Alma Mater Studiorum Università di Bologna

Dipartimento di Ingegneria dell'Energia Elettrica e dell'Informazione "Guglielmo Marconi"

Scuola di Dottorato in Automatica e Ricerca Operativa
XXIX CICLO

Settore Concorsuale: Area 09/G1 Automatica
Settore Scientifico Disciplinare: ING-INF/04 Automatica

Haptic Device Design and Teleoperation Control Algorithms for Mobile Manipulators

Coordinatore Dottorato:
Prof. Daniele Vigo

Supervisore:
Prof. Claudio Melchiorri

Autore:
Alberto Pepe

Tesi conforme ai requisiti
per il rilascio del titolo di Doctor of Philosophy

in

Automatica e Ricerca Operativa

Esame finale anno 2018

Declaration of Authorship

I, Alberto Pepe, declare that this thesis titled, 'Haptic Device Design and Teleoperation Control Algorithms for Mobile Manipulators' and the work presented in it are my own. I confirm that:

- This work was done wholly or mainly while in candidature for a research degree at this University.
- Where any part of this thesis has previously been submitted for a degree or any other qualification at this University or any other institution, this has been clearly stated.
- Where I have consulted the published work of others, this is always clearly attributed.
- Where I have quoted from the work of others, the source is always given. With the exception of such quotations, this thesis is entirely my own work.
- I have acknowledged all main sources of help.
- Where the thesis is based on work done by myself jointly with others, I have made clear exactly what was done by others and what I have contributed myself.

Signed: 

Date: 03/04/2018

“Di tutto un po’.”

Nonna Marta

ALMA MATER STUDIORUM
UNIVERSITY OF BOLOGNA

Abstract

School of Engineering and Architecture
Department of Electrical, Electronic and Information Engineering (DEI) "Guglielmo Marconi"

Doctor of Philosophy

Haptic Device Design and Teleoperation Control Algorithms for Mobile Manipulators

by Alberto Pepe

The increasing need of teleoperated robotic systems implies more and more often to use, as slave devices, mobile platforms (terrestrial, aerial or underwater) with integrated manipulation capabilities, provided e.g. by robotic arms with proper grasping/manipulation tools. Despite this, the research activity in teleoperation of robotic systems has mainly focused on the control of either fixed-base manipulators or mobile robots, non considering the integration of these two types of systems in a single device. Such a combined robotic devices are usually referred to as *mobile manipulators:* systems composed by both a robotic manipulator and a mobile platform (on which the arm is mounted) whose purpose is to enlarge the manipulator's workspace. The combination of a mobile platform and a serial manipulator creates redundancy: a particular point in the space can be reached by moving the manipulator, by moving the mobile platform, or by a combined motion of both. A synchronized motion of both devices need then to be addressed. Although specific haptic devices explicitly oriented to the control of mobile manipulators need to be designed, there are no commercial solution yet. For this reason it is often necessary to control such as combined systems with traditional haptic devices not specifically oriented to the control of mobile manipulators.
The research activity presented in this Ph.D. thesis focuses in the first place on the design of a teleoperation control scheme which allows the simultaneous control of both the manipulator and the mobile platform by means of a single haptic device characterized by fixed base and an open kinematic chain. Secondly the design of a novel cable-drive haptic devices has been faced. Investigating the use of twisted strings actuation in force rendering is the most interesting challenge of the latter activity.

Acknowledgements

The first thanks goes to all the people I have shared the last years with. My supervisor, professor Claudio Melchiorri who gave me the chance to choose my way while kept on steering me in the right direction. He also gave me the great honor to be his teaching assistant in the course of Industrial Robotics. This 4 years activity turned out to be one of the most satisfying professional experiences of my life. A great thanks goes to Gianluca Palli for the everyday support and valuable advices, and for having routed my research activity to the haptic device design. Thanks to Luigi Biagiotti and Alessandro Macchelli for never having lost track of my progress. A great thanks to professor Eugenio Faldella for showing me that there is so much to learn even from coffee-breaks.
I would like to thank my fellow labmates with whom I share much more than the years of PhD: Umberto, Daniele, Lorenzo, Davide, Federico, Roberto, Riccardo and Mohssen. The great Caccia and the wise Christian. I truly thank my family: my parents, Cristina and Gian Marco, my brothers Michele and Francesco but also Eugenia, Betti, Laura Elisa for the unconditional support in everyday life.
Last but not least I sincerely would like to thank all the people that kept on pushing me also in the hard times of this long learning journey. Growing old is mandatory, growing up is optional.

Contents

List of Figures

Dedicated to Francesco *and* Michele, *my little brothers.*

Chapter 1

Introduction

1.1 Research goals

Teleoperation systems have been the first discipline to come to light in the scene of robotics research back in the 40s. Since then, although the research in autonomous robots has made great strides making robots more and more intelligent and able to execute even very complex tasks without the need of human supervision, a costant growth of applications involving robots teleoperation has still been recorded. Main reasons can be found in the native perception capabilities and decision making skills of the human being that cannot be left aside when dealing with operations in remote and unstructured environments.
Teleoperated robots permit the interaction with environments that are dangerous or of difficult access, e.g. space or underwater exploration, or with a different scale with respect to the typical human perspective, as for example in the case of microsurgery [3].
Control problems arises when a the master and the slave robots of a telerobotic system present kinematically dissimilar mechanical structures as the case of the slave robot is a mobile manipulators. A mobile manipulator represent the integration of traditional n-DoF (Degrees of Freedom) fixed-base robotic arm and a standard (nonholonomic or omnidirectional) mobile robot in a single robotic device. Such a integration increases the manipulator's working range potentially to infinite, but also introduces redundancy, which means that there exist an infinite set of solutions in the joint space of both the arm and the mobile base, for a given end-effector configuration. A properly combined motion of both devices needs then to be addressed. Although specific haptic devices explicitly oriented to the control of mobile manipulators need to be designed, there are no commercial

solution yet. For this reason traditional fixed-base haptic devices not specifically oriented to the control of mobile manipulators and in general with a lower number of DoF need to be used.
The hybrid control algorithm for a standard mobile manipulator presented in Chapter 4 tries to overcome the kinematic mishmach between the master and the slave robots providing an intuitive interface to the operator who controls the 8 DoF of the slave robot by means of fixed-base 6 DoF haptic interface.
For a more detailed discussion on the issues related to mobile manipulators teleoperation that have motivated this research please refer to Section 3.3.1.
The second part of the activity has focused on the design of a novel cable-driven haptic inteface addressed to teleoperate generic robotic devices. Many researchers have shown that the availability of haptic interfaces able provide the operator with sufficient kinesthetic information about the interaction forces exchanged between the slave robot and the remote environment can considerably improve the performance of the teleoperation task.
The *ideal* haptic inteface is supposed to have low inertia, low friction, low torque ripple, backdrivability, and low backlash in the actuation and transmission systems. Besides this, many applications requests considerable workspace of the master device in order to properly mimic the slave characteristics. Commercial (sensibly expensive) solutions do not guarantee all these features, which in general are in contrast between each others.
Cable transmission may be promising candidates to solve these limitations because it minimizes the actuators contribution to the haptic's end-point inertia and encumbrance, providing a considerable force-weight ratio.
Despite many solution of haptic interface embedding cable trasmission have been proposed in literature, there seems to be a gap in the investigation of Twisted String Actuation (TSA) in haptic force-rendering.
More details on the issues related to the topic that have motivated the design of the UBHaptic see Section 3.3.2.

1.2 Thesis structure

The thesis is organized as follow:

- In Chapter 2 a bref introduction to robots teleoperation systems is presented. In particular a general overview of the main features and components of a

telerobotic system as well as brief hystorical perspective and main applications is provided. A particular focus has been reserved to the classification of haptic devices and to the introduction of mobile manipulators;

- In Chapter 3 the main issues related telerobotics are introduced. In particular Sec. 3.3.1 and 3.3.2 focus on the issues that have motivated the definition of the hybrid control algorithm for a generic mobile manipulator and the design of the UBHaptic respectevely;

- In Chapter 4 the hybrid control algorithm is presented and discussed as well as the the experimental setup used to validate the proposed approach. Experimental results are provided at the end of the chapter;

- In Chapter 5 the design of the haptic interface based on TSA is presented. First the overall structure is discussed and the inverse and differential kinematic models are introduced. A description of the criteria and the simulation results used for the workspace dimensioning and actuation/trasmission sizing is then provided as well as a preliminary design of the TSA module;

- In Chapter 6 the design of the new TSA module is discussed with a particular focus on the design of the integrated optoelectronic force sensor. The problem of the integration between the different system's components is also addressed and the structure of control system architecture is described. Experimental results are proposed and discussed at the end of the chapter;

- In Chapter 7 the results of the research are summarized drawing guidelines for further developments;

Chapter 2

Focus on Robotic Teleoperation

2.1 Introduction

Robots teleoperation (i.e. *telerobotics*) is perhaps the earliest field of application of robotics. Literally meaning *doing work at a distance* [4], it is generally used to refer to robotic systems with a human operator in control or *human-in-the-loop* [1]. Any high-level, planning, or cognitive decisions are made by the human user, while the robot is responsible for their physical/mechanical implementation (see Fig. 2.1). In essence, the brain is removed or distant from the body. The inclusion of the human operator makes telerobotics very attractive to handle unknown and unstructured environments.

The term *tele*, which is derived from the Greek and means *distant*, implies the idea to have a human operator controlling a robot operating in a remote location as shown in Fig. 2.2.

Besides distance, barriers may be imposed by hazardous environments or scaling to very large or small environments. All barriers have in common that the user cannot (or will not) physically reach the environment.

From a functional point of view a teleoperation system can be divided in two main parts: the *local site* with the human operator and all the hardware needed to implement a physical connection with him/her (e.g joysticks, monitors, keyboards, or other input/output devices), and the *remote site*, which contains the robot and supporting sensors and control elements (i.e. the environment where the robot is requested to operate) [1].

The local and remote robots are called *master* and *slave*, respectively, while the system is referred to as a *master–slave system*. In the most common scenario, the master and the slave robots are kinematically equivalent: the slave robot is

(a) Direct interaction

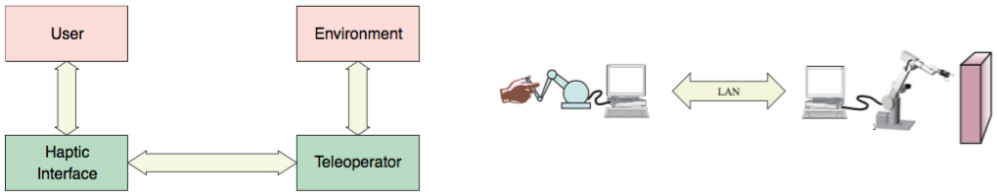

(b) Remote interaction

FIGURE 2.1: Direct interaction with a local environment and interaction with a remote environment by means of a telerobotic system.

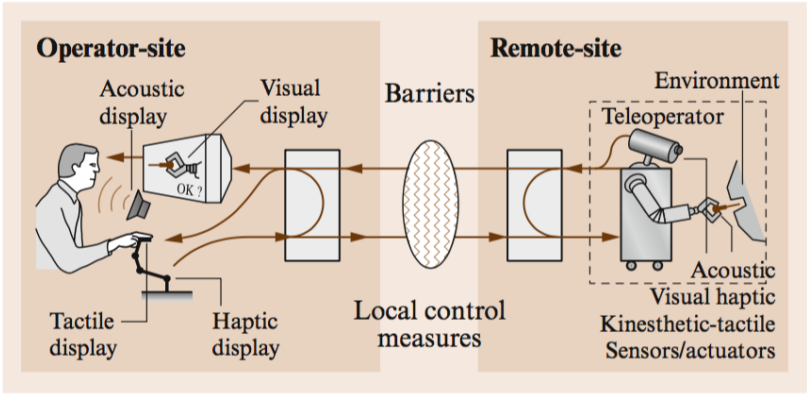

FIGURE 2.2: Overview of a telerobotic system (from [1]).

programmed to follow the motions of the master robot, which is imposed by the user (*direct control*).

Some master–slave systems provide the so called *force feedback* feature. In this kind of systems the master robot is not only able to send motions command (imposed by the user) to the slave robot, but it is also able to provide some kind of information related to the remote environment (where the slave robot operates) back to the operator. This information are usually translated in terms of *interaction forces*. Such telerobotic systems are often called *bilateral* and the master devices able to display force information to the user are often referred to as *haptic devices* (discussed in Sec. 2.4).

The workflow of bilateral teleoperation systems is summarized in Fig. 2.3: the human operator generated forces producing the motion of a master haptic device. The motion signals of the master robot (generally position and/or velocity signals) are transmitted to the slave robot through a communication channel. The

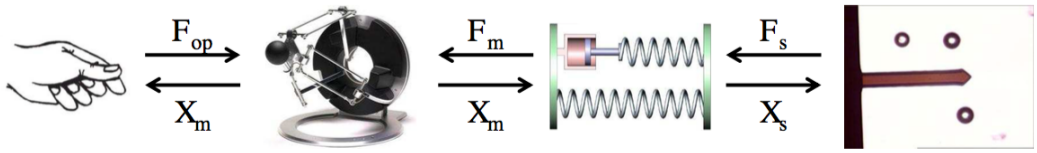

FIGURE 2.3: Bilateral teleoperation system: the user controls the position Xm of the master haptic device which is sent to the slave robot in terms of motion commands. The Interaction forces between the slave robot and the remote environment are transmitted back and displayed to the user as a haptic force Fm (see [2]).

slave robot tracks the motion of the master. During the task execution, the slave robot may exchanges interaction forces with the remote environment. The reaction forces are transmitted back to the haptic master which is able to display them to the human operator. Several researchers showed that the role of haptic devices, able to provide kinesthetic feedback representing the remote mechanical interaction, is essential to extend the information provided to the user beyond the simple visual feedback [5], [6] and improve the sense of *telepresence*, intended as the ideal of sensing sufficient information, and communicating this to the human in a sufficiently natural way that the operator feels to be physically present at the remote site [7]. In the field of telerobotics, the term telepresence is generally used to refer bilateral teleoperation systems that, in addition to haptic interfaces, also include computer vision, computer graphics and virtual reality (multi-modal systems) [8].

The design and implementation of reliable bilateral teleoperation systems present a number of challenges when there is a considerable physical distance between the master robot and slave robot and the information transit back and forth through a communication channel. The first problem is related to the *transparency* of the teleoperation system [9] [10], i.e. the need to couple the human operator as good as possible to the task requested to perform in the remote environment by providing a trusty transmission of the force, position and velocity signals. In other words, the force feedback to the user has to faithfully represent the mechanical interaction of the slave robot with remote objects.

Transparency of the teleoperation system is an important control design goal, since the power requested to perform a certain task has to flow from the user throughout each component before reaching the remote environment. To achieve transparent position coordination the position of the slave robot should converge to the position of the master robot if the forces developed by human operator and the environment are zero. For transparent force reflection, in steady state the

force developed by the environment on the slave robot should be equal to the force developed by the master robot on the human operator [11].
Since the interaction involves power flows between each subsystem, it is important that control algorithms can handle them in such a way that stability of the interaction is preserved regardless of the particular remote environment. This requisite is particularly important for systems that interact with human beings, that have to be intrinsically safe. Stability problems in bilateral systems are related to the presence of not negligible communication delay and package losses in the communication channel.

2.2 Brief history

In this section a few references to the systems, that are seen to be milestones within the history of telerobotics are given.
The first modern teleoperation system was developed between 1940's and 1950's addressing the nuclear research by Raymond C. Goertz in the *Argonne National Laboratory* where a master-slave manipulator addressed to chemical and nuclear material handling in the first nuclear reactor [12] was developed. The need was obvious. The radioactive nuclear material has to be manipulated safely. The nuclear material was placed in a "hot cell" where the operator could manipulate it from behind shielded walls. The visual contact with the target was through a protective window and/or a mirror. The first teleoperation system was completely mechanical. Master and slave were connected by gears, linkages, and cables these systems allowed the operator to use natural hand motions and transmitted forces and vibrations through the connecting structure. The system was clearly limited by the distance between the operator and environment and required the use of kinematically identical devices, see Fig. 2.4. Goertz quickly recognized the value of electrically coupled manipulators. The mechanical manipulators were soon replaced by electro mechanical servos [13]. In 1954, Goertz's team developed the first electro mechanical manipulator controlled by an array of on–off switches to activate various motors and move various axes. The Goertz's work laid the foundations of modern telerobotics and bilateral force-reflecting positional servos.
After this, the teleoperation of manipulators and mobile vehicles extended rapidly to new branches where the advantages of teleoperation techniques could be utilized.
At the beginning of the 1960s the effects of time delay on teleoperation started to become a topic of research. The concept of supervisory control, that will be

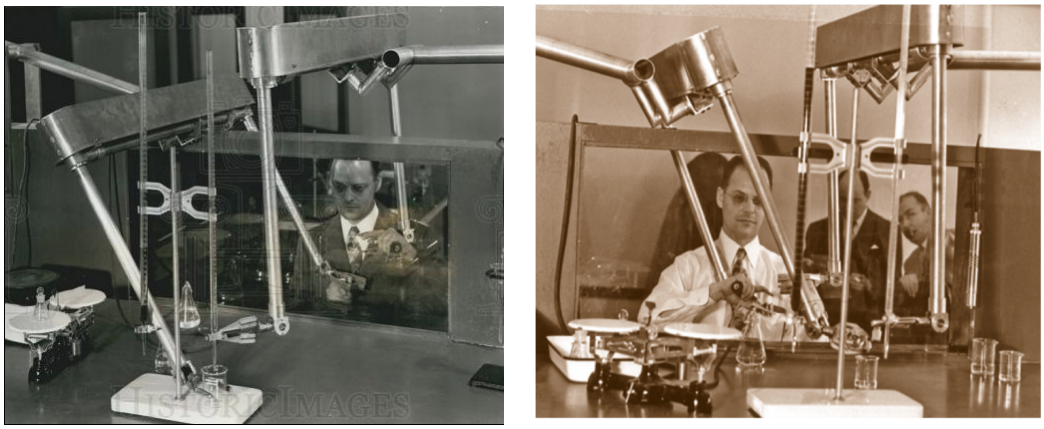

(a) (b)

FIGURE 2.4: Raymond C. Goertz in the early 1950s handling radioactive material using the first (mechanical) teleoperator.

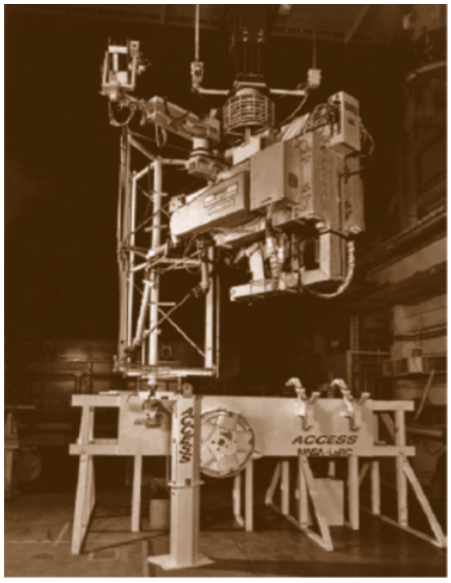

FIGURE 2.5: The telerobotic system CRL Model M2 developed by the Oak Ridge National Laboratory and used by NASA in deep space assembly applications (1982).

detailed in Sec. 3.1.3 was introduced and inspired the next years of development [1].

The first telerobotic system implementing force feedback with separated master and slave electronics was the *model M2* (1982), shown in Fig 2.5, of the Central Research Laboratory. It was developed together with the Oak Ridge National Laboratory and was used for some time for a wide range of demonstration tasks including military, space or nuclear applications. NASA tested the model M2 for remote assembly in space with excellent results.

Still in the field of space applications a dual-arm force reflecting telerobotic system was developed by *Bejczy et al.* at the Jet Propulsion Laboratory (JPL). For

FIGURE 2.6: JPL ATOP control station (early 1980s).

the first time in history kinematically and dynamically different master and slave systems were used, requiring control in Cartesian space coordinates (the same approach is used in the proposed teleoperation control schemes for mobile manipulators discussed in Chapter 4). Figure 2.6 shows the master control station with its two back-drivable hand controllers. This system was used for simulating teleoperation in space.

In the 1980s and 1990s, the attention of the research community on teleoperation systems for space exploration was at the highest stage and started shifted also to other areas such as medicine and undersea/deep-sea exploration. The deep oceans are even today considered too hostile for humans so that most of the deep-sea operations are made with teleoperated submarines called *Remote Operated Vehicles (ROV)*. Often ROVs are equipped with telemanipulators in order to perform underwater work tasks. The growth of the Internet and its use as a communication medium fueled further the trend of looking for new applications for telerobotics, adding also new challenges. Novel commercial haptic devices (e.g. the Phantom device [14], see Sec. 2.4.1) were introduced pushing up research activities in haptic applications and virtual reality.

In 1993 the first telerobotic system was flown in space with the German Spacelab Mission D2 on board the Space Shuttle Columbia. The robot technology experiment (ROTEX) demonstrated remote control of a space robot by means of local sensory feedback, predictive displays, and teleoperation [15]. The system could not be considered a bilateral system since only a one-way communication was embedded. The round trip delay was 6–7 s, such that it was not feasible to include force feedback into the control loop.

Last but not least the first transatlantic telesurgery demonstration in 2001,

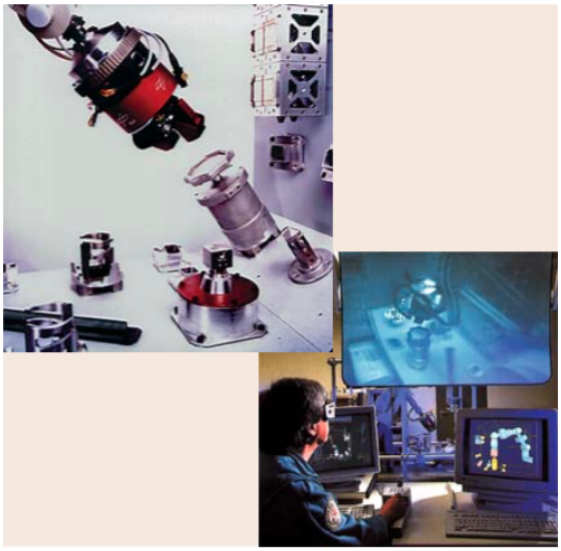

FIGURE 2.7: ROTEX, the first remotely controlled robot in space (1993). Telerobot in space and ground operator station. (Courtesy of the German Aerospace Center, DLR).

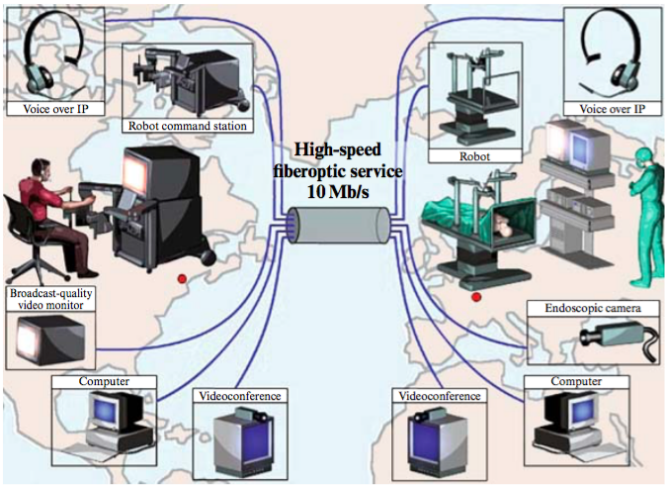

FIGURE 2.8: Operation Lindberg. The first transcontinental telerobotic surgery (2001).

Computer Motion demonstrated the feasibility of telerobotic systems even in the delicate field of surgery [16]. A surgeon in New York (USA) used a ZEUS system to perform a laparoscopic cholecystectomy on a patient located in Strasbourg (France), as depicted in Fig. 2.8. The system did not include force feedback, so the surgeon had to rely on visual feedback only.

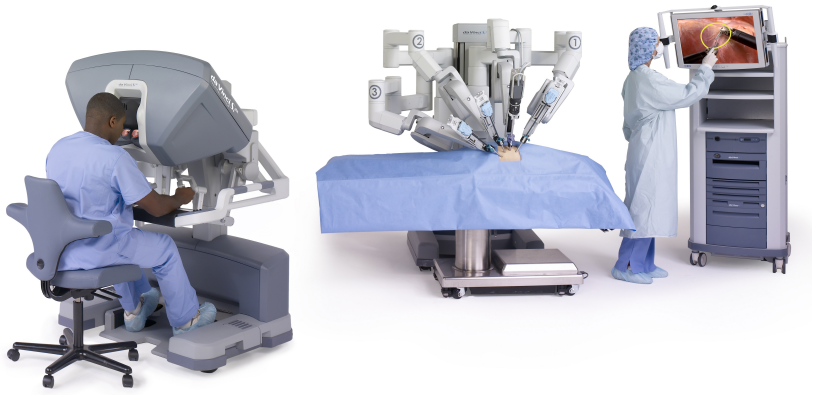

(a) Da Vinci surgical system

(b) Da Vinci master device

FIGURE 2.9: The Da Vinci surgical system.

2.3 Range of application

2.3.1 Telesurgery

A quick look to the history of telerobotics briefly summarized in Section 2.2 points out that such systems can be applied to a variety of areas [17]. Telerobotic systems have been motivated by issues of human safety in hazardous environments (e.g. nuclear or chemical plants), the high cost of reaching remote environments (e.g. space), scale (e.g. power amplification or position scaling in micromanipulation or minimally invasive surgery), and many others. In the following some of the most successful cases of use are provided. A typical modern application of teleoperated robotic systems is represented by assisted surgery. In Fig. 2.9 the Da Vinci robot developed by the *Intuitive Surgical* company is shown. The surgeon safely and precisely controls the surgical tools by means of two haptic joysticks plugged to the thumb and the index of both hands (avoiding in this way dangerous issues related to human hand's tremor, see Fig. 2.9(b)). The system also provides to the user an immersive 3D view of the scene where the tools are operating.

Nowadays a variety of minimally invasive surgical interventions are made by the help of the Da Vinci system: it can perform a variety of laparoscopic surgeries which involves scaling the surgeon's actions into very small movements over a very small communication-delay.
Telesurgery over great distances is still on an experimental stage. In 2001, a team of surgeons from *Johns Hopkins University* in Baltimore (US) operated on 17 patients at Rome's *Policlinico Casilino University* (Italy). In seven of the 17 procedures, the telesurgical connection was stopped and the operations were continued only from the remote site. Two of the 17 were converted to open surgery and during one of the kidney-related procedures problems arised with the manual control of the robotic device. Therefore not all the cases were fully teleoperated and the presence of a surgeon on site is needed in case unexpected problems arise. Anyway it's easy to image a not so far future in which surgeons could operate on a patient from another location all around the world. Other examples of teleoperation in transatlantic surgery can be found in [18], while other generic medical applications in [19] and [20].

2.3.2 Underwater exploration

In the area of underwater applications, teleoperation is used in offshore oil exploration, inspection and maintenance on drill heads, oil platforms and pipelines, marine biology experiments, geological surveys, archaeological search and recovery and classified navy tasks [21]. Americans, British, Japanese have led in this area [8]. ROV often are used in two-arms configurations: one fixed in the structure for stability and the other to perform tests and maintenance [22]. One of the earlier control architectures for underwater manipulator with force feedback is presented in [23].
The *Jason* ROV shown in Fig. 2.10 that was controlled remotely to locate Titanic (but it was later lost at sea). This system was developed as Argo-Jason project at the Woods Hole Oceanographic Institute and named after Jason and his Argonauts of Greek mythology [24]. The name *Argo* identifies a heavy passive assembly of high-energy sonar and photographic equipment suspended by up to 6000 m of cable from its support ship, while the telerobot *Jason* maneuvers on a flexible cable within easy return range from Argo, all controlled from the surface. Jason is programmed with a variety of supervisory control modes (see Chapter 3), and also makes use of some sophisticated techniques such as sliding-control to compensate for unmodeled dynamics common in deep-sea environments.

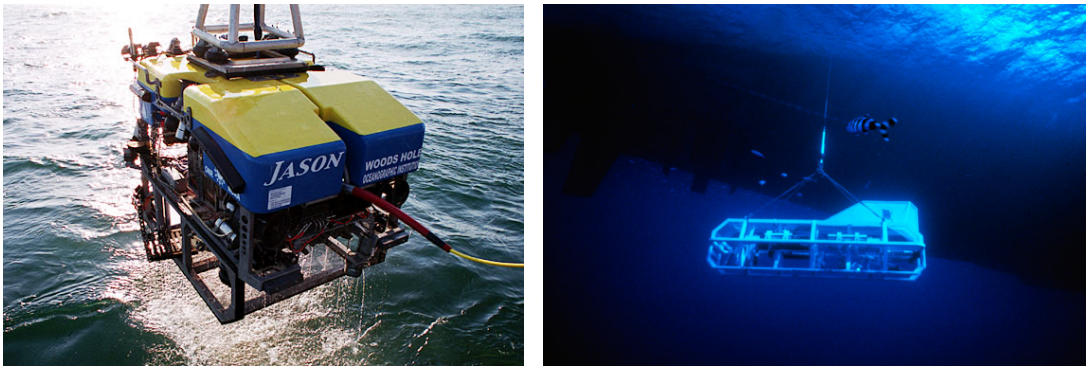

(a) The Jason ROV. (b) The Argo sonar and photographic equipment.

FIGURE 2.10: The remotely controlled Jason ROV (Fig. 2.10(a)) and the system of television cameras and sonars Argo (Fig. 2.10(b)). Both were used to locate the Titanic in 1985.

2.3.3 Space exploration

Space robotics is a classic application, in which distance is the dominating barrier (see Sec. 2.1). The human operators can remotely control robots to perform different tasks in the outer space. It can significantly reduce the cost of operations like assembly, maintenance, repairs. More importantly, it can reduce the risk of safety issues for astronauts [25].

The NASA rovers on Mars are a famous example. Due to the time delay of several minutes, the rovers are commanded using supervisory control (see Sec. 3.1.3), in which the human operator is defining the goal of a movement and the rover achieves the goal by local autonomy using sensory feedback directly [26].

The German technology experiment ROKVISS (Robot Component Verification on ISS) is the most advanced telerobotic system [27]. Launched in 2004, it is installed outside the Russian module of the international space station. In this experiment advanced robot components of a slave system, including torque sensors and stereo video cameras, are validated in real space conditions. Due to a direct communication link between the space station and the operator station at DLR (Germany), the time delay was reduced to about 20 ms allowing a bilateral control architecture with high-fidelity force feedback to the operator [28] (Fig. 2.11).

Figure 2.12, shows the telemanipulation system built by the *German Aerospace Research Center (DLR)*, conceived to support astronauts during maintenance operations in the Space Station. [29].

The master (see Fig. 2.12(a)) is equipped with two anthropomorphic arms that can be plugged to the wrists of the operator. An input device for the hands control is mounted to the flanges of the two arms. The operator can wear a mask

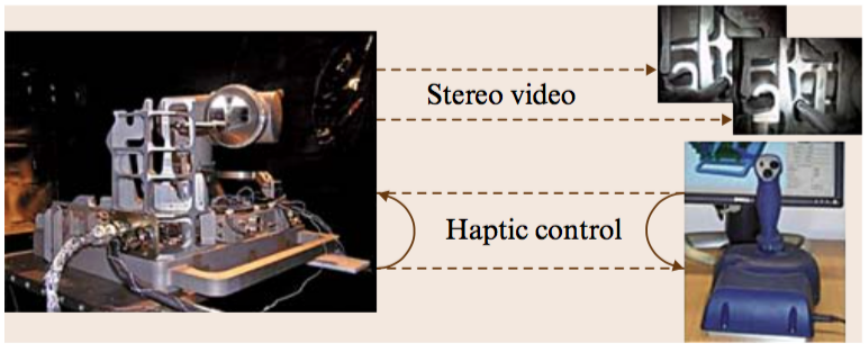

FIGURE 2.11: ROKVISS, a space telerobotic system in which a ground operator by means of stereo vision and haptic feedback controls a slave robot place in the proximity of the ISS (International Space Station).

(a) Master: HUG

(b) Slave: SpaceJustin

FIGURE 2.12: The DLR telemanipulation system.

with a binocular screen to fell immersed in the augmented reality. The slave (see Fig. 2.12(b)) consists of two torque controlled anthropomorphic arm/hand systems and a actuated head. The head has two degrees of freedom and is equipped with a stereo vision system that streams in realtime to the operator. The telemanipulation behavior is realized by means of a cascade of an admittance and an impedance controller block [30].
The operator apply forces to the master arms that are acquired and converted to joints references velocities for the master arms. The current poses of the master TCPs are calculated by means of the forward kinematic and are used as references for the slaves arms. The pose errors are evaluated as the differences of the current TCP poses of the master and the slaves arms. They are used as input for the impedance controller block that translate the pose errors to torques for the joints of the slave arms.

2.3.4 Other applications

Today telerobotics systems are applied to a variety of different fields that is impossible to list all the possible applications in this document.
Good results of teleoperation of mobile robots are addressed in [31–33]. The human operator can remotely control one or several mobile robots to performance different tasks such as formation, co-transportation and multi-robot exploration. There are also many other applications where teleoperation has been applied. These applications include nano-manipulation [34], entertainment and education [35], forestry [36], excavation [37] and many others.

2.4 Haptic devices

This section focuses on specific robotic devices, known as haptic interfaces that, used as master in telerobotic systems, allow human operators to experience the sense of touch in remote environments. As mentioned in Sec. 2.1, force feedback can considerably improve the performance of a master-slave teleoperation system providing the operator with sufficient kinesthetic information about the remote environment.
There are two broad classes of haptic devices: admittance and impedance devices.

Admittance devices sense the force applied by the operator and constrain the operator's position according to the actual dynamics of the slave robot. This approach is currently under investigation mainly in teleoperation of aerial vehicles [38, 39]. In contrast, an impedance haptic device senses the position of the operator, and then applies a force vector according to the physical interaction occurring between the slave robot and the remote environment. In the following we will only refer to impedance-type haptic interfaces.
The force vector imposed by the slave robot on the remote environment is reflected back and imposed by the master on the operator's hand helping him/her to carry out the requested manipulation task. Hannaford et al. [40] compared both task completion time and level of force used for a variety of teleoperation tasks as well as a variety of control modes:

- Position control with visual but no force feedback;
- Regular visual feedback plus force feedback by means of visual display;
- Visual plus kinesthetic (conventional bilateral force) feedback;
- "Shared control" intended as: force feedback is imposed or suppressed as a computer-based function of object contact, recent past forces applied in all degrees of freedom;
- Bare-handed manual control;

Massimino and Sheridan (1994) [5] showed how mean completion time in such tasks is significantly reduced by force feedback independently of visual parameters such as frame rate and spatial resolution of the image.
While force reflection has been accepted in many applications like remote handling of nuclear and toxic wastes, where master-slave positions are considerably close, in all those applications where there is a significant time delay in the control loop (e.g. space applications or transoceanic telesurgery), force feedback produces dangerous instability effects. In all those applications where force feedback is applied (in order to augment the sense of telepresence and increase task performance) haptic interfaces play a fundamental role as the master device. Such a device is able, not only to send motion commands to the slave, but also to display force information to the operator (see Fig. 2.3).
Generally speaking, from a kinematic point of view, there are two main types of haptic interfaces:

- *Serial haptic devices:* characterized by a serial-structured design. The end-effector is mechanically connected to the robot's base by a single open kinematic chain;
- *Parallel haptic devices:* characterized by a parallel-structured design. The en-effector is connected to the base by a number of kinematic chains.

When applied to a teleoperation systems both have some advantages and disadvantages [41] that will be further discussed in Chapter 3.
In the following the state of the art of some well known commercial solutions available on the market as well as research results for both serial and parallel mechanisms is provided.

2.4.1 Serial kinematic structure

In 1977, Teleoperator System Corporation developed a bilateral force-reflecting servo master-slave manipulator called SM-229. SM-229 was the first member of a family of force-reflecting electric master-slave manipulators designed for production and it was designed to be maintainable by the users [42]. In 1980, Jet Propulsion Laboratory (JPL) and Stanford Research Institute (SRI) developed a universal, bilateral force-reflecting six-DoF manual controller [43].
The 7-DOF electrical Force Reflecting EXoskeleton Master was developed for research at Wright-Patterson Air Force Base. The system could provide an operator 25 N of force feedback at the handgrip using cables to transmit forces to the user's hand. The design, control, and evaluation of a hyper-redundant serial haptic device is presented in [44]. A joystick-like general purpose haptic interface is discussed in [45].
Several commercial solutions are also available on the market. The most widely used haptic interface is probably the *PHANToM Omni*® presented in [14], developed at MIT [14], and commercialized by *Geomagic*® under the name *Geomagic Touch* (formerly Sensable Phantom Omni) [46]. The device, shown in Fig. 2.13, is characterized by a six DoF serial kinematic chain and is available in a variety of sizes, three or six actuated DOF and allow interactions through a finger sled or a stylus. The same company also produces an high-end research device called *Phantom Premium*. It offers low dynamic properties but also reduced range in terms of force rendering and reduced workspace. This device has been used in a variety of research experiments focused on robots teleoperation including the one presented in Chapter 4.

(a) PHANToM Haptic by SensAble Technologies (b) Touch Haptic by Geomagic

FIGURE 2.13: The Phantom Omni device by SensAble Technologies and the today's Geomagic Touch by 3D Systems. This low-cost device senses motion in six degrees of freedom and can apply forces in the x, y, and z directions to the stylus tip.

Another serial-designed commercial haptic is the Freedom 7 [47]. One of the disadvantages of such device is limited control stiffness due to the low physical damping present in the joints. A commercial version of Freedom 7 has been realized with the name Freedom 6S (MPB Technologies) [48]. The *HapticMaster* by MOOG [49] is the only admittance controlled haptic interface on the market. Other commercial solutions are distributed by *Haption* [50], *MPB Technologies* [51].

2.4.2 Parallel kinematic structure

A Gimbal-based parallel device has been presented in [52] (floating actuators) and [53] (non-floating actuators). In [54] a solution composed by a center handle connecting four commercial *Phantom Omni* devices is proposed in order to provide six DoF force feedback while two 3 DoF parallel structures connected with a steering handle are presented in [55]. The device proposed in [56] adopts a separable structure composed by lower and upper parallel mechanisms and it is specifically meant to address teleoperation of mobile manipulators. Commercial solutions include the Force Dimension devices [57]: two series of haptic devices with parallel structures (*omega.x and delta.x*) and a 7 active DoF device, *sigma.7* with an extra force feedback DoF for grasping. The *Novit Falcon* [58] is a low-cost version of *omega.3* meant to target the game industry but widely used also in research (Fig. 2.14).

FIGURE 2.14: Novit Falcon: commercial parallel haptic interface addressing the game industry but widely used in research.

Other exaples are produced by *Quanser* [59] and *Butterfly Haptics* [60] that produced *Maglev 200*: the only commercially available haptic interface based on the principle of Lorentz magnetic levitation.

2.5 Mobile manipulators

The importance and popularity toward mobile manipulators has grown in recent years [61]. In research, considerations have focused on the coordination of movements of the robot and the base since redundant degrees of freedom (DoF) are created by adding the moving base (as explained in the following).
In robotics the expression manipulator usually implies some sort of robotic arm involved [62]. A standard serial manipulator consist of a number of links connected with motor-driven joints, where at least one link is connected to the fixed base of the serial kinematic chain. When used as slave in telerobotics systems, the manipulator make it it possible to manipulate objects in the remote environment and exchange interaction forces with it. The joints can either translate or rotate the links in order to place the end-effector to a given position with a desirable orientation. The main drawback in such robotic devices is clearly the limited workspace. Manipulators have been used in the industries since George Devol designed the first programmable robot in the mid-1950s.
On the other hand mobile robots have the ability to freely move in the environment making the available workspace potentially endless. The applications of mobile robots ranges from underwater and aerial vehicles, to ground robots, and are used both by the industry, military and civilian consumers. In the group of

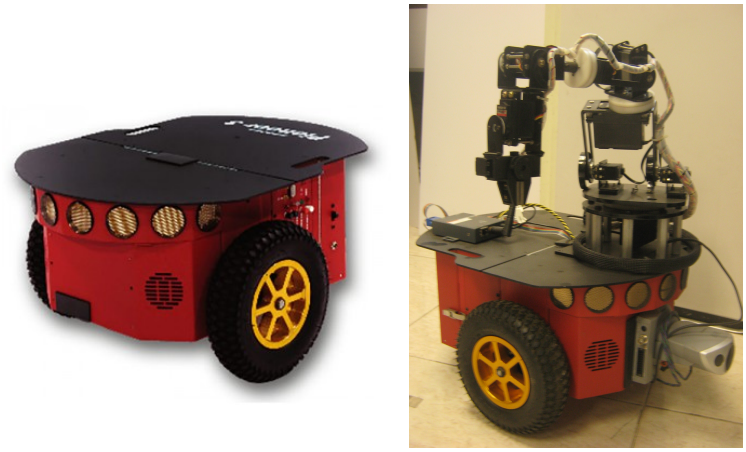

(a) Pioneer robot: one of the most famous unicycle-like differential drive wheeled mobile robot widely used in research.

(b) Pioneer robot with embedded serial manipulator.

FIGURE 2.15: Figure 2.15(a) shows a standard differential drive mobile robot while Figure 2.15(b) shows the same robot equipped with manipulation capabilities.

ground vehicles the wheeled mobile robots are far the most common. A popular mobile robot used in research is the Pioneer robot shown in Fig. 2.15(a). It is driven by a differential drive actuation system and presents a 3 DoF unicycle-like kinematic model.

Mobile manipulators represent the integration of this two type of systems in a single robotic device (Fig. 2.15(b)). Generally speaking it is composed by a mobile platform with integrated manipulation capabilities, provided e.g. by robotic arms with proper grasping/manipulation tools mounted on it. Such a combined robotic devices make it possible to extend the manipulator's workspace to infinite.
The integration of the two different robotic devices also introduces new challenges. The combination of a mobile platform and a multi-link manipulator creates redundancy because the sum of the degrees of freedom of the mobile base and the manipulator is generally greater than six. This implies that a particular point in the environment can be reached by the end-effector by moving the manipulator, by moving the mobile platform, or by a combined motion of both. In other words there exists an infinite set of solutions in the joint space, for a given end-effector configuration. It is then possible to change the robot configuration without affecting the six DoF pose of the end-effector. A complete modeling and control aspects analisys related to mobile manipulators can be found in [63].
Other research challenges in mobile robots teleoperation are related to the different kinematic models of the mobile platform and the manipulator. The manipulator

FIGURE 2.16: Mobile robot with omnidirectional wheels.

is usually a *holonomic* system while the mobile platform may be subject to *nonholonomic constraints*. A system subjected to nonholonomic constrains is limited in the directions that an instantaneous act of motion can be performed. In other words a constraint is said to be nonholonomic if there exists a limitation on the velocity (velocities perpendicular to the wheel's rolling direction are not allowed) but not in the configuration vector (i.e. the configuration that the robot can rich in the environment).

The end-point on a serial manipulator with six (or more) DoF instead, can apply a linear (and/or rotational) velocity in any direction (around any axis in space), but its configuration vector is limited by the dimension of its workspace. Mobile manipulators override the holonomic contraints proper of fixed-base manipulator extending their workspace to infinite. A mobile manipulator has the same reachable area than an infinite numbers of fixed-base manipulators along the path where the mobile base can move, which is insted still nonholonomically constrained. Many studies have been conducted on the whole-body modeling and control of nonholonomic mobile manipulators. There are commonly two ways to model the kinematic system with nonholonomic constraints. One way is to directly add the constraints to the velocity kinematic model [64, 65]. Another way is to model the system to explicitly entail the admissible motions with respect to the nonholonomic constraints [66, 67].

The redundancy resolution methods for standard fixed-base manipulators can then be extended to the nonholonomic mobile manipulator with methods like the Extended Jacobian method [68].

A common way to avoid nonholonomic constraints proper of mobile robots is the use of omni-directional wheels, shown in Fig. 2.16. In this kind of wheel, a series of rollers are attached to its circumference with axis of rotation placed at 45 degrees to the plane of the wheel and at 45 degrees to the line through the centre of the roller and parallel to the axis of rotation of the wheel.

Considering a four-wheeled configuration, like the one shown in Fig. 2.16, alternating wheels with left and right-handed rollers, in such a way that each wheel applies force roughly at right angles to the wheelbase diagonal, the vehicle is stable and can move in any direction and turn by varying the speed and direction of rotation of each wheel. The following actions related to the wheel's actuations are allowed:

- Moving all four wheels in the same direction causes forward or backward movement;
- Moving the wheels on one side in the opposite direction to those on the other side causes rotation of the vehicle (without causing any translation);
- Moving the wheels on one diagonal in the opposite direction to those on the other diagonal causes sideways movements;

Combining these actions permits to obtain three completely decoupled DoF (translations along x and y axis and rotation θ around z axis) and allows the vehicle to perform motions in any direction with any rotation.
The use of omni-wheels permits to obtain a mathematical model of the mobile manipulator in which the 3 decoupled DoF of the mobile platform are considered as new joints and links of a standard redundant manipulators (two endless prismatic joints and one infinite rotary joint) and to extend the traditional control methods for the standard manipulators to the mobile manipulators. However, when implementing these control methods to the actual mobile manipulators many problems occur seriously affecting the control performance of the mobile manipulators in terms of motion accuracy [69]. These issues will be discussed in Sec. 3.3.1.

2.5.1 KUKA youBot

The KUKA youBot was introduced at the *Automatica* conference in 2010 in Munich. The hardware is entirely developed by KUKA. The software was created as part of the European Best Practices in Robotics, or BRICS, project, funded under the EU's FP7 robotics framework. It is a mobile manipulator that was primarily developed for education and research. As any other mobile manipulator, it consists of two main parts [70]:

- *Omni-directional mobile platform* (Fig. 2.17(a)): consists of the robot chassis, four omni-wheels (described in Sec. 2.5), motors, rechargeable battery

(a) KUKA youBot mobile platform. (b) KUKA youBot arm.

FIGURE 2.17: The KUKA youBot mobile manipulator composed by a omni-directional mobile platform Fig. 2.17(a) and a 5 DoF robotic manipulator Fig. 2.17(b).

and an on-board PC running Ubuntu Linux and ROS (Robot Operating System). The wheels motor controllers of can be accessed via Ethernet and EtherCAT both form the on-board PC and an external workstation. An extra Ethernet slot can be used to connect the on-board PC to a LAN via network cable. The overall mobile base weight is 20 Kg with a payload of 20 Kg as well. The geometric dimensions are: length 580 mm, width 380 mm and height 140 mm. The velocity range goes from a minimum of 0.01 m/s to a maximum of 0.8 m/s.

- *The manipulator* (Fig. 2.17(b)): it is characterized by a five DoF (defective) serial kinematic chain (shown in Fig. 2.18) and a two-finger gripper with a 20 mm stroke and a 70 mm range. Similar as for the base, the motor drivers of each individual joint can be accessed via Ethernet and EtherCAT. If connected to the mobile platform, the arm can be controlled by the on-board PC. Alternatively, the arm can be controlled without the mobile platform by using an external workstation connected via Ethernet cable. The total arm's weight is 5.3 Kg with a nominal payload of 0.5 Kg. The available workspace is an ellipsoid-like portion of space with x and y axis equal to 540 mm and z axis equals to 655 mm. The maximum joints rotational speed is 90 deg/s.

Additional sensors and general purpose hardware can be mounted on the robot. The most common integrations involve the use of standard vision sensors (2D cameras), range finders, laser scanners and 3D vision sensors.
The robot is available in a single-arm configuration with a metal plate installed nearby the arm on the mobile base for holding objects and in a dual-arm configuration for advanced bi-manual manipulation tasks. Both solutions are shown

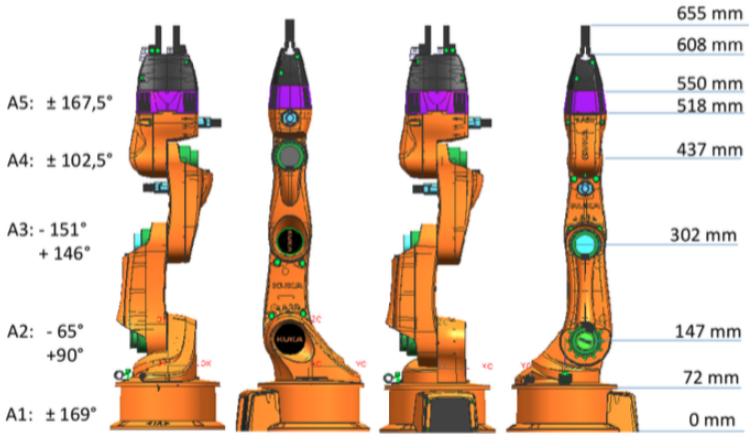

FIGURE 2.18: Overview of the serial kinematic chain of the KUKA youBot arm. The figure illustrates joints limits and links length.

(a) KUKA youBot sigle-arm configuration (b) KUKA youBot dual-arm configuration

FIGURE 2.19: The KUKA youBot mobile manipulator available in single-arm configuration Fig. 2.19(a) and dual-arm configuration Fig. 2.19(b).

in Fig. 2.19. The single-arm configuration is the one used in the experiments discussed in Chapter 4.

Chapter 3

Design and Control Issues in Robotic Teleoperation

3.1 Degree of autonomy

Although the research in robotics has gone a long way towards making robots more and more intelligent and able to execute complex tasks autonomously without the help of human operators, the native perception capabilities and decision making skills of the human being cannot be left aside when dealing with operations in remote and unstructured environments. For this reason, teleoperation of robotic systems still plays an important role in many applications (see Sec. 2.3). As a matter of fact in recent years mainly two research lines have been followed up in order to widen the fields of application of robots. First of all, a higher degree of autonomy has been recognized as an essential requirement in order to reduce the need for human supervision/control and to improve the capability of a robot to self-react to external stimuli, (e.g. the presence of obstacles with unknown positions and velocities) [6]. On the other hand, several tasks such as the manipulation of radioactive materials require the constant supervision of a human operator, that for safety reasons remotely operates an electro-mechanical device [71]. In this situation, the perception by the user of the interaction between the robotic device and the manipulated material is essential in order to successfully complete the required operation.

Several control schemes have been proposed in the literature [72]. These control methods are based on a number of different techniques for dealing with common problems that arise in this area of telerobotics. In order to achieve different degree of autonomy embedded in the slave robot (i.e. the ability to perform some kind

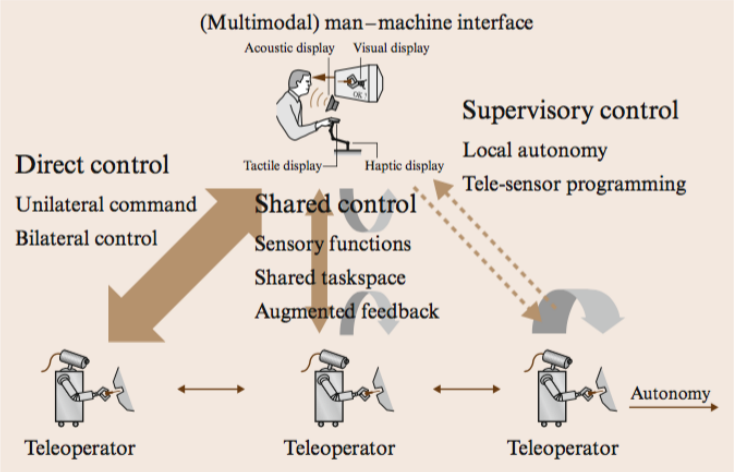

FIGURE 3.1: Different types of control architectures for telerobotics system depending on the degree of autonomy of the slave robot.

of operation in the remote environment without the intervention of the human operator) mainly three control architectures can be considered (Fig. 3.1):

- Direct Control
- Shared Control
- Supervisory Control

Direct control or manual control falls at one extreme, indicating that the user is controlling the motion of the robot directly and without any automated help. At the other extreme, *supervisory control* implies that user's commands and feedback occur at a very high level and the robot requires substantial intelligence and/or autonomy. Between the two extrema lie a variety of *shared control architectures*, where some automated help is available to assist the user [1].

3.1.1 Direct control

The direct control architecture implies that the slave motion is directly controlled by the human operator by means of the master device. In this case the slave robot is usually referred to as telemanipulator (or teleoperator) and do not own any kind of intelligence or local autonomy.
The motion commands sent from the master to the slave, related to the master position displacement imposed by the user, can be computed and mapped on the slave side by means of different strategies depending on the kinematics of the slave

device. Roughly speaking, it is possible to define two main control approaches strongly oriented to the type of robot to be controlled [73]. In case of fixed-base manipulators, a common approach is the so called *position-position* while, in case of mobile robots, the same master displacement is mapped into velocity commands (*position-velocity*).
In the following, the two basic control schemes are briefly reported and discussed. A combination of both schemes has been used in the hybrid scheme addressed to mobile manipulators presented in Chapter 4.

3.1.1.1 Position-position control

The position-position teleoperation control scheme is among the most simple schemes adopted in robots teleoperation (mostly applied to fixed-base manipulators). It has been widely used to perform teleoperation tasks requiring object manipulation and more in general involving interaction with remote environments. This control scheme can be based on a direct kinematic mapping between master and slave devices (involving control in the joint space, i.e. physically identical devices) or can implies control in the workspace to overcome possible mismaches in the master/slave kinematic structures. [74].
This control scheme maps the position displacement of the master device, directly imposed by the operator, to a reference signal for the slave position controller. It is particularly suited in control schemes where the human operator controls object positions directly. The transfer function from human operator to the slave robot movement in position control is a constant (i.e. a *zero order transfer function*, see Fig. 3.2). A proper scaling factor may be used to overcome possible different dimensions in master and slave workspaces.

3.1.1.2 Position-rate/acceleration control

Position-rate/acceleration control on the other hand, controls movement through velocity or acceleration. In this scheme the displacement of the master device defines the velocity or the acceleration of the slave: In other words the transfer function from human input to the slave robot movement is an integral (or double integral) (i.e. *first order or second order transfer function*, see Fig. 3.2). This type of control architecture is particularly suited for mobile robots control (ground, aerial or underwater vehicles) to overcome the mismatch between the master and the slave workspaces dimension.

For six-degree-of-freedom DoF applications, i. e., when the slave needs to be controlled in translation and orientation, a 6D-Space Mouse or alternatively often two joysticks are used as master device for translation and orientation respectively. Acceleration and rate control can require considerable effort for the operator to reach and hold a given target location. Obviously, users can more accurately position a system under rate control than under acceleration control [75]. Indeed acceleration control necessitates users to regulate a second-order system versus a first-order system for rate control.

3.1.1.3 Comparison

In the following a comparison between position-position and position-rate controls is taken into consideration. In general, position control has been proven to be more efficient in task where short and precise movements are involved, (i.e. manipulation tasks) [76].In [77] the authors found out that the position-position scheme can be 1.5 times faster than the position-rate control when the master and slave workspaces are similar. As illustrated in Fig. 3.2, the input control patterns for rate control are more complex than for position control. As a matter of fact in order to cause a change of state from one level to another, a pair of reversal actions has to be given. This might result in being less intuitive then the position-position scheme in case of small displacements.
The position-rate scheme gives better performance when the slave workspace is (much) larger than the master's one. and therefore this control scheme is very suitable in case of teleoperation of mobile robots with infinite workspace. Position control also has its conceivable disadvantages relative to rate control. First, it transfers all human limb movements, whether voluntary or involuntary, to the manipulation task. In contrast, the low pass filtering effect introduced by the integral function in a rate control scheme will suppress many high frequency involuntary noises. Second, by definition, rate control lets the user control the velocity of the controlled robot, resulting in smoother movement. With position control, on the other hand, it is more difficult to maintain control of the velocity of the movement, increasing the likelihood of jerky motions. Third, with position control, the maximum operating range is limited while rate control has an effectively unlimited operational range.

Hybrid position-position and position-rate schemes, that try to take advantage from both approaches, have been proposed in the literature. For example, the case of mobile robots has been addressed in [78], while [76, 79] considers a fixed-base

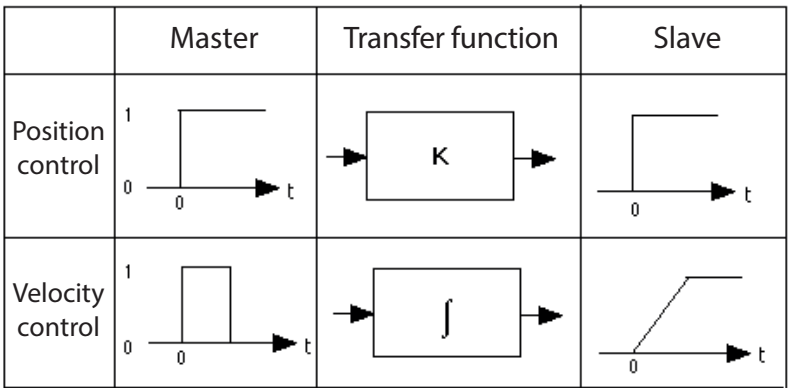

FIGURE 3.2: Transfer function between master and slave in position-position and position-velocity control schemes.

simulated manipulator, and [80, 81] a virtual environment interaction. The idea behind hybrid position-position and position-rate controllers is obviously to exploit the precision of the first and the ability to cover large distances of the latter scheme.

3.1.2 Shared control

Direct control may became impractical in case of not negligible time delays in the communication channel of the telerobotic system (e.g. space or internet-based applications) or in case it is desired to reduce operator workload. To enable telepresence in long-distances telerobotics systems, a so called shared autonomy control [82, 83] appears to be convenient, as it lightens the effort required to the operator [84]. Shared control is based on local autonomous sensory feedback loops [85] at the slave site. The human operator can produce gross motion commands using a kinesthetic haptic device (Sec.2.4), which are fine-tuned by the teleoperator. In applications with large time delays the shared autonomy concept can be even related to a so called task-directed approach [86]. The intelligence is distributed between the operator and the slave robot such that each controls his specific subtask independently. An example can be seen in the telesurgery system shown in Fig. 3.3 [1], where the autonomous skills of the slave robot controls and compensates the patients movement, while the surgeon controls the operation itself on a virtual stabilized patient [87].

In other application of shared control, like the execution of an anthropomorphic grasp task, the user could, for example, simply manifest the intention to grasp

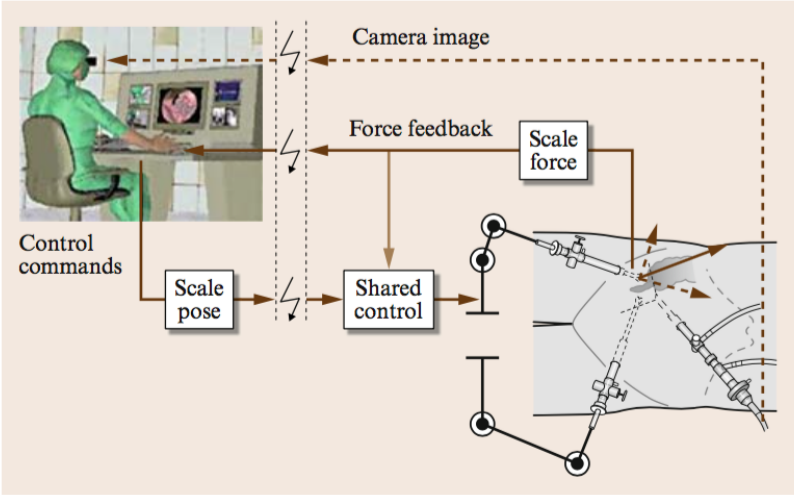

FIGURE 3.3: An example of application of the shared control concept in telesurgery.

an object, while the system autonomously plan the grasp configuration of the anthropomorphic hand. This can be done based on the actual relative pose of the arm with respect to the object, the object shape and the hand kinematic. The implementation of such technique becomes much more feasible if a reactive and accurate vision system able to retrieve objects and obstacles informations, is available on the slave robot [30].
Virtual elements, such as virtual surfaces or generic virtual constraints, can be also imposed to the user. These fixtures help the operator perform manipulation tasks by limiting movement into restricted regions and/or influencing movement along desired paths. Control is thus shared at the master site, taking advantage of a priori-knowledge of the system or task to modify the user's commands and/or to combine them with autonomously generated signals.

3.1.3 Supervisory control

An even higher-level approach, compared to shared control, is the superisory control [88]. In supervisory control the operator is limited to act as a supervisor of the telerobotic system and decides if/when/how to act and what to do. The intelligence is truly distributed between the operator and the slave robot [89]. The user specifies only high-level task operations, local sensory feedback loops are used by the robot system, while global task-level jobs have to be specified interactively by a human operator. In this approach the robot can be teleprogrammed on a task directed level. The teaching of a robot system occurs not on the joint or Cartesian

manipulator level but on a higher language level, i. e. the operator plans activities at a level and the slave robot independently perform the task.
Such a control architecture sometimes includes two control loops working in parallel. One loop running on the real remote system, which contains internal feedback for local autonomy. The other loop, running on the local site, implements a simulated environment which is structurally equivalent to the real system. Since the simulated environment is not affected by any delay in the communication channel, it is predictive with respect to the real system. The main feature of this telerobotic concept is to replace the time-delayed visual feedback with predictive stereo graphics including sensor simulation, providing a supervisory control technique that will allow a shift of more and more autonomy and intelligence to the robot system. This provides the operator with an efficient interface to setup task to configure the task control parameters and debug an entire job execution. Such a telerobotic architecture requires unique tools to implement the required functionality. A sophisticated simulation system has to be provided to emulate the real robot system (including the simulation of sensory perception within the real environment).
In all those applications with large time delays, e.g. in space and undersea applications, this approach has advantages because under time delays of a few seconds, is not feasible for the human operator to handle the robot's movements using a standard direct control approach.

3.2 Master/Slave kinematics comparison

3.2.1 Kinematically equivalent mechanisms

Considering a telerobotics system running under a position-position direct control modality (described in Sec. 3.1.1.1), the simplest scenario involves a master-slave system kinematically equivalent between the two robots. In this case the control of the slave device can be based on a direct mapping between the joint state vector q_m of the master robot (imposed by the user) sent to the slave device as a joint state vector position setpoint q_{sd} for the slave's joints position controllers:

$$q_{sd} = q_m \tag{3.1}$$

Depending on the controllers architecture, the joint velocities of the master and the slave robots may be similarly related, taking derivatives of eq 3.1.

3.2.2 Kinematically unequal mechanisms

Master and slave robots may, in many cases, present completely different kinematics structures. This is a common situation when the slave robot is a mobile robot or in particular a mobile manipulator. The master is connected to the human operator which usually has a limited available workspace with respect to the slave workspace. As a result a direct mapping in the joint space between the two robots is not feasible.
In such scenarios a usual solution is to implement a master-slave mapping in the workspace as stated by the following equation:

$$x_{sd} = \delta \cdot x_m \tag{3.2}$$

$$R_{sd} = R_m \tag{3.3}$$

where x_{sd} and x_m are the desired 3D position of the slave robot and the actual 3D position of the master (imposed by the user) and δ is a proper scaling factor needed to overcome the different dimension between the master and the slave workspace. R_{sd} and R_m represent the desired rotation matrix of the slave device and the current rotation matrix of the master (imposed by the user) respectively. Again velocities and angular velocities may be connected if needed.
It is important to remark that, in case of the slave device presents a lower number of DoF with respect to the master device, the different kinematics may introduces Cartesian configurations of the master that are not physically reachable by the slave. Hybrid approaches between joint space mapping and workspace mapping can then be used. This is the case of the teleoperation algorithm proposed in Chapter 4.

3.3 Motivation and related issues

3.3.1 Mobile Manipulators teleoperation

As described in Sec. 2.3, the range of application of telerobotic systems is considerably extended. The native perception capabilities and decision making skills of the human being cannot be left aside when dealing with operations in remote and unstructured environments (such as space, surgery or nuclear materials handling). Mobile manipulators like the KUKA youBot (presented in Sec.2.5.1) are promising solutions because they significantly increase the workspace of the slave manipulator

(potentially to infinite) as to be worthy of attention from the research community. However, many complications may arise when studying teleoperation solutions in such combined systems.

An important aspect to be considered in this context is that the research activity in controlling teleoperation systems has mainly focused on the control of either standard fixed-base manipulators [6] or mobile robots [31] [11, 90, 91], non considering the integration of these two types of systems in a single device. The increasing of complexity of such robotic systems introduces new DoF in the controlled slave robot that need to be properly managed. The combination of a mobile platform and a multi-link manipulator creates redundancy (see Sec. 2.5): a particular point in the environment can be reached by the end-effector by moving the manipulator, by moving the mobile platform, or by a combined motion of both. There exist then an infinite set of solutions in the joint space, for a given end-effector configuration. Many researchers defined unified whole-body approaches in order to include the wheel's nonholonomic constrains of standard wheels directly in the velocity kinematic model of the mobile manipulator [64, 65, 92, 93].

Another solution includes the use of omni-directional wheels in order to overcome the nonholonomic constraints and obtain 3 decoupled DoF for the mobile base (see Sec. 2.5). This permits to obtain a mathematical model that consider the mobile manipulator as a standard redundant manipulator. The 3 decoupled DoF are considered as new joints and links of the overall kinematic structure (two endless prismatic joints and one infinite rotary joint) and this allow to extend the traditional control methods for the standard fixed-base manipulators to mobile manipulators.

However the practical implementation of these unified approaches in the control strategy is not straightforward. First of all the non-optimal motion distribution between the mobile platform and manipulator creates issues. Traditional control methods try to move the mobile platform and manipulator concurrently not taking in consideration the different working conditions and dynamic behaviors of the manipulator joints and the mobile base joints. Usually, the manipulator is more accurate than the mobile platform, which is especially true when using omni-wheels that are in general affected by low positioning precision.

This lead to not negligible tracking errors of the mobile manipulator's end-effector when considering the unselective motion of all joints together. Intuitively, to achieve a better tracking performance in a generic grasping task, instead of equally using the mobile platform and manipulator during the whole operation, the use of the latter should be preferred as much as possible when the object is placed within the manipulator's workspace, while the mobile base should have a predominant

role during the approaching phase. Unfortunately this procedure would implies the availability of master devices specifically designed to overcome the master/slave kinematic dissimilarities and control the DoF of the manipulator and of the mobile base separately.
The design of custom haptic devices oriented to mobile manipulators teleoperation must also pay a particular attention in keeping the complexity as limited as possible: main reasons are the costs and the period necessary to train the human personnel. Although a good design attempt in this direction is presented in [94] there are no commercial solution yet and it is often necessary to control such as combined systems with traditional haptic devices, as e.g. the PHANToM haptic ([14], [95]) discussed in Sec. 2.4.1. In this scenario, the different kinematic characteristics of the master and slave systems usually involve the need to map the high number of DoF (typically six or nine) of the redundant mobile manipulator into the six DoF proper of standard commercial masters. This requires to design suitable control algorithms able to make the overall teleoperation system intuitive while preserving the feeling of telepresence and transparency to the operator.
These reasons have motivated the design of the hybrid control algorithm for mobile manipulators presented in Chapter 4 which addresses a synchronized motion of both the mobile platform and the manipulator of the slave robot by means of a proper partition of the fixed-base master device's workspace.

3.3.2 Haptic device design

Bilateral force-reflecting telerobotics systems require the availability of special master devices able to display kinesthetic information to the human operator. Many researchers have shown that such haptic interfaces can considerably improve the performance of a master-slave teleoperation system providing the operator with sufficient information about physical interaction occurring in the remote environment (see Sec. 2.4).
An ideal haptic device provides a completely transparent interface to the remote environment (see Sec. 2.1). The transparency and versatility of haptic devices is affected by a number of design criteria characterizing its performance. The haptic devices performance in terms of force display, strictly depends on the actuators properties and the mechanical transmission between the actuators and the interaction point with the human operator (i.e the robot's end-point). The display of a large dynamic range of impedances is the main challenge: a good backdrivability to allow unconstrained motion imposed by the operator and high stiffness to

mimic interaction contacts are desirable. For this reason the primary requirements for actuators and mechanical transmission in impedance-type haptic devices are: low inertia, low friction, low torque ripple, backdrivability, and low backlash. In addition, if the design is such that the actuator itself moves as the user's position changes, a higher power-weight ratio is desired.

On the other hand many applications involve the need of haptic devices with considerable workspace available. This second requirement may be in contranst with the need of low inertia. A maximization of the workspace volume with respect to the length of the kinematical chain requires a serial kinematic chains (see Sec. 2.4.1) with revolute joints which provide spherical workspaces with radius equal to the length of the master arm. This lead to complex and heavy mechanisms where the presence of links and actuators in the moving structure contributes to considerably increase the inertia. For all those tasks requiring large workspaces and high force-rendering capability often standard serial industrial robots are used [96, 97]. These robots are, however, not optimized for interactions with humans: the force capability exceeds by far the strength of a human and the mechanical stiffness is much larger than required for haptic applications [41]. Besides when considering serial structures large areas of the workspace will not be available due to the presence of kinematic singularities: around these positions the robot dynamic properties degrade because high joint velocities only produce small end-effector velocities/displacements. Since the device must be freely moved by the human operator the transition thought these configurations cannot be avoided by trajectory planning methods.

Another important characteristic requested in ideal haptic devices is the extensibility i.e. the capability to host heavy haptic end-effectors such as exoskeleton, able to providing kinesthetic feedback to the operator's hand or tactile interfaces. The addition of such devices requires sufficient mounting space and actuation performance. The commercial haptic device available on the market and discussed in Sec. 2.4 are usually very expensive and do not guarantee the features mentioned above. This considerably slow down the exploration of novel applications involving haptic force rendering.

Cable-based interfaces are promising candidates to solve limitations related to workspace, inertia and cost, at the expense of limited stiffness. The cable transmission minimizes the actuators contribution to the end-point inertia and encumbrance, providing a considerable force-weight ratio. The usage of cable transmissions is not a new concept in haptic interfaces design, as some wire-based haptic displays have been proposed in the literature. In [98] a wearable haptic interface

based on parallel wires in an under-actuated configuration is presented. The discussed device is addressed to blind people and it is the basis of the development of the three-cable haptic interface presented in [99]. A 4-wire driven 3-DoF planar haptic device in proposed in [100], while in [101] a 4 strings 3D spatial interface is presented. Over-actuated solutions for 6 DoF with 9 and 8 strings are proposed respectively in [102] and [103]. The advantages of such a configuration are low-inertia, low-cost, and high safety.

Driven by the considerations reported in this section, the design of a novel cable-driven haptic device (and related actuation module) based on Twisted Strings Actuation (TSA) and addressed to teleoperation of different types of robots is presented in Chapters 5 and 6. This mechanical interface allows to secure the forearm of the user while leaving to her/him the freedom to use the hand to accomplish other tasks, such as teleoperating a robotic gripper.

Chapter 4

The Hybrid Teleoperation Control Scheme

4.1 Motivation

The increasing need of teleoperated robotic systems implies more and more often the use, as slave devices, of mobile platforms (terrestrial, aerial or underwater) with integrated manipulation capabilities, provided e.g. by robotic arms with proper grasping/manipulation tools. Due to the intrinsic integration of the standard manipulators and mobile platforms, mobile manipulators (previously described in Sec. 2.5) have been widely used in many applications including industrial manufacturing, hazardous material operations and space exploration [69, 104–106].
An important aspect to be considered in this context is that the research activity in controlling teleoperation systems has mainly focused on the control of either standard fixed-base manipulators or mobile robots [11, 90, 91], non considering the integration of these two types of systems in a single device (Chapter 3).
In this decoupled approach the motion commands sent from the master to the slave, related to the master position displacement imposed by the user, can be computed and mapped on the slave side by means of different strategies depending on the kinematics of the slave device. Roughly speaking, it is possible to define two main control approaches strongly oriented to the type of robot to be controlled [73]. In case of fixed-base manipulators, a common approach is the so called *position-position* scheme that maps, with proper scaling factors, the displacement of the master device in position reference signals for the slave while, in case of mobile robots, the same master displacement is mapped into velocity commands (*position-velocity*). Both approaches have been described in Sec. 3.1.

Mobile manipulators are combined systems able to perform manipulation tasks in a much larger workspace than a fixed-base manipulators. However, the integration of the two different robotic devices also introduces new challenges such as mismatch in the master/slave kinematic structures and introduction of extra DoF which creates redundancy. The control issues related to mobile manipulators teleoperation has been already discussed in Sec 3.3.1.
These issues have motivated the research described in this chapter, where an hybrid position-position and position-velocity teleoperation control scheme for a generic mobile manipulators, is presented and discussed. The algorithm, (that tries to take advantage of both schemes) is intended to be applied in common teleoperation applications involving mobile manipulators where the slave robot, controlled by a single haptic device characterized by a fixed-base open kinematic chain and not specifically designed for mobile manipulators teleoperation, is requested to grasp objects and move/release them in different locations. Since both the grasping and the releasing position can be placed outside the workspace of the manipulator, a synchronized motion of both the arm and the mobile platform is required.
The proposed control scheme integrates the two control modalities depending on the phase of the task to be executed by the slave robot. In particular, in the grasping/manipulation phase, the robot is controlled with a position-position scheme, while in the motion phase a position-velocity control scheme is adopted. Experimental results are presented at the end of the chapter to illustrate the features and the effectiveness of the proposed control scheme.
The work has been presented at the *International Conference on Intelligent Robots and Systems* (IROS 2016, Daejeon, South Korea) [107].

4.2 The hybrid control algorithm

The human been is a full-fledged *legged mobile manipulator*. In everyday life we have to perform a countless number of interactions with the environment, usually involving grasping or manipulation. As it happens in most cases, the target object is placed far outside the workspace of the human arms and a coordinated motion between the lower and the upper part of the body is required. In most teleoperation applications involving mobile manipulators interacting with unstructured environments, the same need arises and a synchronized motion of the arm and the mobile platform is required.
The novel control strategy presented aims at the simultaneous control of an omnidirectional mobile platform and a robotic manipulator by means of a single,

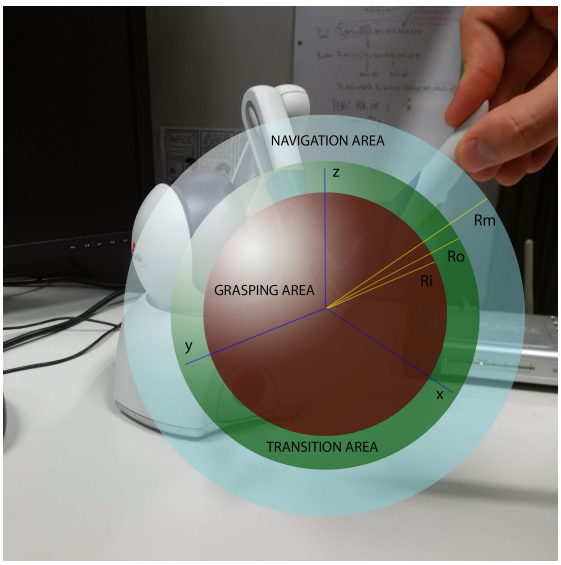

FIGURE 4.1: Characterization of the master device's workspace

commercial, haptic device, characterized by an open kinematic chain with a fixed base (i.e. a Phantom Omni). This result is achieved with a specific partition of the master workspace, as schematically shown in Fig. 4.1.

Given a master device characterized by an open kinematic chain, the volume of its workspace is approximately a portion of a sphere with a radius that depends on the manipulator dimensions.

We define a sphere of radius R_m as the maximum spherical region which can be geometrically contained in the workspace and centered in the workspace itself. The center of the sphere is then assumed to be the origin of the reference frame for the master end-point.

A second concentric sphere of radius $R_o < R_m$ is then defined. This second sphere divides the master workspace in two separate regions. When the haptic interface is inside the inner region, a proper position-position control scheme allows to control the arm of the slave system, while in the outer region a position-velocity mapping is implemented with the aim of controlling the mobile platform. In order to avoid an abrupt stop of the arm motion when the master end-point reaches this surface, a third sphere of radius $R_i = R_o - \epsilon$ ($\epsilon > 0$) is introduced.

By defining $\|p\| = d(P, 0)$ as the Euclidean distance of the haptic interface end-point from the origin during the user operations, the portion of workspace defined by $R_i < \|p\| < R_o$ is meant to be used to perform a proper *smooth transition* between the two control modalities. In conclusion, three different control areas can be identified for the master device:

a) An inner *grasping area*, delimited by the smaller spherical surface of radius R_i in which only the arm is controlled while the mobile base is fixed;

b) An outer *navigation area*, delimited by the two spheres of radius R_o and R_m respectively, mainly assigned to the control of the mobile base;

c) A *transition area*, delimited by the two spheres of radius R_i and R_o and used to perform a gradual transition between the two control modalities.

While the parameter R_m is a design specification and depends on the master workspace dimension, R_o and R_i (i.e. the value of ϵ) are degrees of freedom in the control design that can be properly chosen, as described below.

4.2.1 Grasping Area

In this region, a standard position-position scheme is implemented with the aim to teleoperate the arm of the mobile manipulator. In order to overcome the mismatch of the master/slave workspaces dimensions, a proper scaling factor δ is defined.

Let R_s be the radius of the smallest spherical surface containing the whole workspace of the slave arm. It is possible to define the scaling factor δ as:

$$\delta = \frac{1}{R_o/R_s} = \frac{R_s}{R_o} \tag{4.1}$$

Depending on the value of R_s related to the slave's arm physical characteristics, it is then possible to tune the parameter R_o ($< R_m$) so that the resulting factor δ allows a proper workspace mapping ensuring a good accuracy in the slave end-effector positioning.
Referring to the specific setup used for the teleoperation experiment and presented in Sec. 2.4.1 and Sec 2.5.1, the chosen factor δ is represented by the constant angular coefficient of the red line of Fig. 4.2.

4.2.2 Navigation Area

The sphere of radius R_o acts as an enclosing region for the master's end-point. The outer navigation area can be only reached by forcing a temporary expansion of

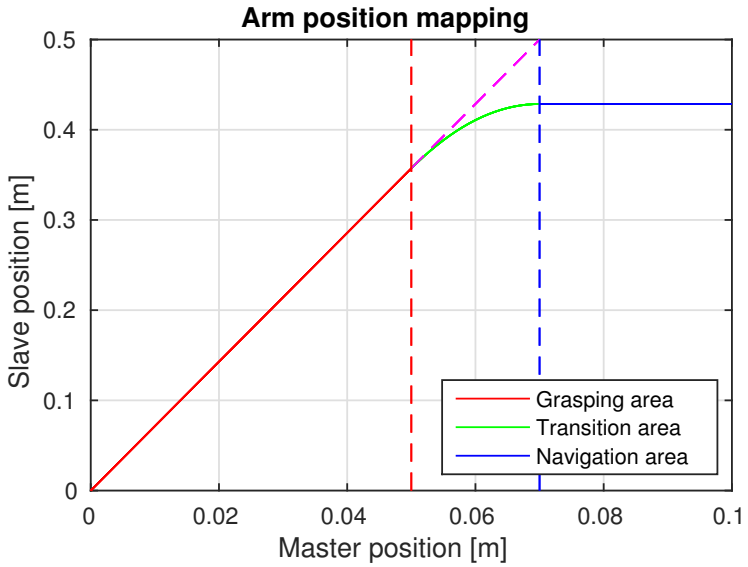

FIGURE 4.2: Mapping between the master and slave arm positions.

the sphere through the application of a force against its surface, that modifies its radius R_o according to the user movements. The end-point is subject to an elastic force, proportional to the expansion of R_o. During the expansion, the increase of the end-point distance from the origin is compensated by a reduction of the scale factor δ due to the radius increase, obtaining a position reference for the arm characterized by a constant absolute value. In this way, in the navigation area the controlled arm modifies only its orientation according to the end-point coordinates and any mismatch in the mapping related to the return of the end-point to the transition area can be avoided.

The elastic force feedback, produced when the sphere is expanded, is defined according to the distance of the end-point from the original surface given by R_o as shown in eq. 4.2:

$$\vec{f_e} = -K_e \cdot (\vec{s} - \vec{p_m}) \tag{4.2}$$

where s is a vector with the same direction of the current end-point position vector p_m and amplitude equal to R_o. The elastic force feedback is produced according to the vector difference between p_m and s.

The position vector p_m of the master's end-point is used to define the direction in the workspace from the origin towards the actual position. The intersection of the direction vector with the inner sphere allows to define vector s of components matching the current position; the components of the two vectors are then compared and, in case at least one of the components of p_m is greater than those of

s (the end effector is outside the grasping region), the force feedback is computed accordingly.

The velocity control law is characterized by a proportional behavior in both the two outer regions (the transition and the navigation areas); the reference velocity is set to zero in the grasping area, and then increases proportionally to the difference between the end-point position p and R_i as shown in eqs 4.3 and 4.4:

$$V_x = K_v \cdot (p_x - R_{i_x}), \qquad V_y = K_v \cdot (p_y - R_{i_y}) \tag{4.3}$$

where:

$$K_v = \frac{V_{max}}{R_m - R_i} \tag{4.4}$$

The elastic force produced by the sphere provides the operator with a feedback of the current mobile base's velocity. The constant factor K_v, used to map the whole velocity range of the mobile platform, is obtained according to the choice of R_o during the design phase. The components R_{i_x} and R_{i_y} are obtained as the x,y components of the vector with the same direction of p_m and amplitude equal to R_i. The resulting velocity control scheme is schematically shown in Fig. 4.3.

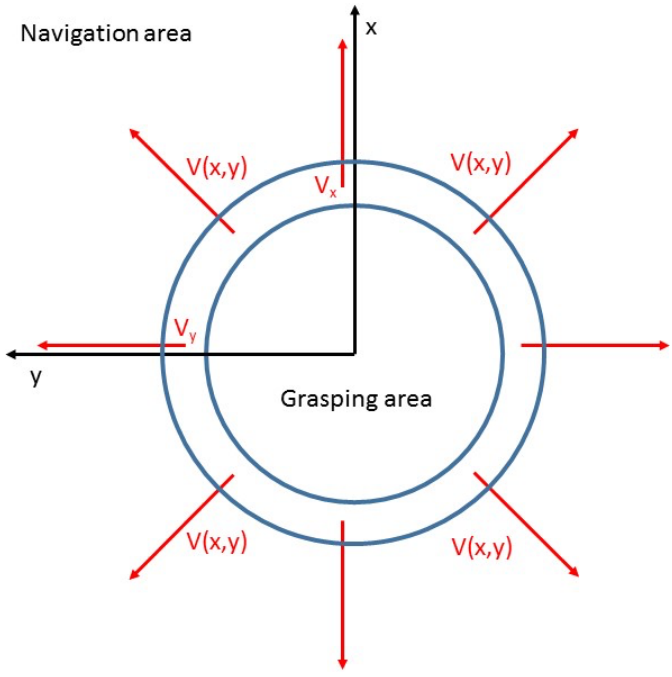

FIGURE 4.3: Velocity generation

The rotational velocity is obtained in a similar way by considering the difference between the z component of the end-point position and R_i (see eq. 4.5).

$$\omega_z = K_p \cdot (p_z - R_i) \tag{4.5}$$

where:

$$K_p = \frac{\omega_{max}}{R_m - R_i} \tag{4.6}$$

In this way, the rotation of the mobile base is defined only in the end-point coordinates whose z components are greater than R_i.

4.2.3 Transition Area

The transition area guarantees a smooth switch between the arm and the base motion: while the master end-point is crossing the region the mobile base starts to increase its velocity according to (4.3) while the arm progressively reduces its speed until it stops when the final position is reached. This reduction is obtained by defining a third order polynomial function in the mapping between the master and slave arm positions, as shown in Fig. 4.2 (green line).
The chosen polynomial trajectory is computed using the following parameters:

$$\begin{aligned} q_i &= \frac{R_i R_o}{R_s} \\ q_f &= \frac{R_s(R_o - R_i)}{2R_o} + q_i \\ q_{v_i} &= \frac{R_s}{R_o} \\ q_{v_f} &= 0 \end{aligned}$$

These four boundary conditions represent the initial and final values of the reference position and of its derivative with respect to the master end-point values. The progressive reduction of the arm motion and the avoidance of the singularity configuration that could arise on the boundary of the slave arm workspace are obtained by choosing as final position the central point between the boundary of the slave arm workspace and q_i.
Since q_i is defined according to the value of R_i, its choice during the design phase can be seen as a trade-off between the percentage of arm workspace mapped with direct proportionality and the distance kept from the singular configuration.
The obtained motion mapping is:

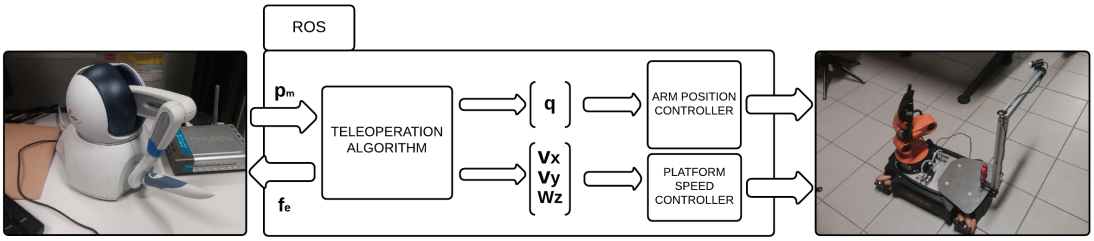

FIGURE 4.4: System used for the experimental evaluation.

$$p_s = -0.5\frac{R_s}{R_o^2 - R_o R_i}(p_m - R_i)^2 + \frac{R_s}{R_o}(p_m - R_i) + \frac{R_s R_i}{R_o} \tag{4.7}$$

4.3 System description

The setup used for the experimental evaluation of the proposed algorithm is shown in Fig. 4.4. The master device is a Sensable Phantom Omni Haptic device (previously described in Sec. 2.4.1), while the slave systems is a Kuka YouBot mobile manipulator (see Sec. 2.5.1).
The control algorithm and communication software infrastructure is based on the Robotic Operating System (ROS). This choice has allowed the creation of a modular scheme, simplifying the debugging and test phases.

4.3.1 The master device

The Sensable Phantom Omni haptic device is a a 6 DoF robotic arm equipped with three motors in the first three joints in order to provide a 3D Cartesian force feedback to the user. Both the Cartesian pose and the joints state vector are transmitted to the network. The 6 DoF of the master end-point Cartesian pose are derived in form of an homogeneous transformation matrix from the joints values by means of the direct kinematics function (DK).
A removable stylus, equipped with two additional switch buttons, can be connected to the end effector in order to provide further customization to the user interaction. In particular, in our experiments, a single button has been used to send open/close commands to the slave's gripper.

4.3.2 The slave device

The Kuka YouBot (described in Sec. 2.5.1) is composed by two different robotic devices: a mobile omnidirectional base provided with an onboard PC and four omnidirectional wheels (see Sec. 2.5), and two 5 DoF robotic arms mounted on the mobile platform. However, the tests have been carried out on a single-arm configuration. The main reference frame is fixed to the base, with origin in the center of mass, with the z axis pointing upwards and the x axis pointing towards the revolute axis of the first joint of the arm. The main control software runs on the onboard PC allowing also the communication over the network.
It is important to remark that the master device has 6 DoF while the slave arm has only 5 DoF. The different kinematics of the master and slave devices introduces configurations that are not physically reachable by the slave. Therefore, the use of two different approaches for the definition of the desired position and rotation is needed. The Cartesian position (with no orientation) of the master end-point is defined by the DK function and depends only on the actual values of the first three joints. The obtained values, properly modified according to the algorithm described in Sec. 4.2, represent the desired position for the slave end-effector (see Sec.3.2.2). The orientation mapping is obtained by defining three *Euler angles* providing the orientation about the $z - y - z$ axes of a reference frame placed in the arm base. The pitch and the roll of the youBot gripper are defined as proportional to the values of the last two joints j_5 and j_6 (see Sec.3.2.1) of the master device, as shown in Fig. 4.5, while the third angle is obtained by the geometric constrains of the arm:

$$\alpha = j_6 \tag{4.8}$$

$$\beta = \frac{j_5 - c}{k} \tag{4.9}$$

$$\gamma = atan2(\frac{p_y}{p_x}) \tag{4.10}$$

The geometric constraint in eqs 4.8, 4.9, 4.10 is imposed by the arm kinematics that forces it to work always in the direction perpendicular to its second joint's revolute axis.
The corresponding rotation matrix, together with the evaluated end-effector position, defines an homogeneous transformation matrix giving the desired pose for the slave end-effector, and is then given as input to the youBot IK function for the computation of the corresponding joint angles for the slave arm. The solution

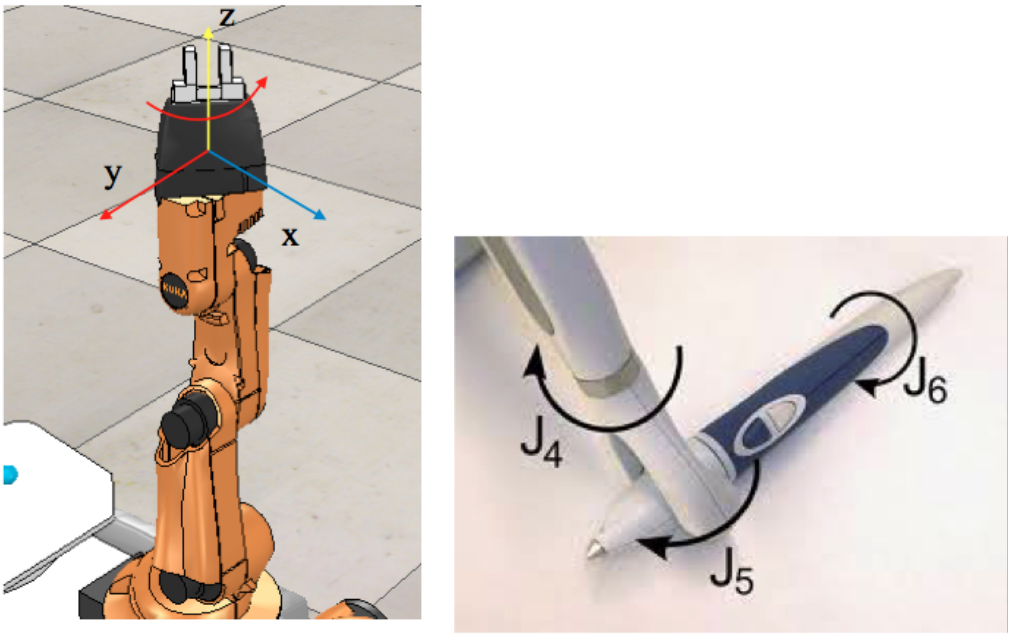

(a) KUKA youBot arm (b) PHANToM haptic device

FIGURE 4.5: The roll angle α of the youBot end-effector is defined according to the value of the last joint j_6 of the PHANToM device while the pitch angle β is related to the value of the fifth joint j_5.

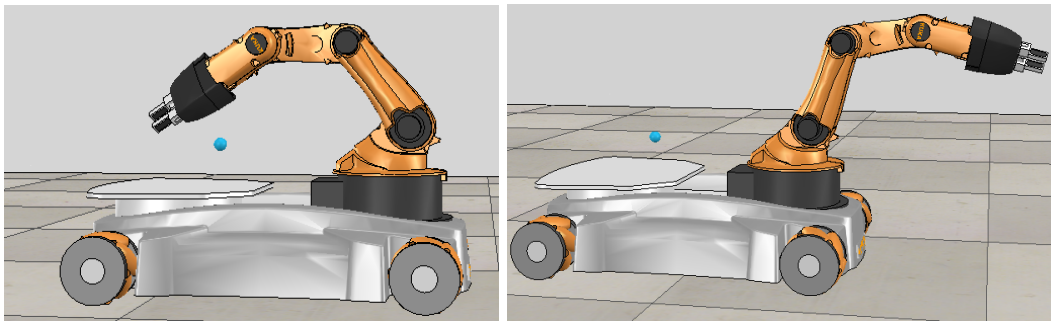

FIGURE 4.6: Inner-arm and outer-arm configurations

with the shortest distance from the current configuration is chosen, in order to avoid unexpected behaviors due to the multiple solutions of the IK.

4.3.3 Configuration switching and singularity issues

With respect to the single arm configuration of the Kuka youBot, the arm workspace can be divided in two main regions depending on the arm configuration, as shown in Fig. 4.6 and referred to as *inner-arm* and *outer-arm* configuration.

The commutation between the inner and outer arm configuration is achieved by using one of the buttons of the Phantom device: during switching operations the

three central joints of the arm invert their angle reference with respect to the z axis before returning the control to the master. The workspace mapping of the arm applied in inner-arm configuration has the y axis reversed to provide a more intuitive interface for the operator. In addition, a generic point in the workspace can be reached in both elbow-down and elbow-up configuration.

4.4 Experimental results

In this section, some experimental tests performed on the system described in Sec. 4.3 are introduced and discussed. The results are related to a generic grasping task characterized by two phases. In the first phase, the slave robot is used to grasp an object initially located inside its arm workspace. The grasping action is properly performed by means of the position-position control of the slave's arm, while the master end-point never leaves the grasping area (inner area). In the second phase the slave robot attempts to place the grasped object far away from the current slave workspace, implying a transition from the grasping area to the navigation area of the master end-point and the resulting movement of the mobile platform. Three specific aspects of the task are discussed and analyzed:

- The position-position mapping between the master and the slave arm during the initial grasping action;
- The position-position mapping between the master and the slave arm while the master goes through the transition area;
- The overall behavior in terms of master arm position, slave arm position and mobile platform velocity while passing through the three control regions.

Considering the physical dimensions of the Kuka youBot arm used for the experiment, it follows the first numerical parameter defined, that is: $R_s = 0.5\ [\ m\ ]$ With regards to eq. 4.1, and given the desired scaling factor $\delta \simeq 7$, it follows:

$$R_o = \frac{R_s}{\delta} = 0.0714 \simeq 0.07\ [m] \tag{4.11}$$

Following the general procedure described in Sec. 4.2, the corresponding chosen parameters are listed in table 4.1 The value $\delta = 7.14$ represents a good trade-off between the necessity to have good accuracy while operating in the grasping

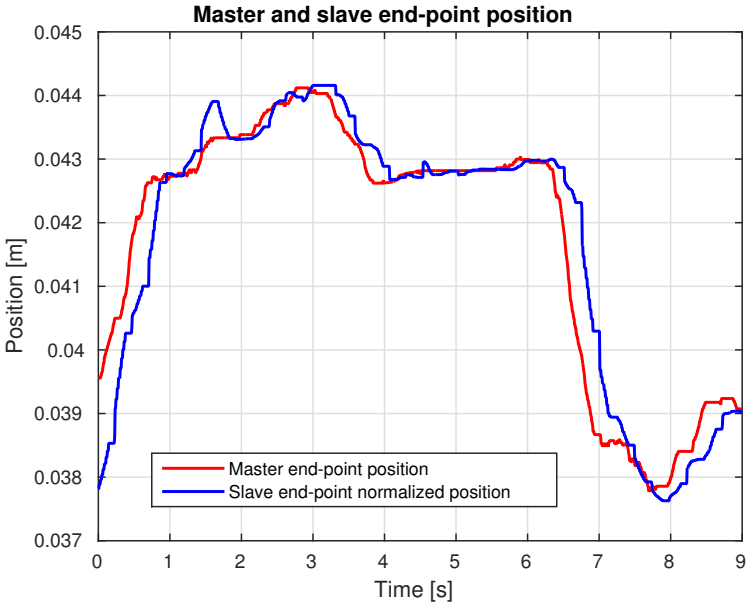

FIGURE 4.7: Master and slave position tracking along x.

TABLE 4.1: Design parameters

Variable	Value	Unit	Variable	Value	Unit
R_m	0.1	[m]	δ	7.14	
R_s	0.5	[m]	R_i	0.05	[m]
R_o	0.07	[m]	V_{max}	0.8	[m/s]

area in a position-position control and the need to equally partition the master workspace between the three control regions.

4.4.1 The grasping task

The grasp of the object is performed inside the inner spherical region of the master device, the grasping area. This region is characterized by a constant scale factor δ and zero velocity for the mobile platform. Fig. 4.7 shows the position tracking of the slave arm's end-effector with respect to the master device's end-point along x. The slave position has been divided by $\delta = 7.14$ in order to normalize its value to the master position scale.

The graph refers to the object's approach and grasping phase and highlights the proper tracking of the slave end-effector despite the presence of a time delay of about 0.2 s between master acquisition and slave execution. This delay can be explained considering the non-real time control environment provided by ROS and the wireless communication channel between the master and the slave devices.

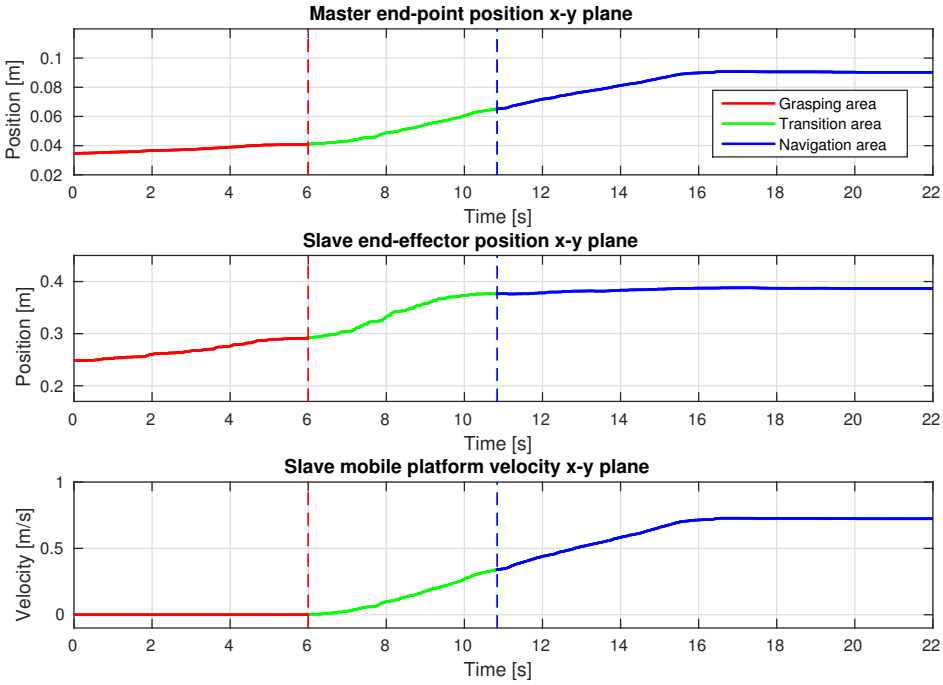

FIGURE 4.8: Master and slave position and mobile platform velocity through the three control regions.

4.4.2 Overall behavior through the three control regions

In order to map the whole velocity range of the slave mobile platform in the whole position displacement achievable by the master end-point in the navigation area, the numerical value of K_v needs to be computed with respect to the specific setup used in the experimental tests. Referring to eq. 4.4 we obtain:

$$K_v = 16$$
$$V_{max} = 0.8 \ [m/s]$$
$$R_i = 0.05 \ [m]$$

where V_{max} is the maximum linear velocity achievable by the Kuka youBot omnidirectional platform and R_i has been chosen as a good trade-off between the percentage of slave arm workspace mapped with direct position-position proportionality and the need to avoid singularity configuration. Figure 4.8 refers to the second phase of the experimental tests (i.e. after the grasping action) in which the robot attempts to place the grasped object outside the current slave workspace. The graphs show the projection of the Cartesian 3-dimensional position p_m, p_s in

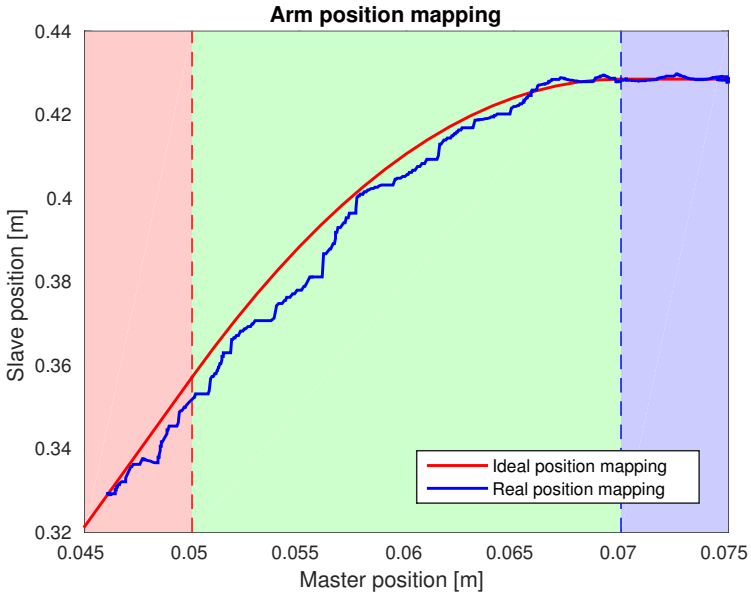

FIGURE 4.9: Master and slave mapping across the transition area. From the left side: grasping, transition and navigation area.

the x-y plane and the mobile platform velocity $V_{xy} = \sqrt{\dot{x}^2 + \dot{y}^2}$ for both the master and the slave robot. The master's end-point position is referred to a reference frame placed in the center of its workspace, the slave's end-effector position is instead referred to the arm's base link reference frame. The figure highlights the effectiveness of the overall arm/base coordination in response to the movement of master end-point. When the master enters the transition area (green line) the slave arm slows down progressively while the base velocity linearly increases. In the end, in the navigation area (blue line), the slave end-point's distance from the $x - y$ origin does not increase anymore and the master displacement is totally mapped in velocity commands for the mobile base, which reaches its maximum speed at the borders of the master workspace.
It is important to notice that the orientation of the slave arm with respect to the mobile base frame keeps changing in order to preserve the position tracking with the master arm when the latter is located in the navigation area. For this reason the slave arm always indicates the direction of motion of the mobile base.

4.4.3 Master/Slave position mapping in the transition area

Figure 4.9 shows the position mapping between the master and the slave device during the transition phase between the grasping and the navigation area. It has been obtained through the comparison of the distances of the master and the slave end-points from the origin of their main reference frame respectively, in each time

instant of the performed task.
The red curve in the graph represents the ideal trajectory generated by the control scheme, while the blue one is obtained from the data measurements. It can be seen that a satisfactory tracking of the desired reference is achieved by the system: the final position reached by the arm is the desired value (far away from singular configurations).

Chapter 5

Design of the UBHaptic

5.1 Motivation

As already mentioned in Chapter 2, a teleoperated robotic system consists of a slave robot remotely controlled by means of an haptic interface, usually referred to as *master device*.
The most common application areas of such systems include space and underwater exploration, mining, surveillance, rescue, surgery and all those application, involving remote interactions, in which is requested to perform and accomplish complex, uncertain tasks in hazardous, dangerous or unstructured environments. Most of this scenarios require the availability of adequate haptic interfaces able to provide the operator a feeling of *telepresence* [7].
Such a system, extends the human capability of interacting and manipulating objects from a remote location by providing kinesthetic sensations to the human operator (commonly force feedback).
Besides the commercial solutions available on the market, many researchers have proposed haptic devices using serial and parallel mechanisms. Both commercial and research devices have been previously discussed in Sec. 2.4.
The cost of standard commercial haptic devices characterized by serial kinematic chains is usually high because of the complex mechanical structure. Other drawbacks of such configurations are high inertia and reduced workspace. In most cases master devices are too heavy and not manipulable enough to allow effective usage [100]. Ideally a master device is supposed to have very low inertia while maintaining the ability to behave very stiffly, allowing a realistic reconstruction of the forces experienced by the slave robot.

In this chapter, the design concept of a new cable-driven haptic interface is proposed. The haptic device, whose name *UBHaptic* stands for *University of Bologna HAPTIC*, is based on Twisted String Actuation (TSA). The TSA [108, 109] represents a very interesting solution for the implementation of very compact, lightweight and low cost linear transmission system for highly-integrated mechatronic devices, such as haptic interfaces.
The proposed haptic interface, which conceptual design is reported in Fig. 5.3, is driven by four TSA modules arranged on the vertex of a tetrahedron, as depicted in Fig. 5.5, allowing to render linear forces along the 3 dimensions of the Cartesian space.
The chapter reports the analysis of the kinematics and force distribution of the proposed device. Moreover, the system design procedure is illustrated by means of simulations, providing the locations, force and displacement the actuators should provide given the desired workspace dimension and the minimum force level the interface must render. To the best of the author's knowledge this is the first attempt of using twisted string actuation in the design of a force reflection haptic devices.
The work has been presented at the *International Conference on Advanced Intelligent Mechatronics* (AIM 2017, Munich, Germany) [110].

5.2 Basic principles of TSA actuation

The basic principle of the TSA is an amazingly simple concept that has been known and used for thousands of years. The basic idea is illustrated schematically in Fig. 5.1: a couple of strings connected to a rotative DC motor to twist them on one end, while on the other end the strings are attached to a linear moving element, i.e. the load. The string twisting produced by the electrical motor reduces the overall string length, thus the rotative motion of the electric motor is converted to a linear motion on the other side of the strings [108].
This actuation concept, because of its high (though configuration dependent) reduction ratio, permits the use of very small, lightweight and low power electric motors and, therefore, is very interesting in applications where size and weight are of crucial importance as well as anywhere it's necessary to produce very cheap form of linear motions.
TSA has been already successfully used for the implementation of different robotic devices like anthropomorphic hands and elbows (see [111]): strings do not take up much space, and they work just like muscles and tendons do in the human body.

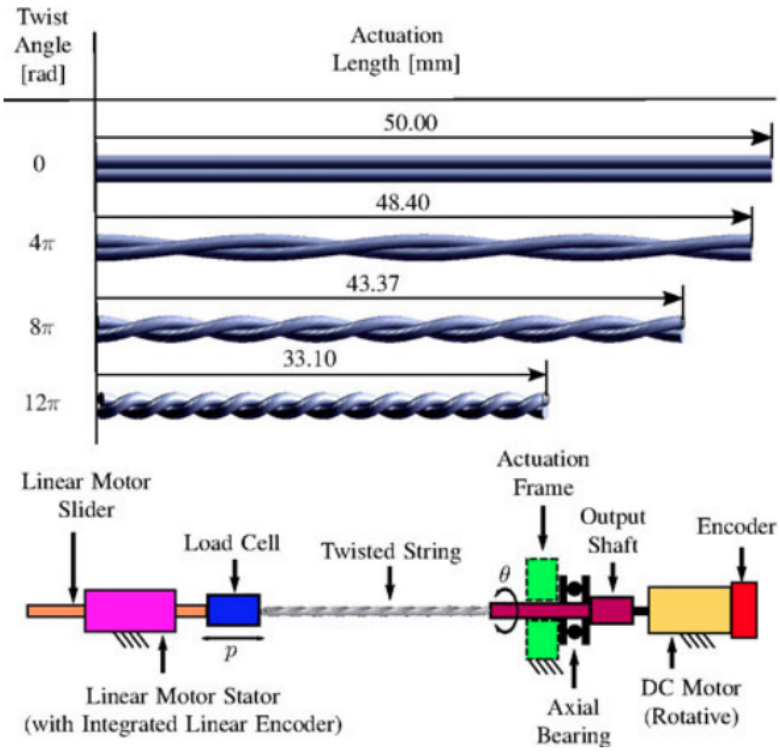

FIGURE 5.1: (Top) Basic concept and (Bottom) schematic representation of the twisted string actuation system.

Probably the most-experienced project regarding the application of TSA in real robotic systems is the European project *DEXMART* [112], in which the LAR lab of the University of Bologna was strongly involved. The main idea behind the project was to use twisted strings to actuate the fingers of a anthropomorphic robotic hand. Fig. 5.2 shows the DEXMART Hand: a total of 24 actuation units were implemented to actuate the five fingers and the wrist.

Other interesting uses of TSA include exoskeletons [113] and tensegrity robots for space applications [114]. A TSA actuation module for robotic hands is presented in [115], while applications on wearable assistance devices can be found in [116].

5.3 System design

The main idea is to design an haptic interface able to move freely in the six-dimensional space (3 linear translations plus 3 orientations) under the intention of the operator and at the same time apply reaction forces in the Cartesian space along the three linear directions *x-y-z*. The device, shown in Fig. 5.3, can be used as mean to control a remote robotic device at a distance and feed the interaction forces acting on the the telemanipulated robot directly to the user's wrist. The

FIGURE 5.2: The 5-fingers DEXMART anthropomorphic hand based on TSA.

connection between the haptic device and the human is implemented by means of a bracelet that is fasten to the user forearm (see Fig. 5.4).

A set of three gimbals, one mounted on the other with orthogonal pivot axes forming a Cardan suspension, are driven by four cable-based actuators, see Fig. 5.5, allowing the user to change freely the orientation of the forearm without affecting the force exerted by the actuators along the linear directions of the Cartesian space. In the following, we will refer to this mechanical interface as the *mobile frame*.

TSA modules, integrating in a very compact space an high speed-low torque DC motor with incremental encoder and a force sensor, are adopted in order to minimize the complexity and the cost of the device. TSA closed loop position and force control are implemented in the module embedded controller discussed in chapter 6. Being the device driven by means of cables, a minimum number of $n+1$ actuators is necessary to control motion and forces in a n-dimensional space. Therefore, being interested in controlling only linear movements, four actuators are needed. The actuators are arranged on the fixed frame, while the strings are connected between the output shafts of the TSA modules and the anchoring points on the mobile frame.

To allow the motor module to be always aligned with the fixing points on the

FIGURE 5.3: 3D CAD rendering of the proposed haptic interface.

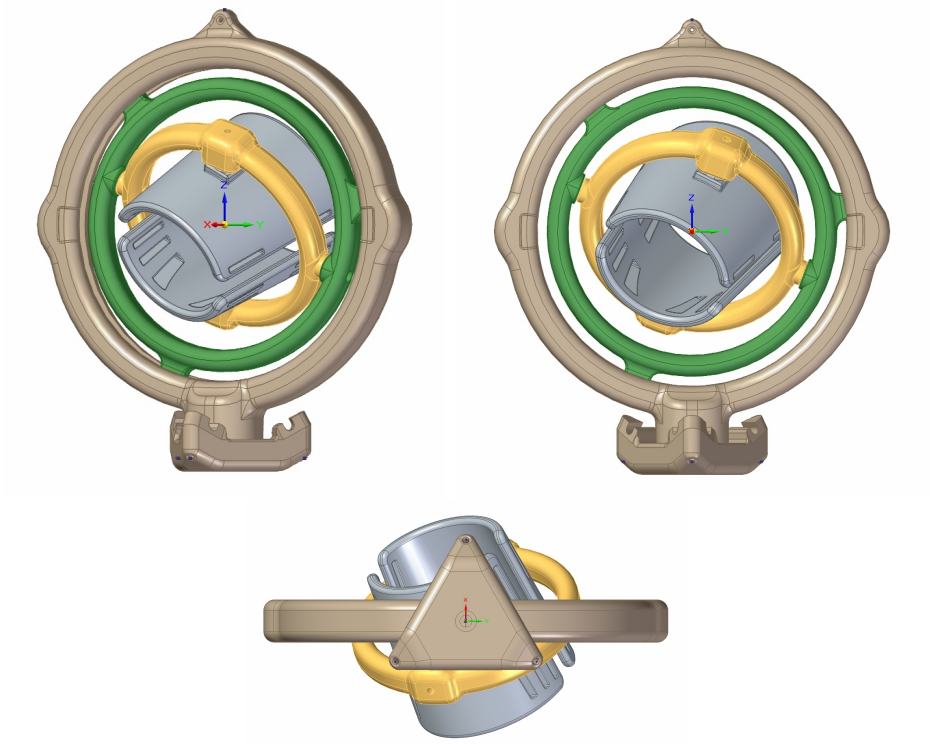

FIGURE 5.4: Different 3D views of the Human-Machine Interface.

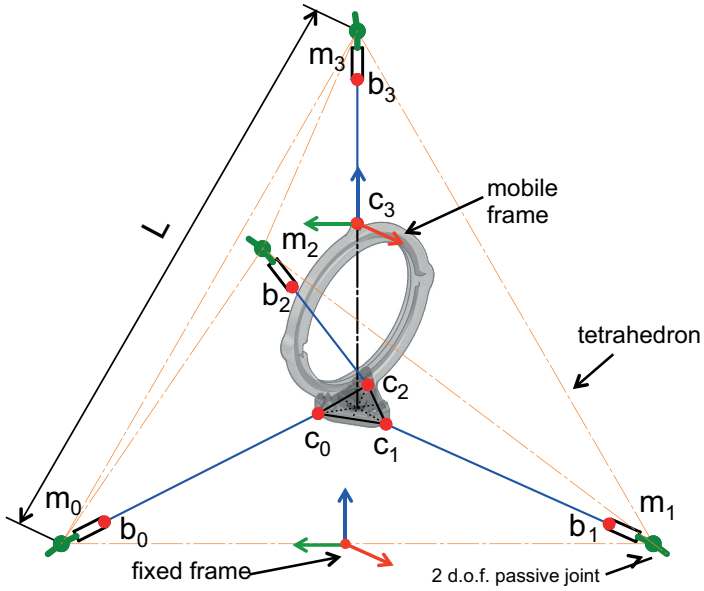

FIGURE 5.5: Schematic view of the haptic interface and actuators arrangement.

frame and the corresponding point on the mobile frame, a *universal joint* has been used to fix the TSA modules to the frame.

5.4 Kinematic model of the haptic interface

The workspace reachable by the mobile frame depends on the relative location of the TSA anchor points on both the fixed and the mobile frame. As a natural choice for achieving a symmetric behavior of the interface in resting conditions, the TSA modules are arranged on the vertices of a regular tetrahedron (i.e. having all the edges with the same length), as depicted in Fig. 5.5. This choice allows to optimize the haptic interface in terms of workspace and generated forces by using a simple geometrical formulation. It is straightforward to note that in case the actuators are ideally connected at the center of the mobile frame (as shown in Fig. 5.7(b)), the reachable workspace would be the entire volume of the tetrahedron itself. Although this solution is very interesting because the tension of the strings would not generate any torque on the mobile frame, due to the practical implementation needs, it is not feasible, since the mobile frame has to hold at its middle the forearm. Therefore the anchor points need to be shifted away from the single point configuration. The solution proposed is to shift down the three connection points corresponding to the ones of the base of the tetrahedron. A schematic view of the anchoring points on the mobile and fixed frame is shown in Fig. 5.5.

In order to compute the kinematic model of the proposed haptic interface, it is

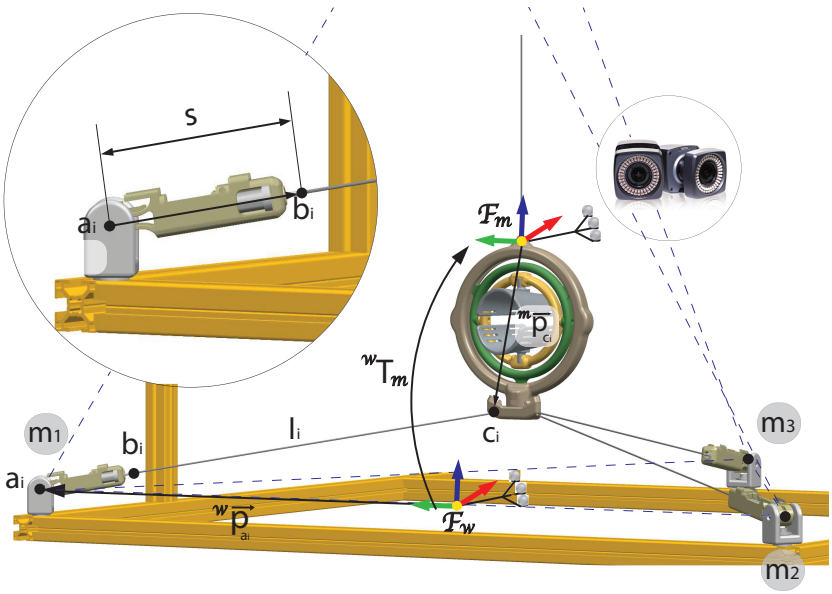

FIGURE 5.6: Kinematics of the haptic interface.

assumed that all the strings are always properly tensioned by minimum strictly positive forces. We define the points $\mathbf{a_i}$, $\forall i \in 0, \ldots, 3$, as the intersection of the two orthogonal axes of the universal joint used to fix the TSA module on the frame. The points $\mathbf{b_i}$, $\forall i \in 0, \ldots 3$, represent the connection points of the string on the TSA modules. The points $\mathbf{c_i}$, $\forall i \in 0, \ldots, 3$, are the anchor points of the strings on the mobile frame. Therefore the string of the i-th TSA module goes from the $\mathbf{b_i}$ to the $\mathbf{c_i}$ point. With reference to Fig. 5.6, a workspace reference frame $\mathcal{F}_w$ is defined with the origin placed at the midpoint of the segment connecting the TSA modules $\mathbf{a_0}$ and $\mathbf{a_1}$ and its x-y plane including the three TSA modules $\mathbf{a_0}$, $\mathbf{a_1}$ and $\mathbf{a_2}$ placed in the vertices of the tetrahedron's base. A mobile reference frame $\mathcal{F}_m$ fixed with the outer gimbal is also defined. Since both these frames are marker-based, the pose of the latter reference frame with respect to the former is known and given by the transformation ${}^w\mathbf{T}_m$ provided by the motion tracking system. The coordinates of the connection points $\mathbf{c}_i$, $\forall i \in 0, \ldots, 3$ with respect to the workspace frame can be expressed as:

$$ {}^w\mathbf{p}_{c_i} = {}^w\mathbf{T}_m \, {}^m\mathbf{p}_{c_i} = [\, {}^w x_{c_i} \;\; {}^w y_{c_i} \;\; {}^w z_{c_i}] \tag{5.1} $$

with ${}^m\mathbf{p}_{c_i}$ being the fixed positions of the $\mathbf{c_i}$ points expressed in $\mathcal{F}_m$ and obtainable form the CAD model of the wearable interface. The known fixed coordinates of the anchor point $\mathbf{a}_i$, $\forall i \in 0, \ldots, 3$ of each TSA module with respect to the workspace frame $\mathcal{F}_w$ are named ${}^w\mathbf{p}_{a_i} = [\, {}^w x_{a_i} \;\; {}^w y_{a_i} \;\; {}^w z_{a_i}]$.

Given the formula of the distance between two points in the 3D space considering

points $\mathbf{c}_i$ and $\mathbf{a}_i$, and taking into account the length of TSA module body s, the length of the i-th string l_i is expressed as:

$$l_i = |\,{}^w\mathbf{p}_{c_i} - {}^w\mathbf{p}_{a_i}| - s \tag{5.2}$$

Specializing eq. (5.2) for each of the four strings the *inverse kinematic model* is obtained. The vector $\mathbf{l} = [l_0\ l_1\ l_2\ l_3]^T$ is the vector of the string lengths and can be considered as the joint position vector of the haptic interface.
Although the *direct kinematic model* can be derived by inversion of eq. (5.2) (which presents a unique solution as long as we consider only positive z coordinates), the computation a closed form direct kinematic expression is not needed since the end-point position will be estimated by the motion tracking system.
The computation of the Jacobian matrix is straightforward if the unit vectors associated with each of the four string are considered:

$$\hat{\mathbf{v}}_i = \frac{\mathbf{v}_i}{|\mathbf{v}_i|} = ({}^w\mathbf{p}_{c_i} - {}^w\mathbf{p}_{a_i})\,\frac{1}{l_i} \tag{5.3}$$

where l_i are computed from eq. (5.2). Specializing eq. (5.3) for each string the four unit vectors, $\hat{\mathbf{v}}_0, \hat{\mathbf{v}}_1, \hat{\mathbf{v}}_2, \hat{\mathbf{v}}_3$ are obtained.
The tensions t_i along the strings are then projected by the unit vectors $\hat{\mathbf{v}}_i$ into a 3D Cartesian force $\mathbf{f}$ acting on the bracelet:

$$\mathbf{f} = t_0\,\hat{\mathbf{v}}_0 + t_1\,\hat{\mathbf{v}}_1 + t_2\,\hat{\mathbf{v}}_2 + t_3\,\hat{\mathbf{v}}_3 = (\mathbf{J}^T)^\dagger\,\mathbf{t} \tag{5.4}$$

where $(\mathbf{J}^T)^\dagger = [\hat{\mathbf{v}}_0\ \hat{\mathbf{v}}_1\ \hat{\mathbf{v}}_2\ \hat{\mathbf{v}}_3]$ and $\mathbf{t} = [t_0\ t_1\ t_2\ t_3]$. The *Jacobian matrix* $\mathbf{J}$ relates the linear 3D velocity of the end-point in the workspace $\dot{\mathbf{x}}_w$ to the actuator contraction velocities $\dot{\mathbf{l}}$

$$\dot{\mathbf{x}}_w = \mathbf{J}\,\dot{\mathbf{l}} \tag{5.5}$$

therefore given a desired force $\mathbf{f}$ the corresponding vector $\mathbf{t}$ of actuation forces is computed as:

$$\mathbf{t} = \mathbf{J}^T\,\mathbf{f} \tag{5.6}$$

where $\mathbf{J}^T$ is computed in eq. (5.4) and the suffix † denotes the *Moore-Penrose pseudoinverse* of a matrix.
It is important to note that, since we are dealing with cable-driven transmissions, only traction forces are allowed (i.e. the strings can only pull). It is then necessary to generate only $t_i \geq 0$. Equation (5.6) does not guarantee that this constraint is

met since the solution for a given desired $\mathbf{f}$ produces a minimum module tensions vector $\mathbf{t}$ with, in general, components $t_i < 0$ as well. For this reason, from a control strategy point of view, it is convenient to modify eq. (5.6) into the following:

$$\begin{aligned} \mathbf{t}^\star &= \mathbf{J}^T \mathbf{f} \\ \mathbf{t} &= \mathbf{t}^\star + \lambda \mathbf{t}^\gamma \end{aligned} \tag{5.7}$$

where $\mathbf{t}^\gamma$ is a base of the null space of $(\mathbf{J}^T)^\dagger$ and $\lambda \in \mathbb{R}$ is chosen in order to impose the strings tensions above a certain threshold $\mathbf{t}^0$ as follow:

$$\lambda = \max_{i \in \{0,..,3\}} \frac{\mathbf{t}_i^0 - \mathbf{t}_i^\star}{t_i^\gamma} \tag{5.8}$$

where t_i^γ is the i-th component of $\mathbf{t}^\gamma$. The term $\lambda \mathbf{t}^\gamma$ of eq. (5.7), being a vector $\in \ker (\mathbf{J}^T)^\dagger$, do not produce any additional Cartesian force $\mathbf{f}^\gamma$ on the bracelet while ensuring vector $\mathbf{t}$ of strings tensions to be always positive [117].

5.5 Device dimensioning

5.5.1 Workspace sizing

Due to the tetrahedral spacial arrangement of the TSA modules, it is straightforward to understand that singular configurations of the overall parallel mechanism occur when an anchor point reaches one of the faces of the tetrahedron. With respect to Fig. 5.7 a spherical region $\mathcal{S}_{R_1}$ of radius R_1, with origin in the tetrahedron's centroid, is defined as the desired workspace in which the bracelet's center must freely move avoiding singular configurations. In order to simplify the analysis, a second sphere $\mathcal{S}_{R_2}$ is defined with origin in the bracelet's actual position and whose radius depends on the mechanical design of the bracelet itself by the relation:

$$R_2 = \max ||^m \mathbf{p}_{c_i}|| \tag{5.9}$$

where $^m\mathbf{p}_{c_i}$ are the fixed position of the anchor points expressed in the mobile frame $\mathcal{F}_m$. Eq. 5.9 ensures that all the anchor points $\mathbf{c}_i$ are enclosed within $\mathcal{S}_{R_2}$. The radius R_3 of the maximum sphere $\mathcal{S}_{R_3}$ inscribed in the tetrahedron and tangent to its faces can be then computed. The side of the tetrahedron, which

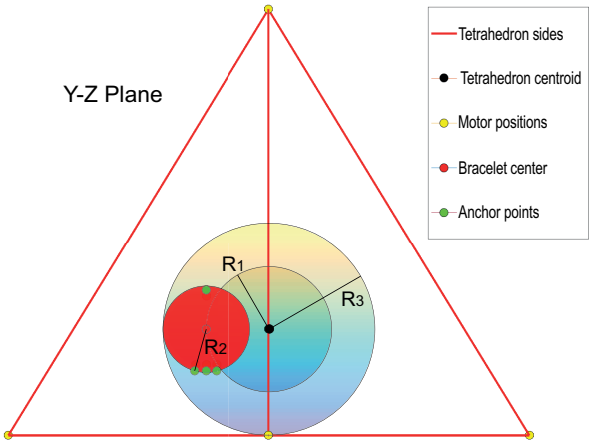

(a) Conceptual scheme used for dimensioning the geometric parameters of the device.

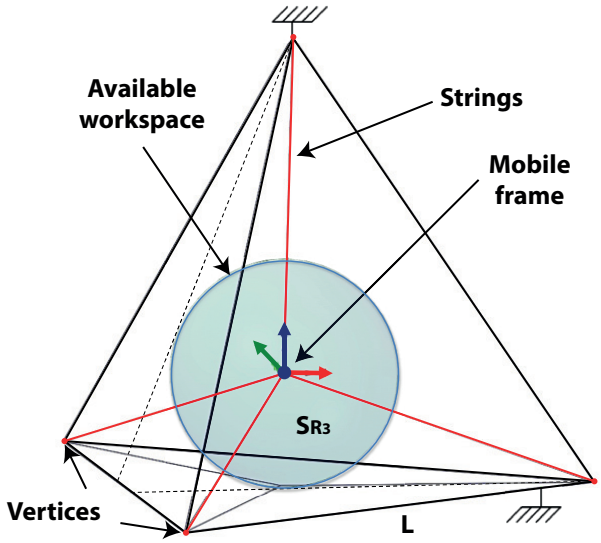

(b) 3D view of the available workspace defined as the maximum sphere $\mathcal{S}_{R_3}$ inscribed in the tetrahedron and tangent to its faces.

FIGURE 5.7: 2D and 3D views of the available workspace of the haptic interface.

determines the total encumbrance of the device is related to R_3 by the following:

$$\begin{aligned} R_3 &= R_1 + R_2 \\ L &= \tfrac{12}{\sqrt{6}} R_3 \end{aligned} \tag{5.10}$$

Table 5.1 summarizes the design parameters of the proposed haptic interface.

TABLE 5.1: Design Parameters

Variable	Value
R_1	0.2 [m]
R_2	0.1062 [m]
R_3	0.3062 [m]
L	1.5 [m]

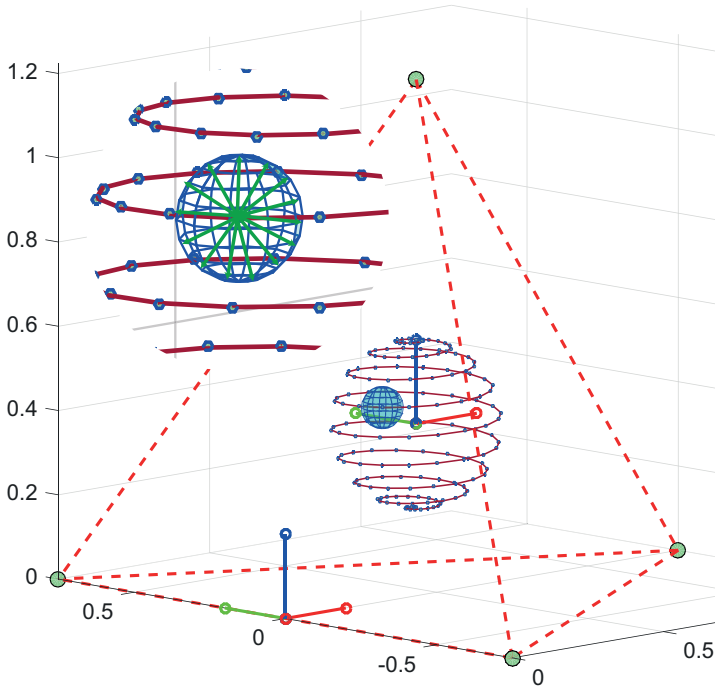

FIGURE 5.8: Sampling of the workspace surface $\mathcal{S}_{R_1}$.

5.5.2 Actuation and transmission sizing

The actuators specifications in terms of maximum force and requested contraction are defined according to the desired forces the haptic device is requested to apply to the user wrist and the workspace dimensions defined in Sec. 5.5.1.
To this end, the kinematic model described in Sec. 5.4 has been implemented in Matlab and used to analyze the actuation requirements over the whole workspace of the haptic interface. It is assumed that in every point of the desired workspace, the system must be able to apply a minimum force of 20 N in every directions. Adopting spherical coordinates the workspace surface $\mathcal{S}_{R_1}$ has been discretized in a finite number of points $\mathcal{P}$ evenly distributed as shown in Fig. 5.8. An analog operation has been done for the three-dimensional force space. The surface of a

sphere with radius 20 N has been discretized in a finite number of points and a set of force vectors $\mathcal{F}$ is computed by connecting the origin of the sphere with the points of the sphere surface (see the magnification of Fig. 5.8).
The algorithm implemented, to determine the size of the actuators, iteratively evaluates each point of $\mathcal{P}$ by computing the lengths of the strings as defined by eq. 5.2 and $(\mathbf{J}^T)^\dagger$ as defined by eq. 5.4. At each iteration, for each force vectors belonging to $\mathcal{F}$, the tendons tensions are computed by means of eq. 5.7. With the assumptions made in Sec. 5.5.1, the behavior becomes critical when the mobile frame is placed to the lower region of the workspace, i.e. $\mathbf{c}_0$, $\mathbf{c}_1$, $\mathbf{c}_2$ are close to $\mathcal{S}_{R_3}$. As shown in Fig. 5.9(a) the string tensions required to generate the set of desired forces $\mathcal{F}$ reaches maximum values much higher than any other region of the workspace ($\approx$ 250 N). A possible solution to mitigate this effect could be to move upwards (positive direction of the z-axis) the origin of $\mathcal{S}_{R_1}$. Running the algorithm recursively we found that an height z=h/3 leads to a uniform distribution of the tendon tensions along the entire set of configurations evaluated as shown in Fig. 5.9(b), which means that singularities are faraway from the workspace considered. It is worth to note that a minimum force of 1 N has been considered to keep a minimum tension on the tendons. Analyzing the results it is easy to conclude that TSA modules with maximum force of 80 N will fulfill the Cartesian force requirements of the proposed haptic interface.
Fig. 5.10 shows the evolution of the tendon lengths within the set of points $\mathcal{P}$. The maximum values for the four tendons lengths are $[0.9693, 0.9687, 0.9701, 0.8050]$ m while the minimum are $[0.3983, 0.3985, 0.3971, 0.4]$ m. A maximum linear displacement equal to the 40% of the untwisted length guarantees that the relation between the twisting angle of the motor shaft and the linear displacement can be accurately predicted and fatigue effects can be avoided [108]. The values computed by means of the simulation are within this working region and therefore the actuation parameters assumed can be considered suitable for further development steps.

5.6 The TSA module

A schematic view of the first version of TSA module that has been designed for the implementation of the proposed haptic interface is represented in Fig. 5.11. It is composed, from left to right, by: i) a connection element to connect the module to the supporting frame; ii) the force sensor to measure the actuation load; iii) a

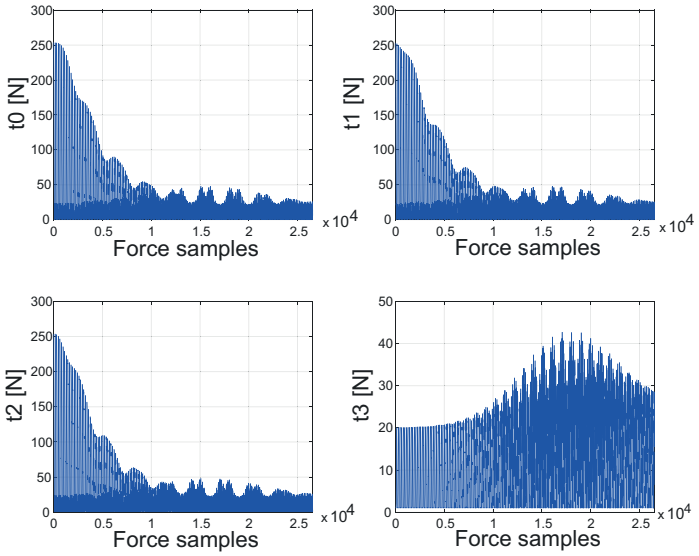

(a) String tensions in the case of $\mathcal{S}_{R_1}$ centered in the tetrahedron centroid.

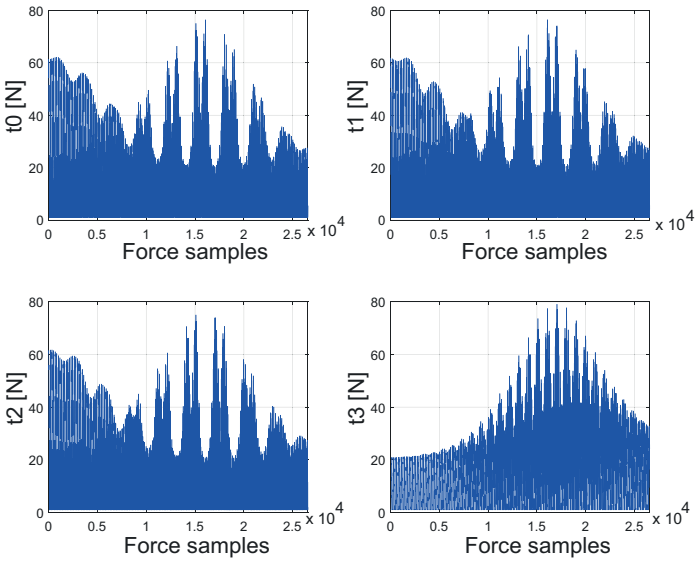

(b) String tensions in the case of $\mathcal{S}_{R_1}$ is lifted to $z = h/3$.

FIGURE 5.9: Result of the sizing simulation

frame hosting the DC motor, the output shaft where the twisted strings are connected and all the electronics; iv) the twisted string itself connecting the motor module with the load, and the load itself represented as a translating mass.
Figure 5.12 reports a detailed 3D view of the TSA module design [118] and [119]. The frame structure is manufactured in ABS plastic [120] by 3D rapid prototyping.

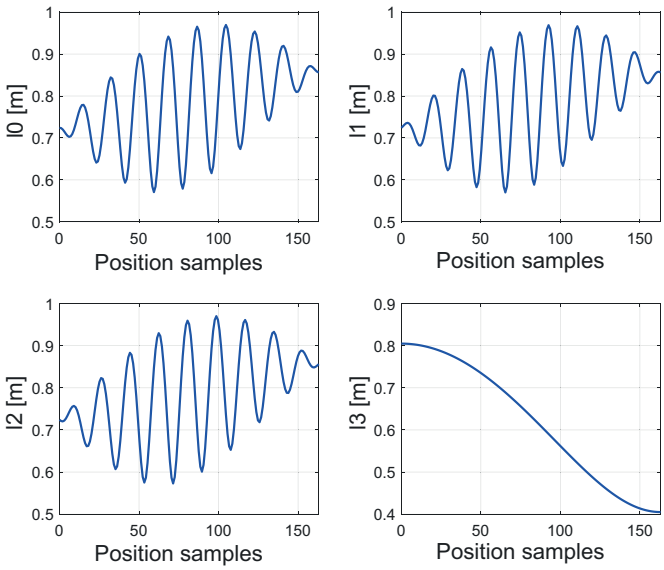

FIGURE 5.10: Result of the simulation with respect to the strings lengths.

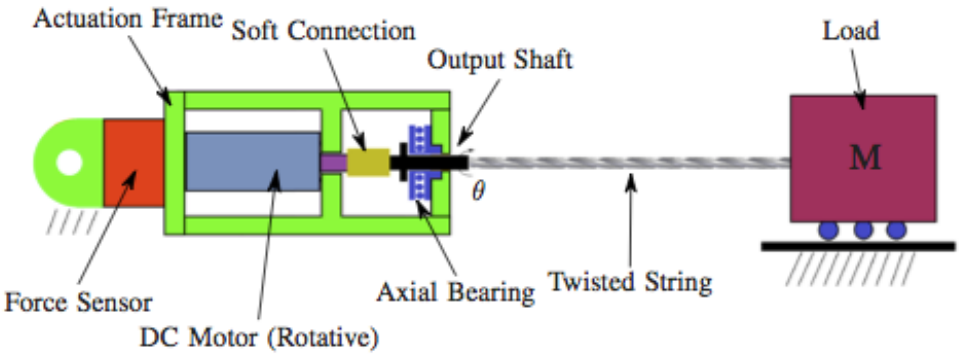

FIGURE 5.11: Schematic representation of the TSA structure.

In the first version it was created, the TSA was composed of a pair of axial-symmetric compliant beams that act as a linear spring, providing to the structure a certain compliance for the implementation of the force sensor. An optoelectronic device is used to detect the frame deformation and convert it back to the applied force. As can be seen in Fig. 5.12, a DC motor equipped with an incremental encoder for angular position sensing is embedded in the module, while the output shaft is supported by an axial bearing at the point of the twisted string connection to both reduce the friction and prevent the transmission force from damaging the motor. A silicon tube is used to connect the transmission shafts and the DC motor in order to solve problems regarding misalignment of the rotational axes of the motor and the module output shaft. The designed TSA module permits the transmission force to be entirely supported by the output shaft through the

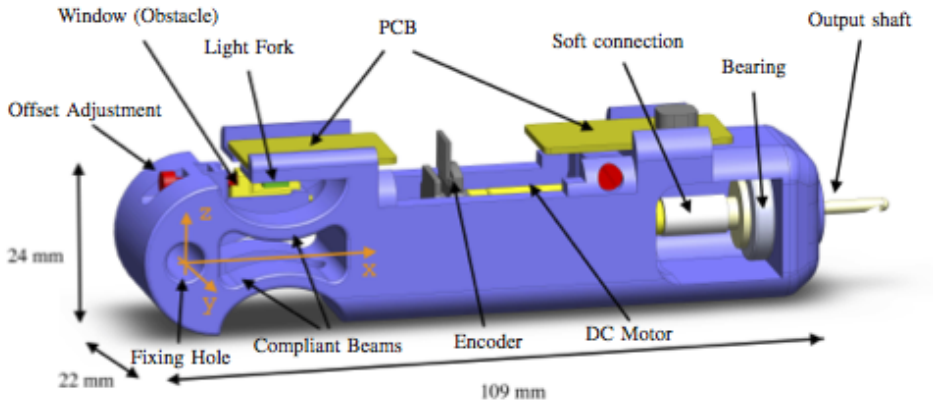

FIGURE 5.12: Design detail of the first version of the TSA module.

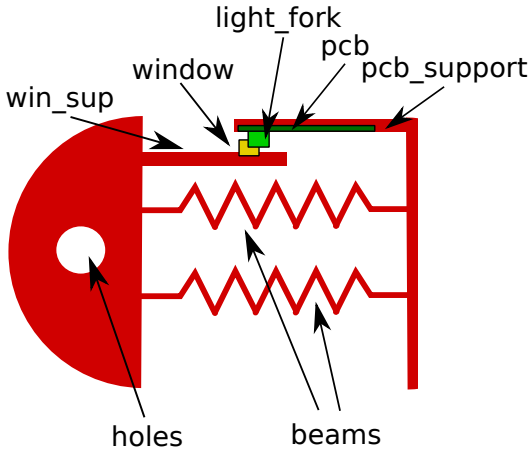

FIGURE 5.13: Scheme of the sensor structure and component arrangement.

combined bearing, while the motor is only used to transmit the necessary torque for driving the twisted string actuation to the output shaft. Figure 5.13 represents the basic concept of the force sensor being mounted in the TSA module. This sensor is crucial to successfully measure the force the actuator applies to the load (see [119]). The main concept is to have a LED illuminating a photodiode (PD), where the current flowing through the PD can be modulated by means of a mechanical component that partially intercepts the light emitted by the LED. The position of the mechanical component depends on the deformations occurring on the sensor's body as a consequence of the application of an external force. As can be seen in Fig. 5.12, the force sensor is located between the frame connection point on the robot structure and the frame hosting the DC motor, i.e. on the opposite side of the twisted strings with respect to the rotative motor.

Figure 5.14 depicts the TSA module embedded controller based on an Arduino NANO board. The actuator electronics provide a digital interface for input and output signals required for the actuation system control, including both the motor

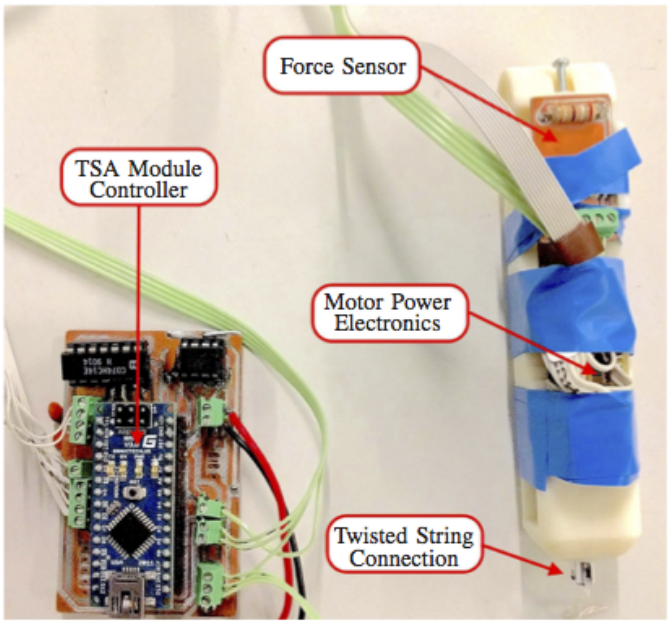

FIGURE 5.14: Detailed view of the TSA module prototype and control electronics.

power electronics, the conditioning system for both the force sensor and the encoder and a microcontroller board for controlling the TSA module, see Fig. 5.14. The communication between the TSA controller and the external system can be implemented with either UART, SPI or I2C interfaces.

5.7 Real setup

The first prototype of the HMI, described in Sec. 5.3, which implements the physical connection between the haptic device and the user forearm is shown in Fig. 5.15. It has been realized with ABS using 3D printing technologies. The user can insert and fix the forearm to the inner ring which allows to change freely the orientation of the forearm without affecting the orientation of the outer ring.
As shown in Fig. 5.15 five reflecting markers has been fixed on the outer ring allowing the the definition of the *mobile frame* needed to compute the kinematic model discussed in Sec. 5.4. In particular the *Jacobian* matrix (necessary to link a desired 3D Cartesian force in the workspace with the corresponding string tensions) is a function of the state vector q (i.e. the vector of the stings length) which depends on the relative position between $\mathcal{F}_w$ and $\mathcal{F}_m$.

With respect to Fig. 5.16 the *workspace reference frame* $\mathcal{F}_w$ is defined with the origin placed at the midpoint of the segment connecting two generic TSA modules and its x-y plane including the three TSA modules placed in the vertices of the

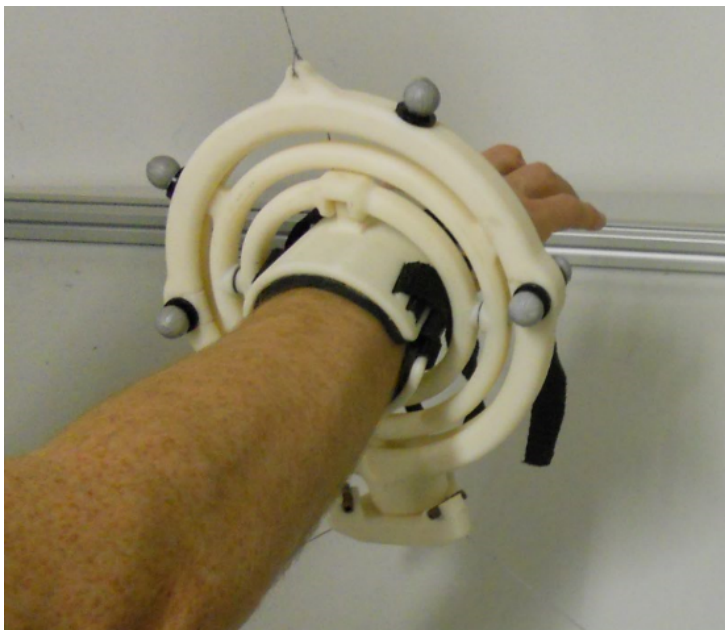

FIGURE 5.15: Prototype of the bracelet-like HMI based on gimbal mechanism.

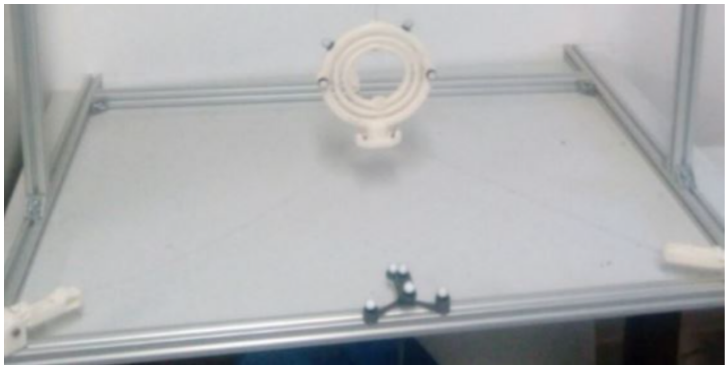

FIGURE 5.16: Arrangment of the *workspace frame* and the *mobile frame* on the haptic device by means of Vicon markes.

tetrahedron's base.

Fig. 5.17(a) and 5.17(b) show the relative position between $\mathcal{F}_w$ and $\mathcal{F}_m$ for a given cartesian pose of the user's wrist in the haptic device's workspace and the corresponding 3D reconstruction given by the visual tracking system.

(a) Real relative pose between the *mobile frame* and the *workspace frame*.

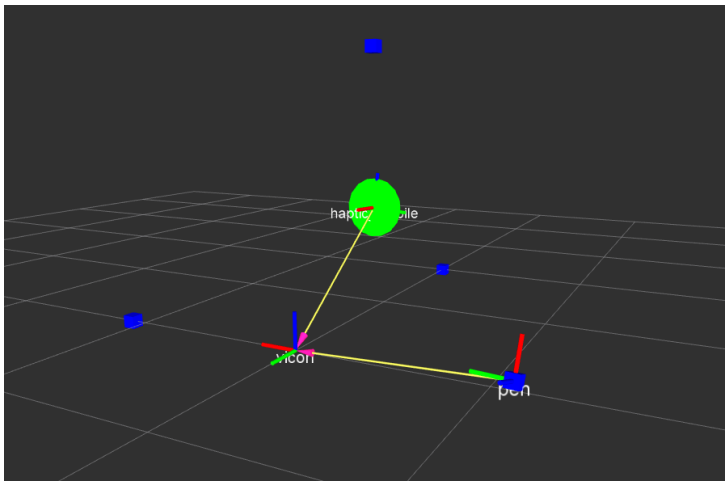

(b) 3D visualization of the *mobile frame* pose with respect to the *workspace frame*.

FIGURE 5.17: *Workspace frame* and *Mobile frame* captured by the Vicon system.

Chapter 6

Design of the TSA Module

6.1 Motivation

The implementation of the TSA actuator reported in this chapter represents the evolution of the previous solution presented in Sec. 5.6. The force sensor was realized by an infrared optical fork mounted on the side of the frame and a window connected to the same side. The fork and the window were fixed to the extremities of two axial-symmetric compliant beams acting as a traction spring. The compliance introduced by the beam allows the relative motion of the two components (fork and window) which is converted back to the force applied to the two extremities of the frame.
During the development of the haptic device described in Chapter 5, the TSA module has shown some critical issues that have pushed to some improvement. First of all, the force sensor based on the compliant beams is quite sensitive to loads misaligned with the x-axis (with reference to Fig. 5.11) which can lead to unpredictable measures in some particular conditions. This effect is amplified by the location of the fork and window with respect to the center of compliance of the beams. Being located at approximately 10 mm on the z-axis, a small torsion along the y-axis leads to a consistent motion on the x-z plane and therefore a significant distortion of the measure. A solution that can mitigate this effect needed to be investigated.
The elastic element has been thought to be produced in one piece with the frame exploiting the capacity of 3D printing technology to realize complex shapes without additional manufacturing effort. On the other hand the parts printed with FDM technology have an uneven distribution of the material which makes difficult to predict precisely the deformation/stress characteristics. With the aim of

having a design that can be simply scaled for different range of measurable force this solution seems to be time consuming since an iterative process of trial and error is needed to reach the desired deformation response to the load of the beams. The TSA module described in this chapter is characterized by integrated force sensor based light forks [121], a DC motor with integrated encoder, embedded microcontroller and power electronics. The custom TSA module controller, developed on purpose for the application, allows position, velocity and force control of the actuators, and provides an Ethernet interface to ease the creation of complex cables actuation networks based on the proposed device (e.g the custom haptic interface presented in Chapter 5).
The TSA module has been evaluated through different experimental tests, presented at the end of this chapter, in which the capability of regulating the force applied on a static load has been evaluated. These tests are particularly significant for the designed system since they involve all the components of the implemented system, i.e. the mechanical design, the force sensor, the custom electronics and the controller. The work is currently under review at the *International Conference on Advanced Intelligent Mechatronics* (AIM 2018, Auckland, New Zealand).

6.2 System description

With respect to Fig. 5.11 the new TSA module with integrated force sensor is composed, from left to right, by: i) a connection element to the supporting frame; ii) the force sensor to measure the actuation load; iii) a frame hosting the DC motor and all the electronics, iv) the output shaft where the twisted strings are connected; v) the twisted string that connects the motor module with the load. Since the twisted string converts the motor rotation into a linear one at the load side, the load is represented as a translating mass.
With respect to solutions presented in Sec. 5.6, the actual design present a number of advantages:

- A more powerful motor is adopted, increasing the module power from 9 to 22W;
- The force sensor is aligned with the twisted string axis to reduce sensitivity to spurious loads;
- Commercial springs are adopted to implement the elastic element to achieve an easy predictable and modular force sensor;

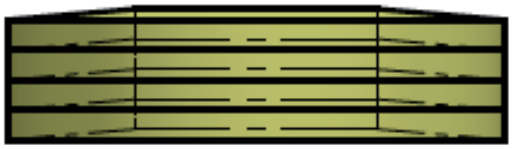

(a) Parallel connection.

(b) Series connection.

FIGURE 6.1: Parallel and series connection of Belleville springs.

- The effect of transversal loads on the complaint elements (i.e. the springs) is annihilated by linear guides embedded into the module structure;
- The firmware running on the TSA controller has been completely redesigned embedding acquisition, control and power electronics with Ethernet interface.

In the following sections, the design of the module components is detailed.

6.2.1 Force sensor

As pointed out in the Sec. 6.2, an important improvement on the TSA module is related to the force sensor implementation. Given the experience acquired during the initial development of the haptic interface described in Chapter 5, the following modifications are introduced:

- The optical force sensor is moved as close as possible to the elastic element center of compliance;
- The motion of the elastic element is mechanically constrained in order to minimize the effect of secondary loads;
- Commercial springs with the desired stiffness characteristics are adopted in order to make the design fully predictable and scalable.

In the solution proposed, the elastic element of the force sensor is implemented by *Beleville springs*. These springs, which shape is schematized in Fig. 6.2, presents

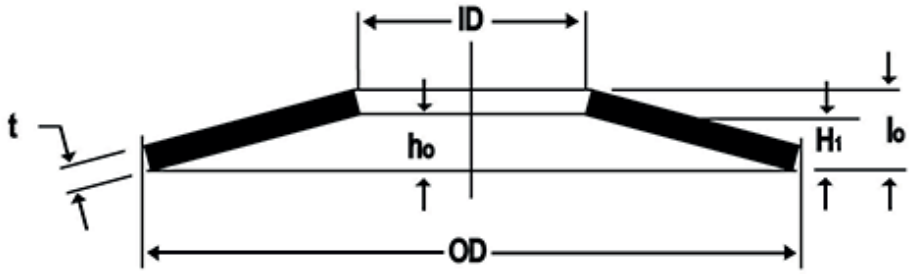

FIGURE 6.2: Main design parameters of a Belleville spring.

a truncated cone shape and can be used for both static and dynamic applications where high loads and relatively small deflections are required. A suitable selection of the mechanical design parameters allows to easily achieve the desired stiffness characteristic. It is worth to notice that these springs can be arranged in stack to implement series and parallel connections by just changing the orientation and coupling among the springs. Springs with opposite cavities, as shown in Fig. 6.1(b), implement a series connection, leading to an equivalent spring with a lower stiffness and larger deflection. In particular, being K_i the stiffness of each spring stacked up in series, the equivalent stiffness of the spring series K_s will result in:

$$\frac{1}{K_s} = \sum_i \frac{1}{K_i} \tag{6.1}$$

Springs stacked up with the same cavity direction, as shown in Fig. 6.1(a), leads to a parallel connection, and therefore to a stiffer equivalent spring K_p equal to the sum of the single spring stiffness K_i:

$$K_p = \sum_i K_i \tag{6.2}$$

To ensure stable working conditions, it is important to mechanically constrain the springs to hold them in position taking into account that, in order to maintain the nominal spring characteristics, a proper clearance has to be guaranteed since, during compression, the spring outer diameter (OD) will increase and the inner diameter (ID) will decrease with respect to their nominal value. The typical materials for the production of this type of springs are steels alloys and plastic. The force sensor, as well as the whole TSA module here presented, are designed according to the requirements of the haptic device described in Chapter 5. In particular, the maximum load expected on the motor module is 80 N.

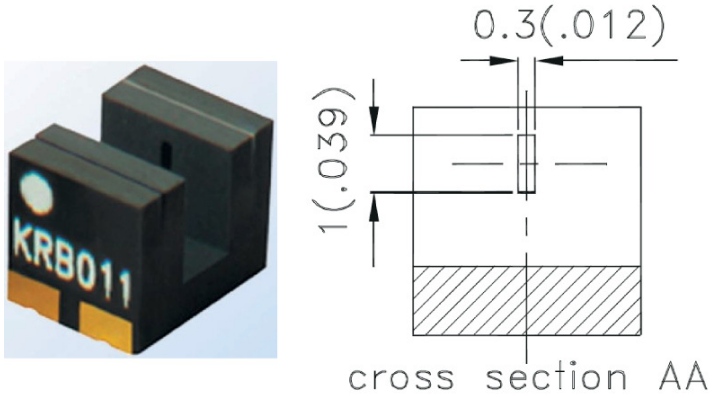

(a) The optical fork KRB011.

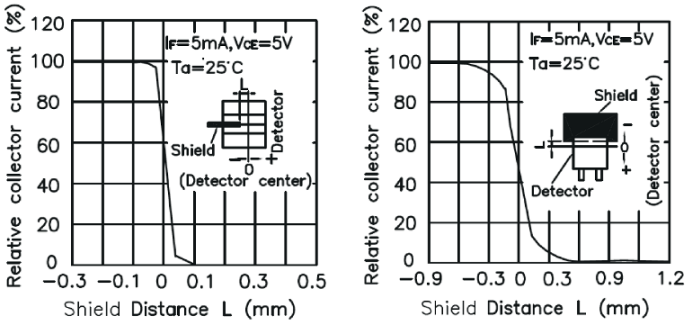

(b) Relative Collector Current vs shield distance in the horizontal and vertical directions.

FIGURE 6.3: Design and characteristics of the light fork KRB011 (from manufacturer datasheet).

The optical component selected to detect the spring deformation is the light fork KRB011, produced by Kingbrigh and shown in Fig. 6.3(a). The component has a fork shape with the infrared emitter placed in front of the detector. It is characterized by a compact footprint of 4x5 mm, and the photo-sensitive region has a rectangular section of 0.3x1 mm. In Fig. 6.3(b) the static characteristics of the collector current (i.e. the output of the sensor) with respect to the distance from the center of an obstacle is given. Note that in the left curve the shield travels horizontally, therefore it spans the 0.3 mm edge of the sensitive area, while the right curve the shield is translated vertically and therefore it spans the 1 mm edge. It is interesting to note that both curves have a linear range centered at the middle of the detector, while the connection with the saturation values is non-linear. In the horizontal configuration the linear interval is smaller then 0.1 mm and the total working range is approximately 0.2 mm. In the vertical configuration, the linear range is about 0.3 mm while the total range approximately 1 mm. During

	D_e [mm]	D_i [mm]	t [mm]	h_0 [mm]	$S_{0,25}$ [mm]	$F_{0,25}$ [N]	$S_{0,5}$ [mm]	$F_{0,5}$ [N]	$S_{0,75}$ [mm]	$F_{0,75}$ [N]	$F_{1,0}$ [N]	M [g]
JTEM-05	10,0	5,2	0,5	0,25	0,06	1	0,13	2,4	0,19	3,6	5	0,04
JTEM-06	12,5	6,2	0,7	0,30	0,08	3	0,15	5,1	0,23	8	12	0,11
JTEM-08	16,0	8,2	0,9	0,35	0,09	4	0,18	8	0,28	11	12	0,20
JTEM-10	20,0	10,2	1,1	0,45	0,11	5	0,22	10	0,33	15	18	0,33
JTEM-12	25,0	12,2	1,5	0,55	0,14	9	0,28	18	0,42	27	35	0,85
JTEM-16	31,5	16,3	1,75	0,70	0,18	15	0,35	32	0,53	51	70	1,44
JTEM-20	40,0	20,4	2,25	0,90	0,23	35	0,45	70	0,68	110	140	3,10

FIGURE 6.4: The available Belleville springs produced by Igus: external diameter D_e, internal diameter D_i, thickness t, maximum deformation h_0, 25% of the maximum deformation $S_{0.25}$, force at 25% of maximum deformation $F_{0.25}$, 50% of maximum deformation $S_{0.5}$, force at 50% of maximum deformation $F_{0.5}$, 75% of maximum deformation $S_{0.75}$, force at 75% of maximum deformation $F_{0.75}$, force at maximum deformation F_1, weight M.

the design process the vertical configuration has been selected for the following reasons:

- It makes easier to place the sensitive element as much as possible close to the center of compliance of the spring;
- The optical sensor presents a lower sensitivity which makes easier the regulation of the initial force sensor offset

Once the load and the deformation range of the force sensor are specified, it is possible to select the appropriate Belleville spring. At this stage, plastic springs of the series Polysorb produced by *Igus* are selected.
The result found with this preliminary prototype might be valid also for steel springs with appropriate load/deformation characteristics. This evaluation will be subject of future work.
Given the available models shown in Fig. 6.4, the spring JTEM-12 is selected to fit with the application needs. This spring has an elastic coefficient of $K_1 = 64.24\,\mathrm{N/mm}$ until the 75% of its maximum deformation, i.e. $S_{0.75} = 0.42\,\mathrm{mm}$, and a slight decrease of the elastic constant in the second part of the characteristics, with $K_2 = 61.53\,\mathrm{N/mm}$. To avoid this region in the working range of the force sensor, a total number of three springs in parallel can be used to guarantee a linear behavior within the 80 N load range, with an equivalent elastic constant $K = 3K_1 = 192.72\,\mathrm{N/mm}$ (see eq. 6.2), leading to a deformation at the maximum load of 0.415 mm. This choice generates a non-linear response of the sensor since the maximum deformation of the spring is larger than the linear range of the optical fork. We assume that the non-linear effect introduced can be characterized

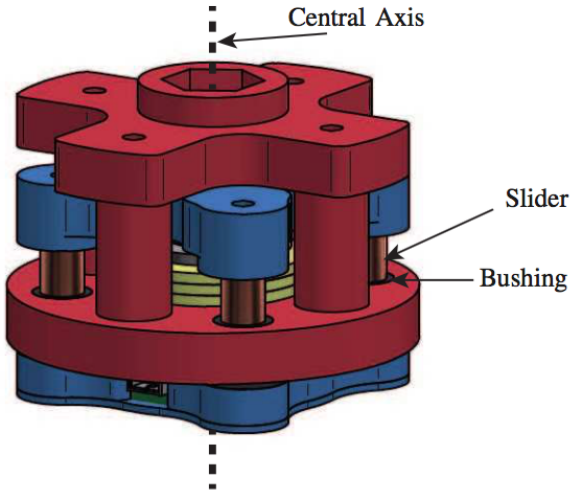

(a) 3D view of the force sensor CAD design.

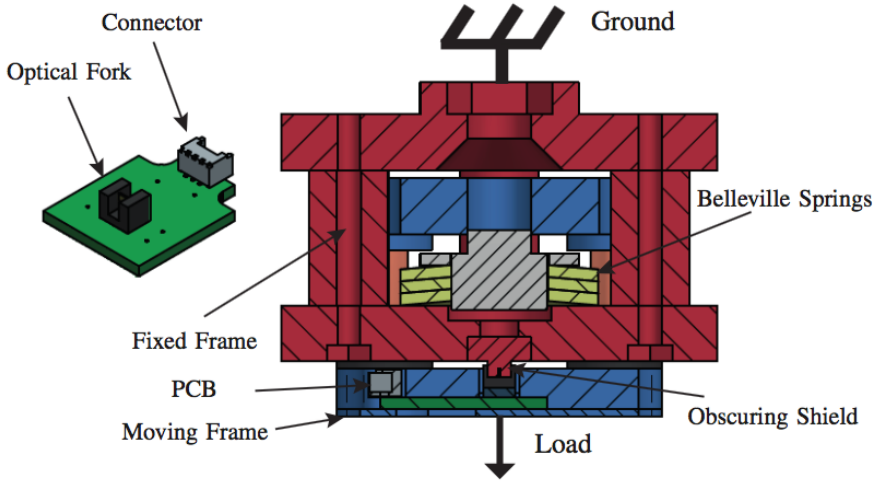

(b) Section view of the force sensor CAD design.

FIGURE 6.5: CAD design of the force sensor.

experimentally during the calibration and managed by a proper polynomial interpolation by the control system.

In Fig. 6.5(a) and 6.5(b) the 3D model and a section view of the proposed force sensor are shown. It consists of two main parts, the red one fixed to ground and the blue one free to move under the action of the load. The relative motion between these two parts is constrained by the use of four pairs of brass sliders and teflon bushings, to prevent spurious motions along other directions w.r.t. the direction of the measured force also in case of transversal loads. The optical fork is soldered on a PCB together with the LED and Phototransistor polarizing resistors, see Fig. 6.5(b). A 3 poles connector is used to supply power to the light fork and to output the sensor signal. The PCB is fixed on the bottom of the moving frame

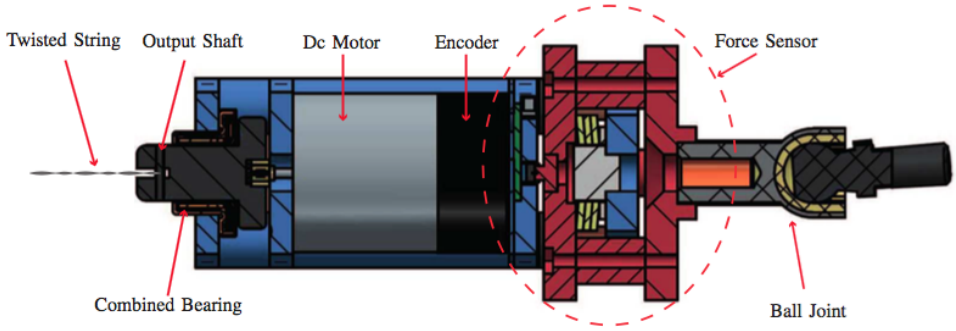

(a) A section view of the motor module with integrated force sensor (fixed together).

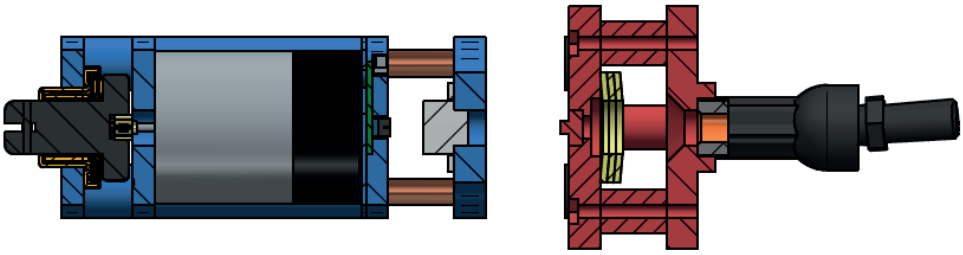

(b) A section view of the motor module with integrated force sensor (separated).

FIGURE 6.6: Section view of the TSA module and the integrated optoelectronic force sensor.

in such a way that the center of the optical fork is aligned with the load axis, see Fig. 6.5(a). On the fixed frame, an obscuring shield is mounted to interfere with the infrared ray of the optical fork. The spring stack is located between the bottom plate of the fixed frame and the upper plate of the moving frame. When a force along the vector represented in Fig. 6.5(b) is applied to the moving frame, the springs get compressed producing the downward motion of the moving frame, moving the shield with respect to the optical fork accordingly. This motion produces a variation of the amount of light that is received by the Phototransistor. The force applied to the moving frame can be then related to the signal variation by means of a proper calibration, as discussed in the next section.

6.2.2 Other components

In order to integrate the force sensor described in Sec. 6.2.1 with the DC motor, a multi-layered frame has been designed. The section views of Fig. 6.6(a) and Fig. 6.6(b) show how the moving frame of the force sensor (the blue frame of Fig. 6.5) is fixed to the structure holding the motor, the output shaft and its bearing. The parallel frames are held in position by spacers and four threaded bars passing

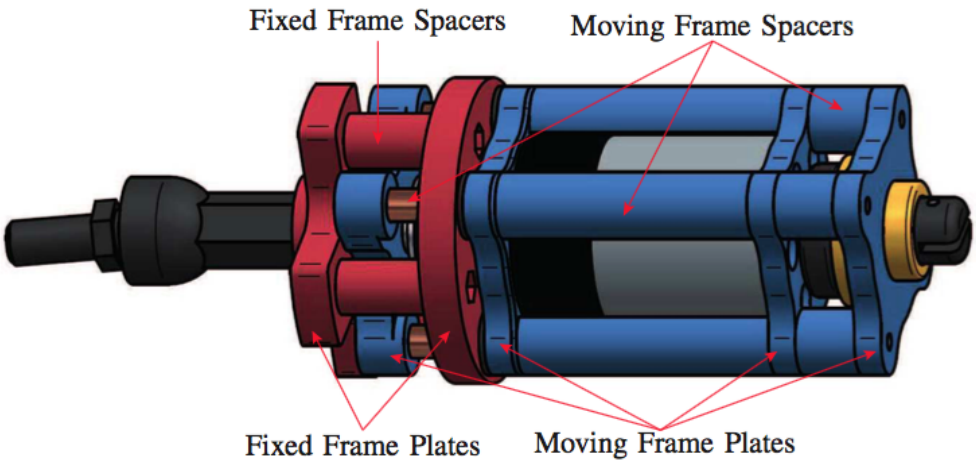

(a) 3D view of the TSA module and the integrated optoelectronic force sensor.

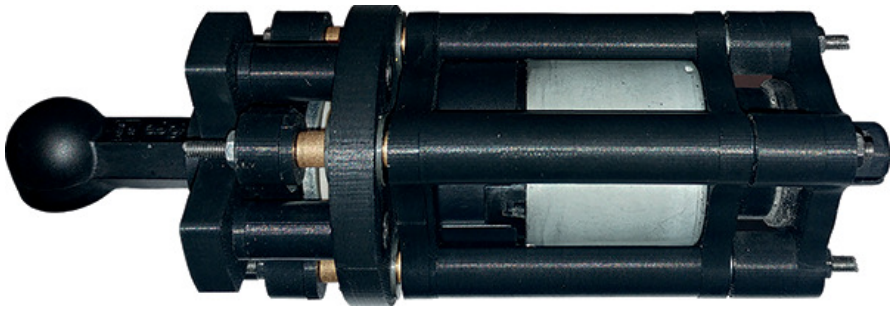

(b) TSA module and the integrated optoelectronic force sensor realized with rapid prototyping.

FIGURE 6.7: CAD design of the motor module and real prototype.

through them. The DC motor shaft is rigidly connected to the TSA output shaft. A combined bearing is mounted on the frame to support the TSA output shaft, decoupling in this way the load acting on the twisted string and the DC motor shaft and reducing rotation friction. The fixed frame of the force sensor (the red frame of Fig. 6.5) is connected to ground by means of a ball joint, that allows the TSA module to follows the orientation of the string within a range of $\pm 25°$ w.r.t. the neutral position.
The 3D view and the real prototype of the proposed TSA module are shown in Fig. 6.7(a) and Fig. 6.7(b) respectively.

6.3 Control system architecture

The proposed TSA module is provided with an embedded control system. All the required functionalities (e.g control, sensors acquisition, communication) are demanded to a custom embedded controller shown in Fig. 6.8. The controller is

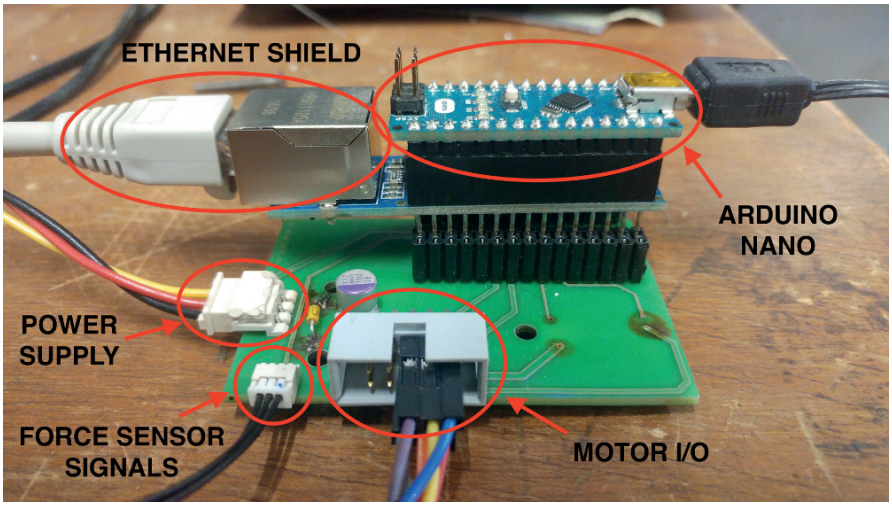

FIGURE 6.8: The TSA controller.

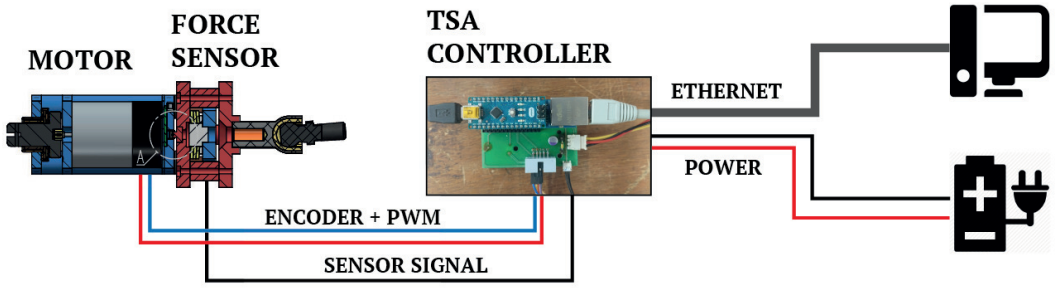

FIGURE 6.9: Interconnection between the TSA module, the embedded controller and the development workstation.

based on the well known Arduino NANO board [122] mounted on a PCB purposely designed for this specific application which provides all the digital and analog interfaces necessary for data exchange with the other system components, as well as the conditioning system for the force sensor signal and the connection to the power supply.

A schematic view of the overall architecture is represented in Fig. 6.9. The connection between TSA controller and the motor module is provided by a 6-pin I/O connector collecting the motor actuation (PWM), encoder signals (quadrature relative encoder) and respective low power supply. Another 3-pin connector connects the TSA controller with the force sensor providing the power supply and the sensor output analog signal. The communication between the TSA controller and the external workstation used for controller design, monitoring and experimental data collection is implemented by means of an Arduino Ethernet Shield placed in-between the PCB and the Arduino board.

The graph shown in Fig. 6.10 represents the structure of the system controller running on the TSA module. The set of functionalities grouped in the *Initial Setup*

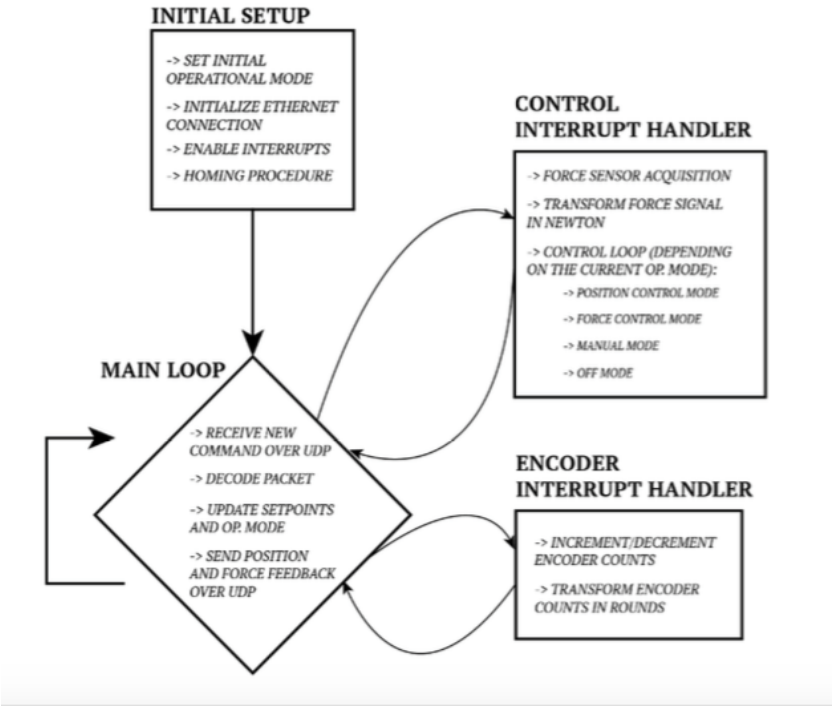

FIGURE 6.10: System controller architecture.

block on top of the graph, run only once at the system startup. First the initial operational mode is set to *off mode*. The operational mode can be chosen between *position mode*, in which the control of the angular position is implemented, *force mode* which implements the control of string's tensioning, *manual mode* which allows setting the PWM's duty-cycle (i.e. the rotational velocity of the motor) manually and *off mode*. Other actions performed in the initial setup include:

- Initialization of the Ethernet UDP connections necessary to exchange data with the workstation;
- Definition of the interrupt handler and enable of all interrupts;
- Execution of the *homing procedure*;

The homing procedure is performed at the system startup to allow a complete untwisting of the string regardless of its current state. This is necessary since the relation between an angular movement of the motor and the corresponding linear displacement of the twisted string strictly depends on how much the string is twisted. The procedure guarantees that the system is always initialized to a known state. The *pseudo code* of the described routine is provided below:

1. Set operational mode to *manual mode*.

2. Move the motor with constant velocity (constant duty cycle) along an arbitrary direction until the force sensor senses a defined arbitrary force value acting on the string.
3. Reset the motor's encoder count.
4. Repeat point 2) with inverted velocity. The string will pass through the untwisted status and will twist in the opposite direction until the force sensor senses the same force value of point 2).
5. Read the angular position from the encoder.
6. Set operational mode to *position mode*.
7. Go to the half of the angular position read at point 5).
8. Reset the encoder.
9. Set operational mode to *off mode*.

The *Main Loop* block iterates every cycle time and take care about the communication with the PC workstation over UDP sockets. At each iteration the presence of a new UDP *control packet* is checked. Fig. 6.11 shows the structure of the control packet sent from the remote workstation to the TSA controller over ethernet connection.
The packet contains 1 byte with the desired operational mode and 4 bytes with the corresponding command. The current operational mode ID and corresponding command are updated each time a new packet is received.
With a similar procedure the current motor state variables, in terms of operational mode, angular position and force acting on the string, are collected into a *state packet* and feed back to the workstation at each iteration.

The control interrupt handler is triggered at 1 kHz by the Arduino board integrated timer. This routine implements:

- The digital conversion of the optical fork signal;
- The transformation of this variable to a force information by means of the calibration parameters;
- The control strategy related to the current operational mode, based on standard PID controllers

1 BYTE	4 BYTE
MODE	COMMAND
Position	Setpoint
Force	Setpoint
Manual	Duty Cycle
Off	None

FIGURE 6.11: Structure of the UDP control packets sent from the workstation.

The encoder count update is demanded to a second interrupt service routine (*encoder interrupt handler* block in Fig. 6.10) which is attached to the signal of one of the two encoder pins. The routine is then triggered at every *rising edge* of the encoder signal (i.e. each time the encoder senses a unit displacement).

6.4 Experimental results

In order to experimentally test the presented actuator, the setup shown in Fig. 6.12 has been developed. The TSA module is connected through a couple of *Dyneema* strings with a diameter of 0.24 mm and length 0.97 m (in accordance to the haptic device's actuation dimensioning given in Sec. 5.5.2) to a linear motor, a *LinMot PS01-37x120*, acting as load for the system.
The control system of the linear motor is based on the servo controller *LinMot E2010-VF* that performs the basic current control, while both position and force control have been implemented on a standard PC equipped with a *Sensoray 626* data acquisition board, used to both communicate with the servo controller and acquire the sensors signals. In particular the position of the motor is measured by an incremental encoder with a resolution of 1μ m integrated in the stator, while the force measurement is obtained via a load cell connected between the slider and the strings.
The linear motor control scheme is designed by using the *MatLab/Simulink/RealTime Workshop* environment. The control scheme also communicates with the actuator's embedded controller through UDP connection in order send control packet to impose the desired working modes (between the ones described in Sec.

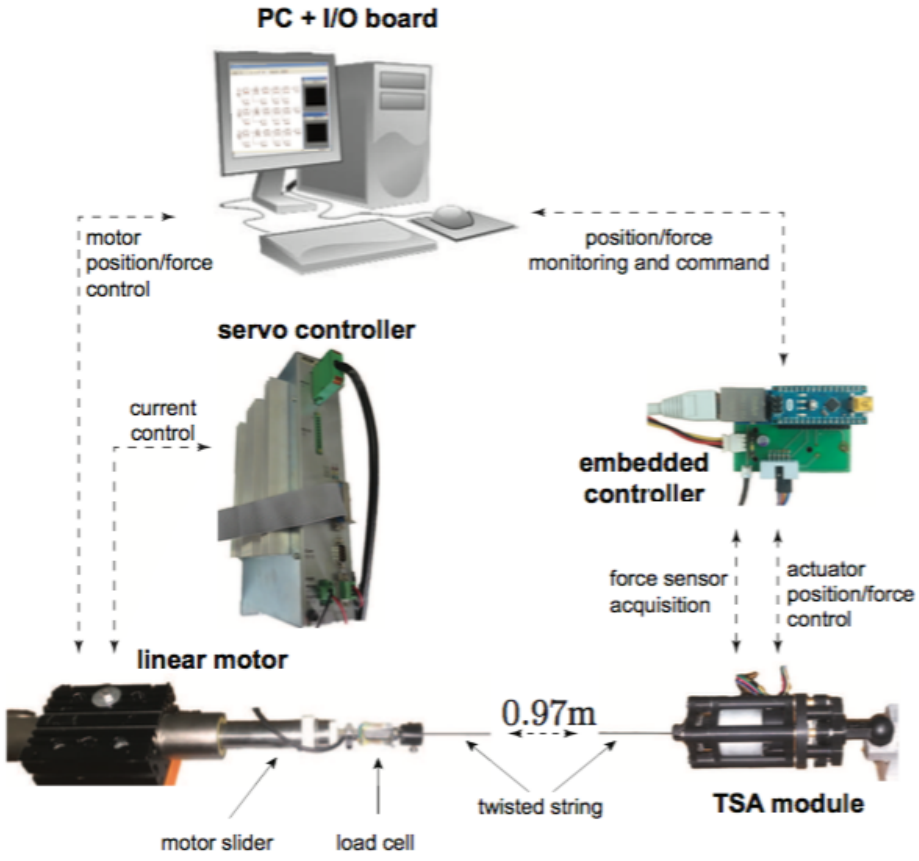

FIGURE 6.12: Schematic view of the experimental setup.

6.3) and acquire position and force feedback. The real-time operating system *RTAI-Linux* allows the controller to run with a sampling period $T_s = 1\,\text{ms}$.

6.4.1 Force sensor calibration

The optical force sensor embedded on the TSA module is calibrated using a commercial load cell used as reference measurement. The load cell is mounted on the linear motor, and the linear motor is used to provide precise pulling forces F_{ref} on the twisted string. Namely, a staircase force profile is commanded to the linear motor, and the sensor raw signal V_{force} is acquired through the A/D converter on the Arduino board. Note that during calibration procedure the TSA motor is not powered and the strings are kept in untwisted position. The calibration data set is then used to numerically find a polynomial interpolation curve fitting in a least-squares sense the experimental data. In Fig. 6.13 the data from several measurement cycles are reported showing the sensor repeatability in case of static measurements.

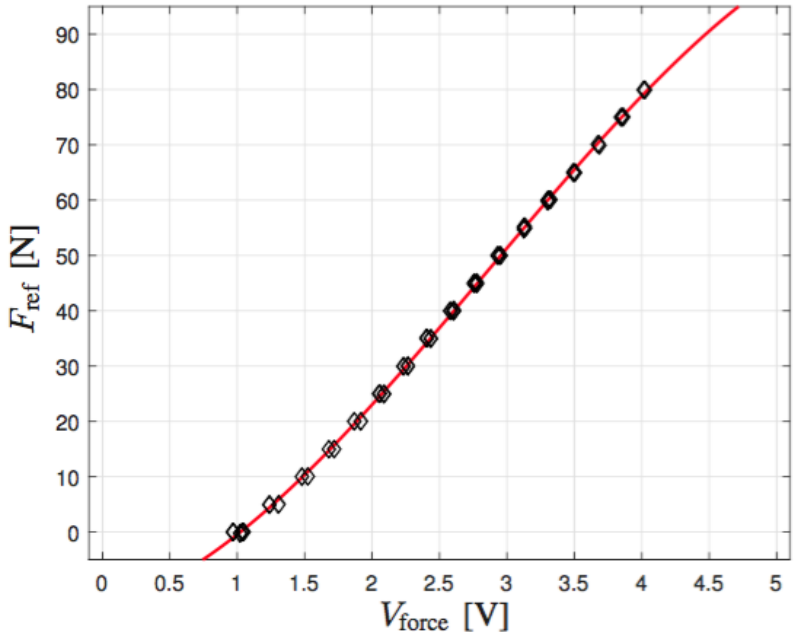

FIGURE 6.13: Calibration data acquired from the sensor (black squares) and corresponding polynomial interpolating curve (red).

In order to provide the best accuracy in force sensing and lowest possible computational burden, a third-order polynomial curve is used to interpolate the sensor output signal V_{force} to the force value F_{TSA}. Note that in this case the elaboration takes just 6 multiplications and 3 additions.
Moreover calibration curve demonstrates the correctness of the design choice in Sec. 6.2.1 where the selection of the spring is motivated in order to guarantee linear behavior within 80N load range. The regulation of the starting offset of the sensor is done by adding graduated washers at the top of the last spring. A good starting point is around the 20% of the characteristics, which allows to avoid the high non-linear response range of the sensor.

6.4.2 Force control tests

In order to test the force control loop embedded on the TSA module, the controller is set to track a fixed force set-point while the linear motor is used as a disturbance source. Namely the linear motor is controlled to track a sinusoidal position profile, which in turn changes the tension of the twisted string accordingly.

As shown in Fig. 6.14(a) - 6.14(b) the controller reacts to disturbances at different frequencies quite well, even if the friction on the shaft bearing affects negatively

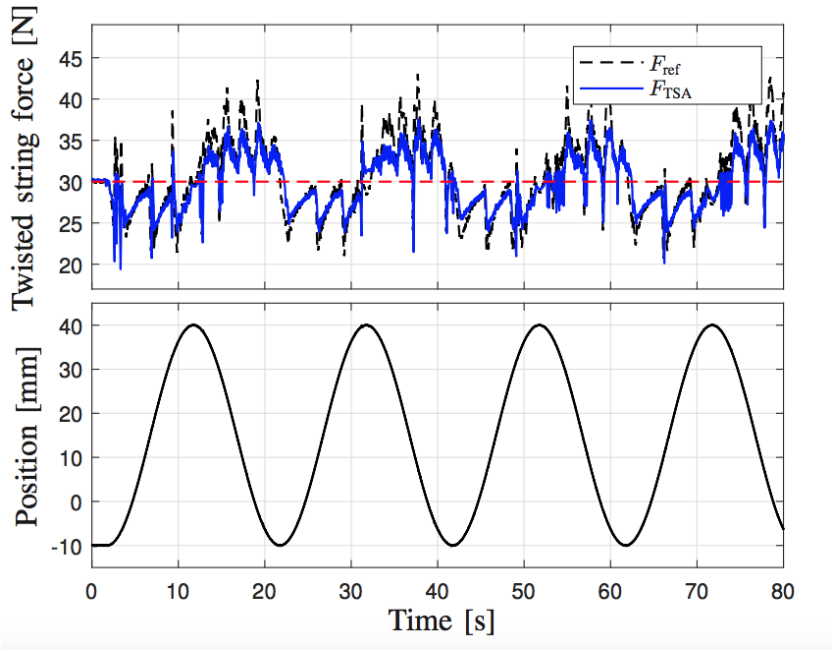

(a) Force control test with a sinusoidal disturbance with frequency 0.05 Hz.

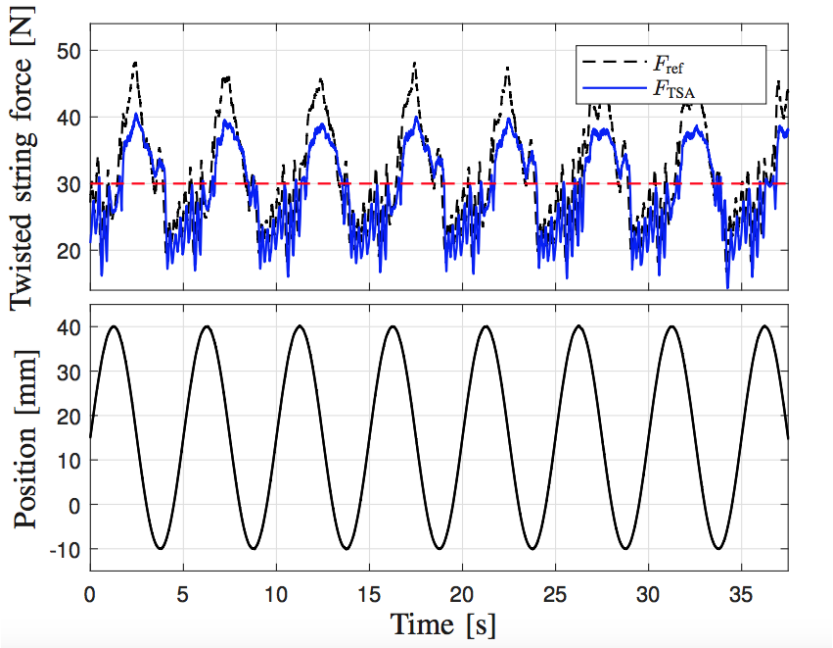

(b) Force control test with a sinusoidal disturbance with frequency 0.2 Hz.

FIGURE 6.14: Tracking of a force set-point of 30 N when sinusoidal disturbances of different frequencies are applied on the twisted string. On top, force measurements are given highlighting the effect of the force feedback, while at the bottom the position profile of the linear motor is shown.

the tracking error. Moreover, it is worth to notice that the force reconstruction of the TSA module is consistent with the load cell measurement.

Chapter 7

Conclusions and Future Works

7.1 Hybrid control scheme

Control problems in remote robots teleoperation arise when the master and the slave robots present kinematically dissimilar mechanical structures as the case of mobile manipulators controlled by standard fixed-base haptic devices.
The integration of standard robotic arms mounted on the top of mobile robots introduces redundancy that needs to be properly managed. A synchronized motion of both devices needs then to be achieved by means of a generally not redundant master device.
The hybrid position-position and position-velocity control algorithm for teleoperation of a generic mobile manipulator presented and discussed in Chapter 4 achieves this purpose by means of a proper partition of the master workspace. The scheme has been successfully applied to a 8 DoF Kuka youBot controlled by means of a 6 DoF PHANToM haptic device, not properly design for mobile manipulators teleoperation. The interaction approach offered by the algorithm appears intuitive to the operator and overcomes the problems due to the kinematic differences between the master and the slave robots. A further extension to the non-holonomic mobile platform case can be easily implemented starting from the actual motion control law and it is currently under investigation.
In the next future, the extension of the control scheme to the dual arm mobile manipulators case is planned. For this purpose, a proper switch between an arm-oriented and an object-oriented teleoperation scheme will be developed. A proper force reflection, when operating the arm inside the bubble, also needs to be implemented and the resulted bidirectional communication will require stability analysis.

In order to move in the direction of a truly multi-sensorial system, visual information coming from a depth camera mounted on the arm's end-point could be embedded in the system. The gaze direction of the camera (i.e the orientation of a generic reference frame placed on the arm end-point) could be adjusted according to the orientation of the operator's head, retrieved by mean of a proper visual tracking system. All this feedback integrations will contribute to augment the sense of telepresence and transparency for the operator through the definition of a functional multi-modal teleoperation framework.
Another possible development concerns the analysis of dynamic effects, i.e. when inertial effects of the slave device become more relevant due to high masses and/or velocities/accelerations. In this research these effects have been neglected and will be possibly considered in a future extension.
Finally, a proper local autonomous obstacle avoidance that takes advantage from the redundant kinematics of the mobile robot can be implemented in order to move in the direction of a shared control architecture.

7.2 Haptic interface design

In the last decades many researchers have shown that the creation of fully bidirectional systems able to display force information to the operator can considerably improve the performance of a remote manipulation task. This requires the availability of haptic interfaces able provide the operator with sufficient kinesthetic information about the interaction forces exchanged between the slave robot and the remote environment.
The main challenge in the design of haptic interfaces is to successfully display of a large dynamic range of impedances. The ideal haptic device must be characterized by a good backdrivability to allow unconstrained motion imposed by the operator and high stiffness to mimic interaction contacts. This request the haptic interface to have low inertia, backdrivability while preserving the opportunity to extend the workspace dimension at will depending on the application's request. Commercially available haptics based on heavy serial kinematic chains do not satisfy this requests.
The development of the novel cable-driven haptic interface presented in Chapter 5 moves in this direction. The device is able to allow a free 6 DoF movement imposed by the user (measured by visual motion tracking system), and render a 3D linear force feedback by means of four TSA modules arranged on the fixed frame in a tetrahedric configuration. To the best of the author's knowledge the

use of twisted string transmission in such a device has never been investigated.
One of the main benefit of rendering forces by means of string tensions is the scalability of the haptic workspace. This aspect makes cable-driven mechanisms potentially suited for overcoming the workspace limitations that characterize haptic solutions based on serial chains.
The tetrahedron-like structure of the proposed haptic interface has been obtained by considering a spherical workspace, a minimum level of feedback that can be transmitted and the fact that at least 4 tendons are necessary to render linear forces in all the directions of the Cartesian space.
The inverse kinematic model and the equations of direct and inverse statics were derived and discussed as well as a procedure for obtaining feasible string tensions for control purposes.
The design, prototyping, and preliminary tests of a modular TSA module for force rendering applications has been also presented and discussed. The use of the Belleville springs to realize the force sensors has met the need of simplifying the dimensioning of the elastic element with regard to the desired range of force required from the specific application.
The second great advancement is the independence of the force sensor measure with respect to spurious loads. This has been achieved with the installation of the photo-detector aligned with the central axis, the use of guides that constrain the relative motion of the frame fixed to ground and the one subjected to the load, and the use of a ball joint to allow the self-alignment of the module to the string direction.
The whole structure of the module has been designed in such a way that it can be easily scaled according to different motor sizes. At this stage all the structural parts has been realized in ABS by means of rapid prototyping techniques to make it easier the preliminary validation of the solutions. However CNC manufactured aluminum parts might make more rigid the frame reducing the friction between the output shaft and the bearing, and therefore improve the force control performance.
Since the device is still under development, further activities are necessary in order to complete the real setup and demonstrate the effectiveness in terms of force reflection through experimental results.
The next step is the validation of the behavior of multiple coordinated actuators acting on a common load as required from the haptic device. Other future extensions will include the study of a complex mechanical structure, based on Gimbal-like mechanisms, able to allow the actuation forces always to be aligned with the bracelet's center point, avoiding the creation of undesired torques acting

on the mobile frame.
The long-term goal is to merge different perceptive solutions and control architectures into a single multi-modal master device for telerobotic systems able to immerse the user in full 3D reconstruction of the remote environment (as well as 3D visors for VR-aided visual feedback.) augmenting the felling of telepresence.
Besides, the integration of fingers force feedback mechanisms with the aim of enabling telemanipulation tasks is also a target for the future, but this goes beyond the present Ph.D. activity.

Bibliography

[1] Bruno Siciliano and Oussama Khatib. *Springer Handbook of Robotics*. Springer-Verlag New York, Inc., Secaucus, NJ, USA, 2007. ISBN 354023957X.

[2] A. Bolopion and S. Régnier. A review of haptic feedback teleoperation systems for micromanipulation and microassembly. *IEEE Transactions on Automation Science and Engineering*, 10(3):496–502, July 2013. ISSN 1545-5955. doi: 10.1109/TASE.2013.2245122.

[3] Claudio Melchiorri. Robotic telemanipulation systems: an overview on control aspects. *IFAC Proceedings Volumes*, 36(17):21 – 30, 2003. ISSN 1474-6670. 7th IFAC Symposium on Robot Control (SYROCO 2003), Wroclaw, Poland, 1-3 September, 2003.

[4] S. Lichiardopol. *A survey on teleoperation*. PhD thesis, Eindhoven University of Technology, 2014.

[5] Michael J. Massimino and Thomas B. Sheridan. Teleoperator performance with varying force and visual feedback. *Human Factors*, 36(1):145–157, 2018/03/30 1994. doi: 10.1177/001872089403600109. URL `https://doi.org/10.1177/001872089403600109`.

[6] Y. Jia. *Teleoperation of mobile manipulators*. PhD thesis, Michigan State University, 2014.

[7] Thomas B Sheridan, Dana S Kruser, and Stanley Deutsch. Human factors in automated and robotic space systems: Proceedings of a symposium. part 1. 1987.

[8] Jianhong Cui, Sabri Tosunoglu, Rodney Roberts, Carl Moore, and Daniel W Repperger. A review of teleoperation system control. 03 2018.

[9] Y. Yokokohji and T. Yoshikawa. Bilateral control of master-slave manipulators for ideal kinesthetic coupling. In *EEE International Workshop on Intelligent Robots and Systems, Towards a New Frontier of Applications*, pages 355–362 vol.1, Jul 1990. doi: 10.1109/IROS.1990.262411.

[10] D. A. Lawrence. Stability and transparency in bilateral teleoperation. *IEEE Transactions on Robotics and Automation*, 9(5):624–637, Oct 1993. ISSN 1042-296X. doi: 10.1109/70.258054.

[11] Peter F. Hokayem and Mark W. Spong. Bilateral teleoperation: An historical survey. *Automatica*, 42(12):2035–2057, 2006. ISSN 0005-1098.

[12] J. Vertut and P. Coiffet. *Teleoperation and Robotics Evolution and Development*. Robot Technology Volume 3A. Kogan page, 1985.

[13] R. C. Goertz. Fundamentals of general-purpose remote manipulators. 1952.

[14] T H Massie and J K Salisbury. The phantom haptic interface: a device for probing virtual objects. 55, 01 1994.

[15] G. Hirzinger, B. Brunner, J. Dietrich, and J. Heindl. Sensor-based space robotics-rotex and its telerobotic features. *IEEE Transactions on Robotics and Automation*, 9(5):649–663, Oct 1993. ISSN 1042-296X. doi: 10.1109/70.258056.

[16] Jacques Marescaux, Joel Leroy, Francesco Rubino, Michelle Smith, Michel Vix, Michele Simone, and Didier Mutter. Transcontinental robot-assisted remote telesurgery: Feasibility and potential applications. *Annals of Surgery*, 235(4): 487–492, 04 2002.

[17] Mark W. Spong, Seth Hutchinson, and M. Vidyasagar. Robot modeling and control. *IEEE Control Systems*, 26(6):113–115, 2006. ISSN 1066-033X. doi: 10.1109/MCS.2006.252815.

[18] Jacques Marescaux, Joel Leroy, Michel Gagner, Francesco Rubino, Didier Mutter, Michel Vix, S.E. Butner, and Michelle K. Smith. Transatlantic robot-assisted telesurgery. 413:379–80, 10 2001.

[19] J. Funda, R. H. Taylor, B. Eldridge, S. Gomory, and K. G. Gruben. Constrained cartesian motion control for teleoperated surgical robots. *IEEE Transactions on Robotics and Automation*, 12(3):453–465, Jun 1996. ISSN 1042-296X. doi: 10.1109/70.499826.

[20] A. J. Madhani, G. Niemeyer, and J. K. Salisbury. The black falcon: a teleoperated surgical instrument for minimally invasive surgery. In *Proceedings. 1998 IEEE/RSJ International Conference on Intelligent Robots and Systems. Innovations in Theory, Practice and Applications (Cat. No.98CH36190)*, volume 2, pages 936–944 vol.2, Oct 1998. doi: 10.1109/IROS.1998.727320.

[21] T.B. Sheridan. Teleoperation, telerobotics and telepresence: A progress report. *Control Engineering Practice*, 3(2):205 – 214, 1995. ISSN 0967-0661. doi: https://doi.org/10.1016/0967-0661(94)00078-U. URL `http://www.sciencedirect.com/science/article/pii/096706619400078U`.

[22] J. Yuh. Design and control of autonomous underwater robots: A survey. *Auton. Robots*, 8(1):7–24, January 2000. ISSN 0929-5593. doi: 10.1023/A:1008984701078. URL `https://doi.org/10.1023/A:1008984701078`.

[23] R. Uhrich. Terminus controlled deep ocean manipulator. In *Ocean 73 - IEEE International Conference on Engineering in the Ocean Environment*, pages 301–304, Sept 1973. doi: 10.1109/OCEANS.1973.1161223.

[24] S. Marier, A. El Mhamedi, and Z. Binder. Analysis of a computer-aided teleoperation process by means of generalized stochastic petri nets. *Control Engineering Practice*, 5(7):931 – 942, 1997. ISSN 0967-0661. doi: https://doi.org/10.1016/S0967-0661(97)00080-4. URL `http://www.sciencedirect.com/science/article/pii/S0967066197000804`.

[25] T. Imaida, Y. Yokokohji, T. Doi, M. Oda, and T. Yoshikawa. Ground-space bilateral teleoperation of ets-vii robot arm by direct bilateral coupling under 7-s time delay condition. *IEEE Transactions on Robotics and Automation*, 20(3):499–511, June 2004. ISSN 1042-296X. doi: 10.1109/TRA.2004.825271.

[26] J. Wright, F. Hartman, B. Cooper, S. Maxwell, J. Yen, and J. Morrison. Driving on mars with rsvp. *IEEE Robotics Automation Magazine*, 13(2):37–45, June 2006. ISSN 1070-9932. doi: 10.1109/MRA.2006.1638014.

[27] Gerd Hirzinger, K Landzettel, Detlef Reintsema, Carsten Preusche, Alin Albu-Schäeffer, Bernd Rebele, and Matthias Turk. Rokviss - robotics component verification on iss, 08 2005.

[28] Carsten Preusche, Detlef Reintsema, K Landzettel, and Gerd Hirzinger. Robotics component verification on iss rokviss - preliminary results for telepresence, 11 2006.

[29] K. Hertkorn, M.A. Roa, M. Brucker, P. Kremer, and C. Borst. Virtual reality support for teleoperation using online grasp planning. In *Intelligent Robots and Systems (IROS), 2013 IEEE/RSJ International Conference on*, pages 2074–2074, Nov 2013.

[30] U. Scarcia. *Design and Control of Robotic Hands.* PhD thesis, University of Bologna, 2015.

[31] N. Diolaiti and C. Melchiorri. Teleoperation of a mobile robot through haptic feedback. In *IEEE International Workshop HAVE Haptic Virtual Environments and Their*, pages 67–72, 2002. doi: 10.1109/HAVE.2002.1106916.

[32] Sun-Gi Hong, Ju-Jang Lee, and Seungho Kim. Generating artificial force for feedback control of teleoperated mobile robots. In *Proceedings 1999 IEEE/RSJ International Conference on Intelligent Robots and Systems. Human and Environment Friendly Robots with High Intelligence and Emotional Quotients (Cat. No.99CH36289)*, volume 3, pages 1721–1726 vol.3, 1999. doi: 10.1109/IROS.1999.811726.

[33] N. C. Mitsou, S. V. Velanas, and C. S. Tzafestas. Visuo-haptic interface for teleoperation of mobile robot exploration tasks. In *ROMAN 2006 - The 15th IEEE International Symposium on Robot and Human Interactive Communication*, pages 157–163, Sept 2006. doi: 10.1109/ROMAN.2006.314411.

[34] Metin Sitti, Baris Aruk, Hiroaki Shintani, and Hideki Hashimoto. Scaled teleoperation system for nano-scale interaction and manipulation. *Advanced Robotics*, 17(3):275–291, 2003.

[35] Nat Durlach. The potential of teleoperation for entertainment and education. *Presence: Teleoperators and Virtual Environments*, 6(3):350–351, 1997. doi: 10.1162/pres.1997.6.3.350. URL `https://doi.org/10.1162/pres.1997.6.3.350`.

[36] S. Westerberg, I. R. Manchester, U. Mettin, P. La Hera, and A. Shiriaev. Virtual environment teleoperation of a hydraulic forestry crane. In *2008 IEEE International Conference on Robotics and Automation*, pages 4049–4054, May 2008. doi: 10.1109/ROBOT.2008.4543833.

[37] Quang Ha, M. Santos, Quang Nguyen, D. Rye, and H. Durrant-Whyte. Robotic excavation in construction automation. *IEEE Robotics Automation Magazine*, 9 (1):20–28, Mar 2002. ISSN 1070-9932. doi: 10.1109/100.993151.

[38] Xiaolei Hou, Hua Lan, Xiaojun Xing, Yaohong Qu, Dongli Yuan, Jianguo Yan, and Panfeng Huang. Environmental force reflection in an admittance configured haptic interface for teleoperation of vtol aerial robots. *IFAC-PapersOnLine*, 50 (1):10262 – 10267, 2017. ISSN 2405-8963. 20th IFAC World Congress.

[39] X. Hou, R. Mahony, and F. Schill. Comparative study of haptic interfaces for bilateral teleoperation of vtol aerial robots. *IEEE Transactions on Systems, Man, and Cybernetics: Systems*, 46(10):1352–1363, Oct 2016. ISSN 2168-2216.

[40] B. Hannaford, L. Wood, D. A. McAffee, and H. Zak. Performance evaluation of a six-axis generalized force-reflecting teleoperator. *IEEE Transactions on Systems,*

Man, and Cybernetics, 21(3):620–633, May 1991. ISSN 0018-9472. doi: 10.1109/21.97455.

[41] Manuel Ferre Martin Buss Rafael Aracil Claudio Melchiorri and Carlos Balaguer. *Advances in Telerobotics*. Springer Tracts in Advanced Robotics, 2007.

[42] Walter Conklin and Sabri Tosunoglu. Conceptual design of a universal bilateral manual controller. In *Florida Conference on Recent Advances in Robotics*, pages 187–191, 1996.

[43] W. Kim. *A study On the Design and Operation of Force Feedback Controllers*. PhD thesis, University of Texas, 1991.

[44] Marc Ueberle, Nico Mock, and Martin Buss. Design, control, and evaluation of a hyper-redundant haptic device. In *Advances in Telerobotics*, 2007.

[45] Soo S. Lee and Jang M. Lee. Design of a general purpose 6-dof haptic interface. *Mechatronics*, 13(7):697 – 722, 2003. ISSN 0957-4158. doi: http://dx.doi.org/10.1016/S0957-4158(02)00038-7.

[46] URL `http://www.geomagic.com/en/products/phantom-omni/overview`.

[47] Vincent Hayward, Pedro Gregorio, O Astley, S Greenish, and Michel Doyon. Freedom-7: A high fidelity seven axis haptic device with application to surgical training. 232:445–456, 01 1998.

[48] J.-G.S. Demers, J.M.A. Boelen, and I.P.W. Sinclair. Freedom 6s force feedback hand controller. *IFAC Proceedings Volumes*, 31(33):115 – 120, 1998. ISSN 1474-6670. doi: https://doi.org/10.1016/S1474-6670(17)38396-9. URL `http://www.sciencedirect.com/science/article/pii/S1474667017383969`. IFAC Workshop on Space Robotics (SPRO'98), St-Hubert, Canada, 19-22 October.

[49] Richard Q Van der Linde, Piet Lammertse, Erwin Frederiksen, and B Ruiter. The hapticmaster, a new high-performance haptic interface. In *Proc. Eurohaptics*, pages 1–5, 2002.

[50] URL `http://www.haption.com/`.

[51] URL `http://www.mpb-techlonogies.ca/`.

[52] Y. Tsumaki, H. Naruse, D. N. Nenchev, and M. Uchiyama. Design of a compact 6-dof haptic interface. In *Proceedings. 1998 IEEE International Conference on Robotics and Automation (Cat. No.98CH36146)*, volume 3, pages 2580–2585 vol.3, May 1998. doi: 10.1109/ROBOT.1998.680730.

[53] Sung-Uk Lee, S Hochul, and S Kim. Design of a new haptic device using a parallel gimbal mechanism. In *International Conference on Computer Applications in Shipbuilding. ICCAS*, 2005.

[54] Tian Qiu, William R Hamel, and Dongjun Lee. Design and control of a low cost 6 dof master controller. In *Robotics and Automation (ICRA), 2014 IEEE International Conference on*, pages 5313–5318. IEEE, 2014.

[55] Minh Hung Vu and Uhn Joo Na. A new 6-dof haptic device for teleoperation of 6-dof serial robots. *IEEE Transactions on Instrumentation and Measurement*, 60 (11):3510–3523, 2011.

[56] Dongseok Ryu, Jae-Bok Song, Changhyun Cho, Sungchul Kang, and Munsang Kim. Development of a six dof haptic master for teleoperation of a mobile manipulator. *Mechatronics*, 20(2):181–191, 2010.

[57] Force Dimension website. Force Dimension Haptic Devices, 2017. URL `http://www.forcedimension.com/`.

[58] URL `http://www.novint.com/`.

[59] URL `http://www.quanser.com/`.

[60] URL `http://butterflyhaptics.com/products/`.

[61] Roger Bostelman, Tsai Hong, and Jeremy Marvel. Survey of research for performance measurement of mobile manipulators. *in Journal of National Institute of Standards and Technology*, 2016.

[62] Bjorn Heber Skumsnes. *Teleoperation of mobile manipulators*. PhD thesis, NTNU - Norvegian University of Science and Technology, 2012.

[63] Ignacy Duleba. Modeling and control of mobile manipulators. *IFAC Proceedings Volumes*, 33(27):447 – 452, 2000. ISSN 1474-6670. doi: https://doi.org/10.1016/S1474-6670(17)37970-3. URL `http://www.sciencedirect.com/science/article/pii/S1474667017379703`. 6th IFAC Symposium on Robot Control (SYROCO 2000), Vienna, Austria, 21-23 September 2000.

[64] Homayoun Seraji. A unified approach to motion control of mobile manipulators. *The International Journal of Robotics Research*, 17(2):107–118, 1998.

[65] François G. Pin, K.A. Morgansen, Faithlyn A. Tulloch, Charles J. Hacker, and Kathryn B. Gower. Motion planning for mobile manipulators with a nonholonomic constraint using the fsp (full space parameterization) method. 13: 723–736, 11 1996.

[66] John Gardner and Steven A. Velinsky. Kinematics of mobile manipulators and implications for design. 17:309 – 320, 06 2000.

[67] Bernard Bayle, Jean-Yves Fourquet, and M Renaud. Manipulability of wheeled mobile manipulators: Application to motion generation. 22, 07 2003.

[68] Olav Egeland. Task-space tracking with redundant manipulators. 3:471 – 475, 11 1987.

[69] Y. Jia. *Teleoperation of mobile manipulators*. PhD thesis, Michigan State University, 2014.

[70] *KUKA youBot User Manual*.

[71] R. Goertz. Manipulator systems development and anl. 1964.

[72] T. B. Sheridan. Space teleoperation through time delay: review and prognosis. *IEEE Transactions on Robotics and Automation*, 9(5):592–606, Oct 1993. ISSN 1042-296X. doi: 10.1109/70.258052.

[73] S. Hirche, M. Ferre, J. Barrio, C. Melchiorri, and M. Buss. *Bilateral Control Architectures for Telerobotics*, volume 31 of *STAR, Springer Tracts in Advanced Robotics*, pages 147–160. Springer Verlag, 2007. ISBN 978-3-540-71363-0.

[74] H.Y.K. Lau and L.C.C. Wai. Implementation of position-force and position-position teleoperator controllers with cable-driven mechanisms. *Robotics and Computer-Integrated Manufacturing*, 21(2):145 – 152, 2005. ISSN 0736-5845.

[75] M. J. Massimino, T. B. Sheridan, and J. B. Roseborough. One handed tracking in six degrees of freedom. In *Conference Proceedings., IEEE International Conference on Systems, Man and Cybernetics*, pages 498–503 vol.2, Nov 1989. doi: 10.1109/ICSMC.1989.71346.

[76] J. Barrio, F. Suarez-Ruiz, M. Ferre, and R. Aracil. A rate-position haptic controller for large telemanipulation workspaces. In *IROS, 2012 IEEE/RSJ Int. Conf. on*, pages 58–63, Oct 2012.

[77] W.S. Kim, F. Tendick, S.R. Ellis, and L.W. Stark. A comparison of position and rate control for telemanipulations with consideration of manipulator system dynamics. *Robotics and Automation, IEEE Journal of*, 3(5):426–436, October 1987. ISSN 0882-4967.

[78] I. Farkhatdinov and Jee-Hwan Ryu. Hybrid position-position and position-speed command strategy for the bilateral teleoperation of a mobile robot. In *Control, Automation and Systems, 2007. ICCAS '07. International Conference on*, pages 2442–2447, Oct 2007.

[79] L. Liu, G. Liu, Y. Zhang, and D. Wang. A modified motion mapping method for haptic device based space teleoperation. In *The 23rd IEEE International Symposium on Robot and Human Interactive Communication*, pages 449–453, Aug 2014.

[80] L. Dominjon, A. Lecuyer, J.-M. Burkhardt, G. Andrade-Barroso, and S. Richir. The "bubble" technique: interacting with large virtual environments using haptic devices with limited workspace. In *Eurohaptics Conf. 2005*, pages 639–640, March 2005.

[81] R. A. Pavlik and J. M. Vance. Interacting with grasped objects in expanded haptic workspaces using the bubble technique. *J. of Computing and Information Science in Eng.*, 15(4), 2015.

[82] L. Conway, R. Volz, and M. Walker. Tele-autonomous systems: Methods and architectures for intermingling autonomous and telerobotic technology. In *Proceedings. 1987 IEEE International Conference on Robotics and Automation*, volume 4, pages 1121–1130, Mar 1987. doi: 10.1109/ROBOT.1987.1087923.

[83] S. Hayati and S. T. Venkataraman. Design and implementation of a robot control system with traded and shared control capability. In *Proceedings, 1989 International Conference on Robotics and Automation*, pages 1310–1315 vol.3, May 1989. doi: 10.1109/ROBOT.1989.100161.

[84] B. Pitzer, M. Styer, Christian Bersch, C. DuHadway, and J. Becker. Towards perceptual shared autonomy for robotic mobile manipulation. In *Robotics and Automation (ICRA), 2011 IEEE International Conference on*, pages 6245–6251, May 2011.

[85] G. Hirzinger, B. Brunner, J. Dietrich, and J. Heindl. Rotex-the first remotely controlled robot in space. In *Proceedings of the 1994 IEEE International Conference on Robotics and Automation*, pages 2604–2611 vol.3, May 1994. doi: 10.1109/ROBOT.1994.351121.

[86] B. Brunner, K. Arbter, and G. Hirzinger. Task directed programming of sensor based robots. In *Intelligent Robots and Systems '94. 'Advanced Robotic Systems and the Real World', IROS '94. Proceedings of the IEEE/RSJ/GI International Conference on*, volume 2, pages 1080–1087 vol.2, Sep 1994. doi: 10.1109/IROS.1994.407532.

[87] T. Ortmaier, M. Groger, D. H. Boehm, V. Falk, and G. Hirzinger. Motion estimation in beating heart surgery. *IEEE Transactions on Biomedical Engineering*, 52(10):1729–1740, Oct 2005. ISSN 0018-9294. doi: 10.1109/TBME.2005.855716.

[88] W. R. Ferrell and T. B. Sheridan. Supervisory control of remote manipulation. *IEEE Spectrum*, 4(10):81–88, Oct 1967. ISSN 0018-9235. doi: 10.1109/MSPEC.1967.5217126.

[89] G. Hirzinger, J. Heindl, K. Landzettel, and B. Brunner. Multisensory shared autonomy - a key issue in the space robot technology experiment rotex. In *Proceedings of the IEEE/RSJ International Conference on Intelligent Robots and Systems*, volume 1, pages 221–230, Jul 1992. doi: 10.1109/IROS.1992.587324.

[90] Jeffrey D. Will, Kevin L. Moore, and Ian K. Lynn. Optimizing human-robot teleoperation interfaces for mobile manipulators. *Industrial Robot: An International Journal*, 40(2):173–184, 2013.

[91] P. Arcara and C. Melchiorri. Control schemes for teleoperation with time delay: A comparative study. *Int. Journ. on Robotics and Autonomous Systems*, 38(1): 49–64, 2002. ISSN I0921-8890.

[92] Andrea De Luca, Giuseppe Oriolo, and Paolo Giordano. Kinematic modeling and redundancy resolution for nonholonomic mobile manipulators. 2006:1867 – 1873, 06 2006.

[93] Jindong Tan and Ning Xi. Integrated task planning and control for mobile manipulators. In *Proceedings 2002 IEEE International Conference on Robotics and Automation (Cat. No.02CH37292)*, volume 1, pages 382–387 vol.1, 2002. doi: 10.1109/ROBOT.2002.1013390.

[94] Dongseok Ryu, Changhyun Cho, Munsang Kim, and Jae-Bok Song. Design of a 6 dof haptic master for teleoperation of a mobile manipulator. In *Robotics and Automation, 2003. Proceedings. ICRA '03. IEEE International Conference on*, volume 3, pages 3243–3248 vol.3, Sept 2003.

[95] 3D Systems. Specifications for the phantom omni haptic device. `https://www.3dsystems.com/haptics-devices/touch`, Online.

[96] C. L. Clover, G. R. Luecke, J. J. Troy, and W. A. McNeely. Dynamic simulation of virtual mechanisms with haptic feedback using industrial robotics equipment. In *Proceedings of International Conference on Robotics and Automation*, volume 1, pages 724–730 vol.1, Apr 1997.

[97] Jens Hoogen, Robert Riener, and Günther Schmidt. Control aspects of a robotic haptic interface for kinesthetic knee joint simulation. 10:1301–1308, 11 2002.

[98] C Bonivento, A Eusebi, C Melchiorri, M Montanari, and G Vassura. Wireman: A portable wire manipulator for touch-rendering of bas-relief virtual surfaces. In

Advanced Robotics, 1997. ICAR'97. Proceedings., 8th International Conference on, pages 13–18. IEEE, 1997.

[99] Robert L Williams, Venkat Chadaram, and Federica Giacometti. Three-cable haptic interface. In *ASME 2006 International Design Engineering Technical Conferences and Computers and Information in Engineering Conference*, pages 817–824. American Society of Mechanical Engineers, 2006.

[100] Paolo Gallina, Giulio Rosati, and Aldo Rossi. 3-dof wire driven planar haptic interface. *Journal of Intelligent & Robotic Systems*, 32(1):23–36, 2001.

[101] Masahiro Ishii and Makoto Sato. A 3d spatial interface device using tensed strings. *Presence: Teleoperators and Virtual Environments*, 3(1):81–86, 2017/02/18 1994. doi: 10.1162/pres.1994.3.1.81. URL `http://dx.doi.org/10.1162/pres.1994.3.1.81`.

[102] Randel Lindemann and Delbert Tesar. Construction and demonstration of a 9-string 6 dof force reflecting joystick for telerobotics. 1989.

[103] M Ishii and M Sato. Six degree-of-freedom master using eight tensed strings. In *ISMCR'98, Proc. of the Eighth Internat. Symp. on Measurement and Control in Robotics*, volume 455, pages 251–255, 1998.

[104] B. Bayle, J. Y. Fourquet, and M. Renaud. Manipulability of wheeled mobile manipulators: Application to motion generation. *The International Journal of Robotics Research*, 22(7-8):565–581, 2018/03/09 2003.

[105] A. Dietrich, T. Wimböck, A. Albu-Schäffer, and G. Hirzinger. Singularity avoidance for nonholonomic, omnidirectional wheeled mobile platforms with variable footprint. In *2011 IEEE International Conference on Robotics and Automation*, pages 6136–6142, May 2011.

[106] Serdar Soylu, B Buckham, and R.P. Podhorodeski. Dexterous task-priority based redundancy resolution for underwater-manipulator systems. 31:519–533, 01 2007.

[107] A. Pepe, D. Chiaravalli, and C. Melchiorri. A hybrid teleoperation control scheme for a single-arm mobile manipulator with omnidirectional wheels. In *2016 IEEE/RSJ International Conference on Intelligent Robots and Systems (IROS)*, pages 1450–1455, Oct 2016. doi: 10.1109/IROS.2016.7759236.

[108] G. Palli, C. Natale, C. May, C. Melchiorri, and T. Würtz. Modeling and control of the twisted string actuation system. *IEEE/ASME Trans. on Mechatronics*, 18 (2):664–673, 2013.

[109] G. Palli, M. Hosseini, and C. Melchiorri. Experimental evaluation of guided twisted actuation. *IFAC-PapersOnLine*, 49(21):380 – 385, 2016. ISSN 2405-8963. 7th IFAC Symposium on Mechatronic Systems MECHATRONICS 2016.

[110] A. Pepe, M. Hosseini, U. Scarcia, G. Palli, and C. Melchiorri. Development of an haptic interface based on twisted string actuators. In *2017 IEEE International Conference on Advanced Intelligent Mechatronics (AIM)*, pages 28–33, July 2017.

[111] Takashi Sonoda and Ivan Godler. Multi-fingered robotic hand employing strings transmission named "twist drive". In *Intelligent Robots and Systems (IROS), 2010 IEEE/RSJ International Conference on*, pages 2733–2738. IEEE, 2010.

[112] Gianluca Palli, Claudio Melchiorri, Gabriele Vassura, U Scarcia, Lorenzo Moriello, Giovanni Berselli, Alberto Cavallo, Giuseppe De Maria, Ciro Natale, Salvatore Pirozzi, et al. The dexmart hand: Mechatronic design and experimental evaluation of synergy-based control for human-like grasping. *The International Journal of Robotics Research*, 33(5):799–824, 2014.

[113] D. Popov, I. Gaponov, and J. H. Ryu. A preliminary study on a twisted strings-based elbow exoskeleton. In *2013 World Haptics Conference (WHC)*, pages 479–484, April 2013. doi: 10.1109/WHC.2013.6548455.

[114] In-Won Park and Vytas SunSpiral. Impedance controlled twisted string actuators for tensegrity robots. In *Control, Automation and Systems (ICCAS), 2014 14th International Conference on*, pages 1331–1338. IEEE, 2014.

[115] G. Palli and S. Pirozzi. Integration of an optical force sensor into the actuation module of the DEXMART Hand. *International Journal of Robotics and Automation*, 29(2):193–201, 2014.

[116] M. Hosseini, R. Meattini, G. Palli, and C. Melchiorri. A wearable robotic device based on twisted string actuation for rehabilitation and assistive applications. *Journal of Robotics*, page Article ID 3036468, 2017.

[117] Richard M Murray, Zexiang Li, S Shankar Sastry, and S Shankara Sastry. A mathematical introduction to robotic manipulation. chapter 6. CRC press, 1994.

[118] M. Hosseini, R. Meattini, G. Palli, and C. Melchiorri. Development of semg-driven assistive devices based on twisted string actuation. In *Proc. IEEE Conf. on Control, Automation, Robotics (ICCAR 2017)*, 2017.

[119] M Hosseini, G Palli, and C Melchiorri. Design and implementation of a simple and low-cost optoelectronic force sensor for robotic applications. In *Advanced*

Intelligent Mechatronics (AIM), 2016 IEEE International Conference on, pages 1011–1016. IEEE, 2016.

[120] ABSplus-P430 Production Grade Thermoplastic for Design Series 3D Printers. URL `http://usglobalimages.stratasys.com/Main/Files/Material_Spec_Sheets/MSS_FDM_ABSplusP430.pdf`.

[121] G. Palli, M. Hosseini, and C. Melchiorri. A simple and easy-to-build optoelectronics force sensor based on light fork: Design comparison and experimental evaluation. *Sensors and Actuators A: Physical*, 269:369 – 381, 2018.

[122] Arduino NANO - Getting started guide. URL `https://www.arduino.cc/en/Guide/ArduinoNano`.

My Publications

- U. Scarcia, L. Moriello, A.Pepe, A.M. Galiano, G.Palli, C. Melchiorri, F. Ficuciello, B. Siciliano. Experimental Evaluation of Synergy-Based In-Hand Manipulation. HFR2013 - *6th International Workshop on Human-Friendly Robotics*, Roma, Italy;

- A. Pepe, D. Chiaravalli, and C. Melchiorri. A hybrid teleoperation control scheme for a single-arm mobile manipulator with omnidirectional wheels. In *2016 IEEE/RSJ International Conference on Intelligent Robots and Systems (IROS)*, pages 1450–1455, Oct 2016. doi: 10.1109/IROS.2016.7759236

- A. Pepe, M. Hosseini, U. Scarcia, G. Palli, C. Melchiorri. Development of an haptic interface based on twisted string actuators. In *2017 IEEE International Conference on Advanced Intelligent Mechatronics (AIM)*, pages 28–33, July 2017.

- U. Scarcia, L. Moriello, A.Pepe, G. Palli and C. Melchiorri. Design of a twisted-string actuator for applications in haptic force rendering. UNDER REVIEW In *2018 IEEE International Conference on Advanced Intelligent Mechatronics (AIM)*, Auckland, New Zealand.